ChEMference 2011

Think Share Relish

September 23 - 24

Organised by

Department of Chemical Engineering
Indian Institute of Science
Bangalore 560 012 INDIA

We Sincerely Thank Our Sponsors

सत्यमेव जयते

CSIC ESSAR Oil

M/S Swastik Oil Products Mfg. Co. Navsari

Quality Industries

Binary Computer Systems Aakar Group

ChEMFERENCE 2011

Think Share Relish

SEPTEMBER 23 - 24

Organised by

DEPARTMENT OF CHEMICAL ENGINEERING
INDIAN INSTITUTE OF SCIENCE
BANGALORE 560 012
INDIA

WELCOME MESSAGE

ChEmference, a national conference of graduate students in chemical engineering, presents a unique opportunity for students to share their latest research findings with their peers, engage in a fruitful exchange of ideas, and come face-to-face with senior colleagues from the academia and the industry. Following the initiative of the Department of Chemical Engineering, IIT Kanpur in 2008, ChEmference has become an annual event and is growing in stature. It is our privilege to host the fourth ChEmference at the Department of Chemical Engineering, IISc Bangalore.

The two day event this year will commence with a plenary lecture by Prof. Ashutosh Sharma, IIT Kanpur. This will be followed by four sessions of oral presentations, each containing a keynote lecture by a faculty member and presentations by students selected from submitted abstracts, and a poster session. In addition, the last session, an added attraction this year, is a special session on entrepreneurship, which will expose students to the avenues for and the challenges in starting-up in chemical engineering in India. It is only appropriate that Bangalore, the epicenter of start-up activities in India, adds this new flavor to ChEmference.

The contributions and support of many institutions and individuals have made this event possible. We are grateful to the administration of IISc for enabling the hosting of the event on our campus. We thank DST and our corporate sponsors for their generous support. Our special thanks go to NIAS for accommodating our student participants in their guest house. Our chairman, Prof. Prabhu Nott, and the faculty and staff of our department have contributed in numerous ways to the organization of the event. And, finally, it is the long, tireless and enthusiastic hours that our student volunteers have put in that brings this event alive before you.

It gives us great pleasure to welcome you to ChEmference 2011.

Narendra M. DIXIT
Convener

K. Kesava RAO
Convener

TECHNICAL PROGRAMME

Day 1: September 23, 2011

08 : 00 - 09 : 00	Registration
09 : 00 - 09 : 30	Opening Ceremony Welcome address by Prof. K. Kesava Rao Department of Chemical Engineering, Indian Institute of Science Bangalore
	PLENARY LECTURE
	Sponsored by SABIC Innovative Plastics
09 : 30 - 10 : 30	Prof. Ashutosh Sharma Department of Chemical Engineering, Indian Institute of Technology Kanpur
10 : 30 - 11 : 00	**Tea**
	SESSION-I
	Sponsored by SABIC Innovative Plastics
11 : 00 - 11 : 45	Keynote address by Prof. Supreet Saini Department of Chemical Engineering, Indian Institute of Technology Gandhinagar
11 : 50 - 12 : 08	Smruti Ranjan
12 : 09 - 12 : 27	Vaidyanathan M. S.
12 : 28 - 12 : 46	Saeikh Zaffar Hassan
12 : 47 - 13 : 05	Pranesh Padmanabhan
13 : 05 - 14 : 30	**Lunch**
	SESSION-II
	Sponsored by Bristol-Myers Squibb
14 : 30 - 15 : 15	Keynote address by Dr. S. K. Dhawan National Physical Laboratory New Delhi
15 : 20 - 15 : 38	Ravi Sankannavar
15 : 39 - 15 : 57	Urmi Mullick
15 : 58 - 16 : 16	Sagnik Chakraborty
16 : 17 - 16 : 35	K. Sivagami
	BOOK RELEASE
16 : 35 - 17 : 00	Release of Book: *Heat and Mass Transfer: A Transport Phenomena Approach* Author: Prof. K. S. Gandhi Department of Chemical Engineering, Indian Institute of Science Bangalore
17 : 00 - 17 : 30	**High Tea**
	POSTER SESSION
	Sponsored by Hindustan Petroleum Corporation Limited
17 : 30 - 19 : 00	Poster presentations by participants*
20 : 00	**Dinner**

Day 2: September 24, 2011

SESSION-III

Sponsored by Shell, India

09 : 00 - 09 : 45	Keynote address by Prof. Raghunathan Rengaswamy Department of Chemical Engineering, Indian Institute of Technology Madras
09 : 50 - 10 : 08	Manoj Krishna K. N.
10 : 09 - 10 : 27	M. Kranthi Kumar
10 : 28 - 10 : 46	Manohar Kakunuri
10 : 47 - 11 : 05	Siddhartha Sengupta
11 : 00 - 11 : 35	**Tea**

SESSION-IV

Sponsored by
Tata Research Development and Design Centre

11 : 35 - 12 : 20	Keynote address by Prof. Mahesh Tirumkudulu Department of Chemical Engineering, Indian Institute of Technology Bombay
12 : 25 - 12 : 43	Radhe Shyam
12 : 44 - 13 : 02	Abhilasha Krishnamurthy
13 : 03 - 13 : 21	Parul Sahu
13 : 22 - 13 : 40	Anjana Ramachandran
13 : 40 - 15 : 00	**Lunch**

SESSION ON ENTREPRENEURSHIP

15 : 00 - 15 : 30	Dr. Dhananjaya Dendukuri CEO & Co-Founder, Achira Labs Pvt. Ltd., Bangalore
15 : 30 - 16 : 00	Mr. Anupam Kunwar Director Technology, SuRe Energy Systems Pvt. Ltd., Hyderabad
16 : 00 - 16 : 30	Dr. Vivek V. Ranade Founder & Chairman, Tridigonal Solutions, Pune
16 : 30 - 17 : 00	Discussion
17 : 00 - 17 : 30	**High Tea**

CLOSING CEREMONY

17 : 30 - 18 : 00	Prize distribution Vote of thanks

List of Participants for Poster Presentations*

1) Ammar Arab Beddai

2) Chandra Shekhar Besta and V K Naveen Kumar

3) Debadrita Bhattacharya

4) Deepak Ojha

5) Dhrubajit Konwar

6) Dinesh Thakare and Nikhil Gharat

7) Fasnabi P. A.

8) G.Keerthiga

9) J. Jaishree

10) Keka Sinha

11) Nandini Bhandaru

12) Rajmohan K. S.

13) Rohit Kumar Gupta

14) Rupesh Singh

15) Sudeshna Roy

16) Swapnil Dharaskar

GENERAL INFORMATION

- **Venue**
  Faculty Hall
  Indian Institute of Science Bangalore

- **Registration**
  Participants are requested to be present on September 23, 2011 at 08:00 am in Faculty Hall, IISc to collect their conference kit.

- **Name Badges**
  Name badges will be issued at the registration desk. Please display your badge when requested. Entry to auditorium, food areas, etc. will not be permitted without the badge.

- **Accommodation**
  Accommodation for student participants has been arranged at the Guest House, National Institute of Advanced Studies (NIAS).

- **Speaker Check-In Information**
  Participants are requested to load their presentation file well ahead of the start of the session. Student volunteers will help you in the process. Kindly preview your slides before the presentation.

  The meeting schedule is rather tight and hence no extra time will be given to the participants for oral presentation.

- **Mobile Phone Policy**
  Kindly switch your mobile phone off inside the auditorium.

CAMPUS MAP OF IISC BANGALORE

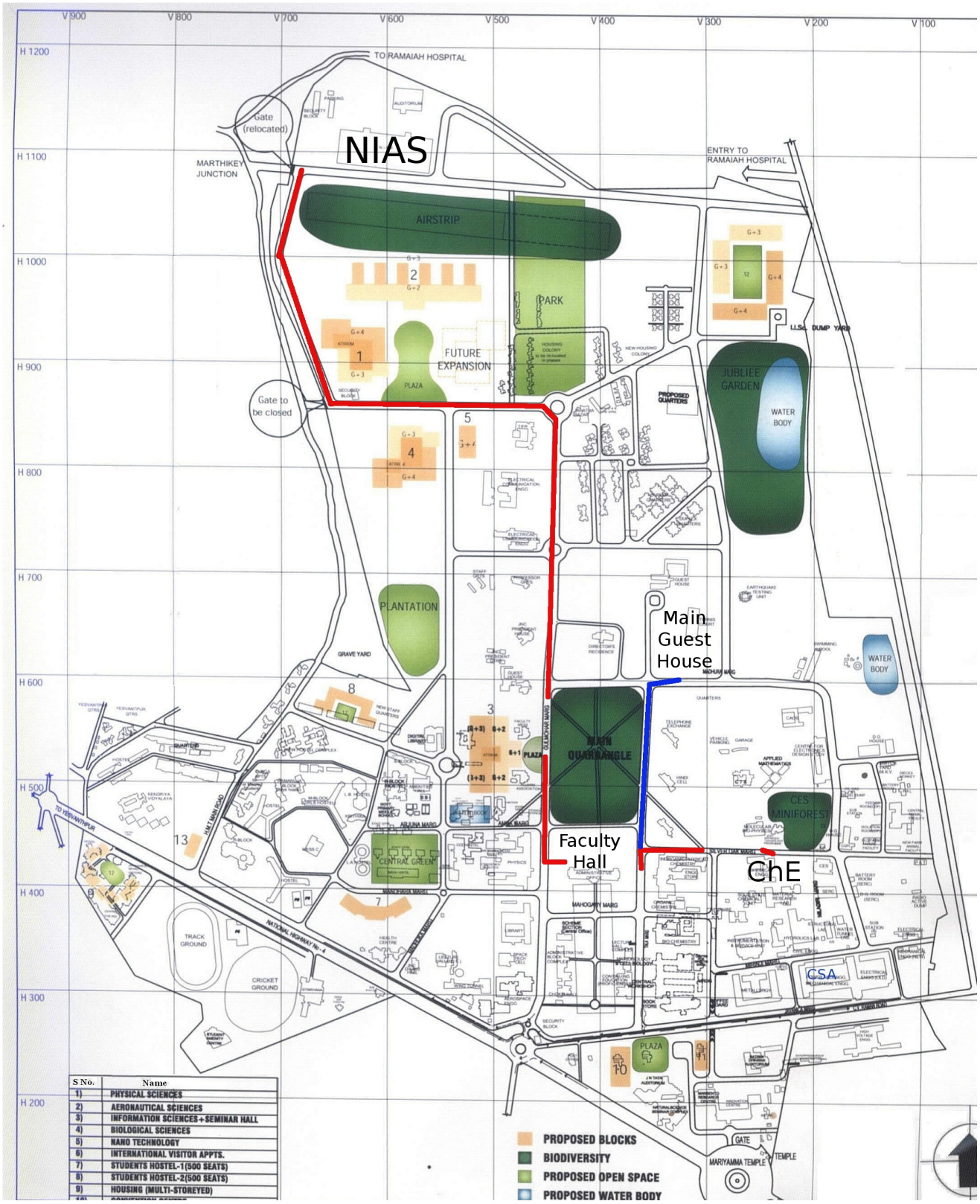

S.No.	Name
1)	PHYSICAL SCIENCES
2)	AERONAUTICAL SCIENCES
3)	INFORMATION SCIENCES+SEMINAR HALL
4)	BIOLOGICAL SCIENCES
5)	NANO TECHNOLOGY
6)	INTERNATIONAL VISITOR APPTS.
7)	STUDENTS HOSTEL-1(500 SEATS)
8)	STUDENTS HOSTEL-2(500 SEATS)
9)	HOUSING (MULTI-STOREYED)

CONTENTS

PLENARY LECTURE

Sponsored by

SABIC Innovative Plastics

Scientific Commonsense & Creativity: Some Case Studies in New Process and Product Development

Ashutosh Sharma
Department of Chemical Engineering,
Indian Institute of Technology, Kanpur
Email: ashutos@iitk.ac.in

Dear Friends:
I would like to explore with you some ideas about what innovation and creativity may mean and their roles in the context of modern chemical engineering research. I will touch upon some aspects of creative scientific thinking illustrated by a few examples from my own experiences. There is already a paradigm shift in chemical engineering research that demands that we not only do scaleup of known processes, but also integrate in a seamless way the many concerns of materials science, physics, chemistry, biology, mechanical and electrical sciences; in fact pretty much everything on demand as dictated by the problem at hand!. These challenges include, but are not limited to, such diverse areas as biomedical and electronic materials and devices, functional and smart materials, computational biology/genomics, bio- mimetics, colloids and interfaces, new separation/reaction processes & their intensification, green chemistry, novel ways of harnessing and utilization of energy and water resources and scale-down of materials and processes (nanotechnology) towards both novel and traditional ends. The potentialities are truly staggering, but their understanding and the action plans require synthesis of a diverse body of knowledge which now stands compartmentalized over different departments. Thus, new advances demand two major ingredients: (1) acquiring a life-long capacity to learn and assimilate new ideas regardless of the name tag they carry, and (2) capacity for learning not just from the printed material, but an innovation/creativity centric style of functioning, especially in the realm of research and long term developments. I would like to share with you some thoughts about the second ingredient by giving some examples from my own experience of seeking scientific solutions to some problems of product and process development (both the terms meant in their general modern context). These examples include:

1) Search for a reusable pressure sensitive adhesive that functions both in dry and wet environments with equal ease [1].
2) How to make small micro/nano 3-D objects?—search for a new fabrication method [2].
3) How to sculpt small scale features in carbon including nano-interconnects?— Fabrication of carbon-MEMS/NEMS platforms including micro-batteries, sensors, cell supports and environmental remediation [3].
4) How to make nano-channels without the use of slow and expensive tools such as ion-beams?[4]
5) How to use self-organization for micro/nano fabrication?[5]

The examples are intended only to guide and incite some intuitive thoughts about the creative processes, rather than provide a comprehensive catalogue of the many facets of innovation and creativity! Thank you. Enjoy!

ACKNOWLEDGEMENT

Collaborations with Marc Madou (UCI), Nishith Verma (IITK), Animangsu Ghatak (IITK), G. U. Kulkarni (JNCASR), K. S. Narayan (JNCASR), Rabibrata Mukherjee (IITKgp) and Chandra Sharma (IITH) are gratefully acknowledged.

REFERENCES

[1] Microfluidic adhesion induced by subsurface microstructures, Science, 318, 258 (2007). Perspectives Article: W. J. P. Barnes, Biomimetic solutions to sticky problems, Science, 318, 203 (2007) ; A bioinspired wet/dry microfluidic adhesive for aqueous environments, Langmuir, 26, 521 (2010).

[2] Generation of sub-micrometer-scale patterns by successive miniaturization using hydrogels, Advanced Materials 19, 1943-1946 (2007); Contact instability of elastic bilayers: miniaturization of instability patterns, Advanced Functional Materials 17, 2356 (2007).

[3] Multi-scale Carbon MEMS: Fabrication and conductivity measurement of suspended carbon nanofiber arrays, Carbon 49, 1727 (2011); Micro-fabrication of carbon structures by pattern miniaturization in resorcinol-formaldehyde Gel, ACS App. Mater. Interf. 2, 2193 (2010); Multiscale carbon structures fabricated by direct micro-patterning of electrospun mats of SU-8 photoresist nanofibers, Langmuir 26, 2218 (2010);Controlling the morphology of resorcinol-formaldehyde based carbon xerogels by sol concentration, shearing and surfactants, Ind. & Eng. Chem. Res. 48, 8030 (2009); Synthesis of resorcinol-formaldehyde based carbon xerogel particles and fractal-like structures, Chem. Eng. Sci. 64, 1536 (2009).

[4] Stress engineered polymeric nanostructures by self-organized splitting of microstructures, Ind. & Eng. Chem. Res. 47, 6374-6378 (2008).

[5] Self-organized nanofabrication: Multiscale pattern generation in viscoelastic polymer films by spatio-temporal modulation of electric field and control of rheology, Advanced Functional Materials 21, 324 (2011); Ultrafast large area micropattern generation in non-absorbing polymer thin-films by pulsed laser diffraction, Small 7, 758 (2011); Enhanced self-organized dewetting of ultrathin polymer films under water-organic solutions: fabrication of sub-micron spherical lens arrays, Advanced Materials 22, 5306,(2010); Stability and dewetting of metal nanoparticles filled thin polymer films: control of instability length-scale and dynamics, ACS Nano 4, 3709 (2010); Electric field induced patterns in soft visco-elastic films: from long waves of viscous liquids to short waves of elastic solids, Phys. Rev. Lett. 102, 254502 (2009).

SESSION-I

Sponsored by

SABIC Innovative Plastics

How do cells count? Flagellar regulation in Salmonella.

Supreet Saini
Assistant Professor,
Department of Chemical Engineering
Indian Institute of Technology Gandhinagar
Email: saini@iitgn.ac.in

Abstract

Cells, including bacteria, house a number of discrete organelles. While in some cases the cell only needs to build a single copy of a given organelle, in other cases it needs to build many. This suggests that cells must employ an active mechanism for sensing and controlling organelle abundance. For, if the cell builds too few, then the integrated activity of these organelles may be insufficient to complete necessary tasks; and if the cell builds too many, then critical resources are wasted.

Using the flagellum from the pathogen Salmonella as a model system for organelle number control, I will talk about the strategies employed by the bacterium to do number control. Using modeling and experimental analysis, I will demonstrate how Salmonella employs protein secretion as a proxy for flagellar abundance and then uses this signal to dynamically regulate flagellar gene expression.

Synthesis and Surface Engineering of Mesoporous $CoFe_2O_4$ Particles for Targeted Drug Delivery

Sasmita Mohapatra and Smruti R. Rout
Department of Chemistry
National Institute of Technology
Rourkela, Odisha, India
Email: sasmitam@nitrkl.ac.in

***Abstract*— Amine-functionalized monodisperse $CoFe_2O_4$ nanoparticles with a size of 35-40 nm have been produced by simple thermal decomposition method. The surface of the nanoparticle was conjugated with folic acid and rhodamine isothiocyanate through surface amine groups. Antitumor drugs such as methotrexate and/or doxorubicin were successfully conjugated with the particles through pH sensitive amide bond. The drug conjugate particles showed excellent aqueous dispersion stability with hydrodynamic size of 61 nm. These drug conjugated nanoparticles exhibit elevated cytotoxicity and high internalization efficiency as investigated in a folate receptor positive Hela cell. The high drug loading capacity owing to its high surface area and favorable pH- sensitive drug release property make the synthesized magnetic nanoparticles a promising material for drug delivery application.**

***Index Terms*—Monodisperse Mesoporous Super paramagnetic Nanoparticles, drug delivery.**

I. Introduction

Recently spinel ferrite has conceived considerable attention due to extensive application in biomedical field such as contrast enhancing agent in MRI and an active agent in drug delivery [1],[2]. More importantly spinel cobalt ferrite has been proposed for biomedical application due to its large anisotropy compared to other ferrites. In this study, in virtue of the advantage of thermal decomposition method, we developed a facile synthetic route to prepare water soluble $-NH_2$ functionalized superparamagnetic $CoFe_2O_4$ nanoparticles with high surface area in one-pot. We have loaded these $-NH_2$ functionalized particles with anticancer drug methotrexate and a fluorescent marker RITC. The entire MTX conjugated $CoFe_2O_4$ nanoparticles have been characterized in terms of their structure, morphology, size, and magnetic property. The in vitro biocompatibility of $CoFe_2O_4$-MTX was investigated through MTT assay. The intracellular uptake efficiency was thoroughly investigated through fluorescent microscopy and flow cytommetry (FACS). The MTX release profile was investigated by mimicking the lysosomal conditions in presence of bovine protease. In addition to this, the effective loading and pH sensitive release behavior of another anticancer drug doxorubicin have also been demonstrated using synthesized $CoFe_2O_4$ nanospheres.

II. Results and Discussions

It is very clear from the image that each particle is a spherical assembly of ultrafine ferrite particles. These spherical nanoassemblies are of size 35-40 nm which are assembly of primary nanocrystals of 4-5 nm (Figure 1b) and are discrete, well defined and porous in nature. The high resolution TEM of a single aggregate (Figure 1c) shows lattice planes. The inter planner distance d is calculated from the image as 2.97 angstroms which corresponds to reflection of [220] plane. Here it may be noteworthy that dispersion state of magnetic nanoparticles is the most important factor so far the magnetic property is concerned. The field dependent magnetization at room temperature (300K) shows no hysteresis representing superparamagnetic nature of the nanoparticles (Figure 1d). The saturation magnetization was found to be 59.4 e.m.u./g corresponding to its bulk counterpart 71.2 e.m.u/g. The stability of MTX-conjugated particles investigated by measuring hydrodynamic size against time shows that there is almost no change of hydrodynamic size and zetapotential even after several months. This observation implies that such stable drug conjugates can be circulated in blood stream for a long period minimizing the rapid clearance of particles by macrophages. Similar result was also obtained in case of $CoFe_2O_4$-FA-DOX nanoparticles.

We investigated the effect of $CoFe_2O_4$ nanoparticle, $CoFe_2O_4$-MTX nanoparticles (Particle without FA) and $CoFe_2O_4$-MTX-FA nanoparticle on the proliferation of HeLa cells in vitro(Figure 2A). It was observed that $CoFe_2O_4$ nanoparticle did not induce any significant change in the proliferation with concentration up to 20μg/mL with respect to the control suggesting an absence of toxicity of the $CoFe_2O_4$ nanoparticle. Subsequently the proliferation of HeLa cells reduced significantly in presence of $CoFe_2O_4$-MTX nanoparticles and at a dose of 10μg/ml, the cell proliferation was uninhibited by 50% (IC_{50} value). This is possibly attributable to the affinity of MTX towards folate receptor owing to its structural similarity with folic acid, which results in higher intake of $CoFe_2O_4$-MTX particles as compared to $CoFe_2O_4$

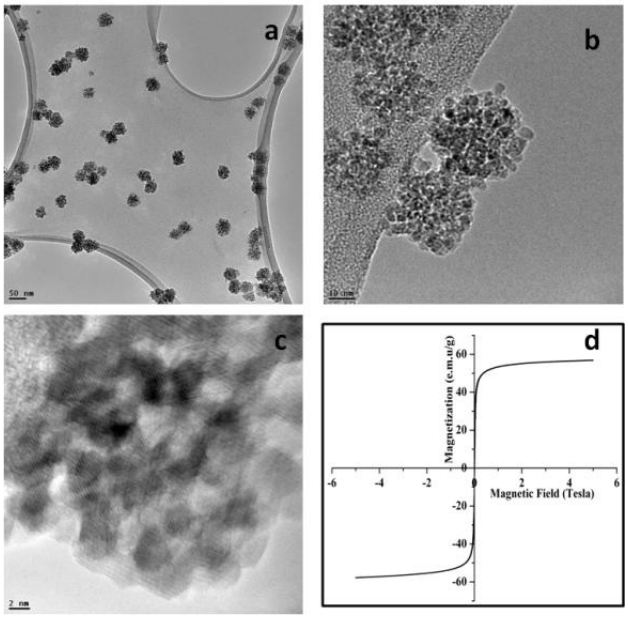

Fig. 1. (a,b) TEM images of synthezised mesoporous cobalt ferrite nanoparticles, (c) image at high resolution showing lattice imaging of [220] plane,(d) Field dependent magnetization curve of mesoporous $CoFe_2O_4$ nanoparticles.

nanoparticle. However, the proliferation of HeLa cells reduced drastically in a dose dependent manner in presence of 5μg/ml $CoFe_2O_4$-MTX-FA nanoparticles and its IC_{50} was 5μg/mL. This is attributed to the active uptake of nanoparticles in a folate receptor mediated endocytosis that interfered with the cell proliferation, which ultimately results in the target specific delivery of MTX to HeLa cells.

We further investigated whether the resulting reduction of proliferation is due to the uptake of $CoFe_2O_4$-MTX-FA nanoparticles. HeLa cells were incubated with 5μg/ml of $CoFe_2O_4$-FA-RITC-MTX nanoparticles for 0, 30, 60, 90 and 120 min. The uptake of $CoFe_2O_4$-FA-RITC-MTX nanoparticles was evident by 30 min and the internalization increased with time. The RITC signal from the $CoFe_2O_4$-FA-RITC-MTX nanoparticles progressively increased in the cytoplasm surrounding the nuclear region (Figure 2B). It suggests that nanoparticles are selectively targeted to the cells through the folate receptor mediated endocytosis and localized into the cytoplasm. Here the uniform distribution of $CoFe_2O_4$-FA-RITC-MTX nanoparticle in the HeLa cells is because of its stable dispersion in the culture media. To confirm the receptor specificity of the $CoFe_2O_4$-FA-RITC-MTX nanoparticles the uptake as well as cell viability data of HeLa cells were also compared with folate receptor-negative NIH/3T_3 cells.

III. Conclusion

This work demonstrates a simple method to produce biofunctionalized, highly water-soluble, mono-disperse, mesoporous, $CoFe_2O_4$ nanoassemblies with the diameter of 35-40 nm. The nanoparticle modified with folic acid was effectively targeted to cancer cells thereby causing the optimal delivery of methotrexate and resulted in the cell death following the induction of apoptosis.

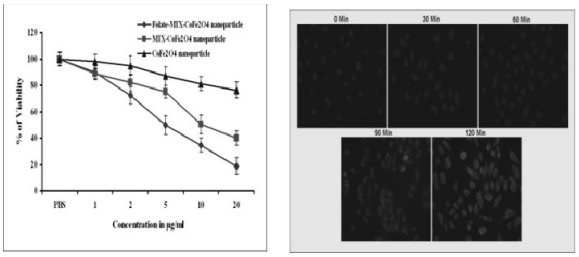

Fig. 2. A. Cytotoxicity assay of nanoparticles. B. Uptake study of nanoparticles in HeLa cells.

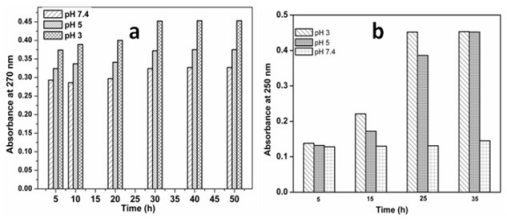

Fig. 3. pH dependent drug-release behaviors of (a) $CoFe_2O_4$-FA—RITC-MTX and (b) $CoFe_2O_4$-FA-DOX. The highest absorbance was observed at pH 3.

Acknowledgement

Authors gratefully acknowledge DBT (Ref. BT/PR11548/NNT/28/420/2008), Govt. of India for financial support.

References

[1] K.Gupta and M. Gupta,"Synthesis and surface engineering of iron oxide nanoparticles for biomedical applications" Biomaterials, , vol 26,pp 3992-4021.June 2005..

[2] N. Kohler, C. Sun, J. Wang and M. Zhang, "Methotrexate modified superparamagnetic nanoparticles and their intracellular uptake into human cancer cells"Langmuir, vol, 21, pp 8858-8864.June 2005.

[3] M. Das, D. Mishra, P. Dhak, S. Gupta, T. K. Maiti, A. Basak andP. Pramanik, "ultrasmall iron oxide nanoparticles for combined targeted cancer therapyand multimodal imaging" Small, vol,5 pp2883-2893.sept 2009.

Understanding the Action of Pore Forming Toxins

Vaidyanathan M.S[†]*, Pradeep S*[‡]*, K.G Ayappa*[†]*, Sandhya S. Viswesariah*[‡]
[†]*Department of Chemical Engineering, Indian Institute of Science*
[‡]*Department of Molecular Reproduction and Development Genetics, Indian Institute of Science*
Bangalore, India
Email: ayappa@chemeng.iisc.ernet.in

***Abstract*— We propose a three step (adsorption-conformation-oligomerization) model for capturing the essential physics of pore formation and cell lysis due to the action of a class of protein toxins called pore forming toxins. Experiments with a typical pore forming toxin, Cytolysin-A (ClyA), on red blood corpuscles (RBC) show a sharp jump in the rate of cell lysis above a threshold toxin concentration. The model yields bounds for the critical number of pores per cell and good agreement with the experimental lysis data is obtained.**

***Index Terms*—Kinetic model, Critical number of pores.**

I. Introduction

Pore forming toxins (PFTs) are a class of toxins which disrupt the cell metabolism by creating unregulated pores on the cell membrane. Despite their widespread prevalence, there is very little knowledge on the exact mechanism of pore formation. Pore forming toxins are classified as α PFTs and β PFTs according to their mode of pore formation. We focus on a typical α PFT called Cytolysin-A (ClyA) whose crystal structure has been recently identified[1],[2].

II. Model Development

A three step mechanism (Fig 1)is envisaged to describe the pore formation process. Toxins which are present in the bulk solution adsorb onto the surface of the cell membrane. This constitutes the adsorption step. On adsorption, the toxin monomer undergoes a conformational change to a membrane bound protomer. This conformational step is found to be the rate limiting step from experimental observations [1]. The protomers oligomerize to form a dodecamer which corresponds to a single pore. Once the number of pores in an RBC exceeds a critical number, cell lysis is initiated. The cell lysis is assumed to follow a first order process and is a function of the number of pores in excess of the critical number of pores per RBC. Experiments at different toxin conentrations are carried out to measure the optical density in a solution of RBC's as a function of time.

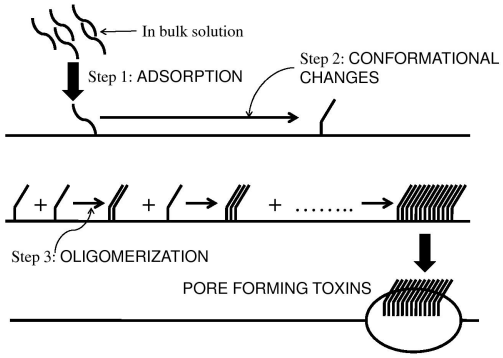

Fig. 1. Schematic for pore formation. Step-1 shows the adsorption of bulk toxin from the solution onto the cell membrane. The membrane bound monomer undergoes conformational change to form the membrane bound protomer in Step-2. The membrane bound protomers on sequential oligomerization, as shown in Step-3, form a dodecamer which corresponds to a pore.

III. Results And Discussions

The model is able to match the experimental data (Fig 2) for both high and low toxin conentrations. An important prediction made by the model is the critical number of pores required for the rupture of cells to take place. The critical number of pores range from 200-600. The simulated mass of haeomoglobin due to cell lysis with respect to time also matches with the experimental data as shown in Fig 3.

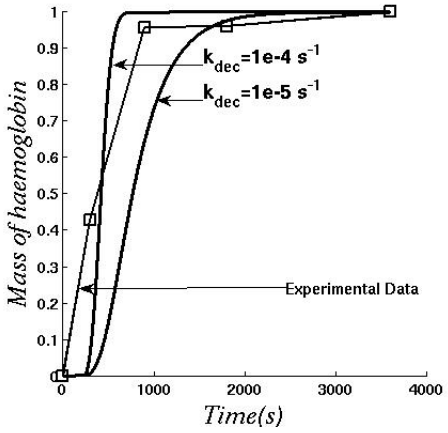

Fig. 2. Maximum amount of haemoglobin, H_{max} observed after the exposure of RBCs to ClyA toxins for 1 hour. λ, which is the ratio of the conformation to adsorption time constant is varied to match the initial toxin concentration, c_{in}. This data is obtained assuming the critical number of pores, n_{pc} as 210.

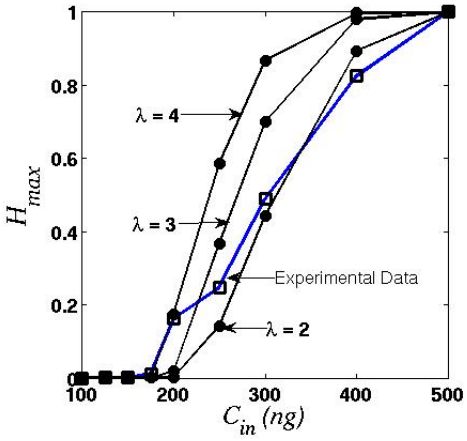

Fig. 3. The variation in the mass of haemoglobin released from the RBC's as a function of time is illustration for a 500ng toxin concentration. The model predictions for different lysis rate constants, k_{dec} are compared with the experimental data. The data shown is for $\lambda = 3$.

ACKNOWLEDGEMENT

We thank the Department of Science and Technology (DST), Government of India for financial assistance under the IRHPA (Intensity of Research in High Priority Area) Scheme.

REFERENCES

[1] Marcus Mueller, Ulla Grauschopf, Timm Maier, Rudi Glockshuber, and Nenad Ban. The structure of a cytolytic alpha-helical toxin pore reveals its assembly mechanism. Nature, 459(7247):726–730, June 2009.

[2] Eifler, N. et al. Cytotoxin ClyA from Escherichia coli assembles to a 13-meric pore independent of its redox-state. EMBO J. 25, 2652–2661 (2006).

Rate Constant of Homogeneous Acid-Catalyzed Reactions is Re-Defined Using Taguchi Approach

Saeikh Zaffar Hassan and Madhu Vinjamur
Department of Chemical Engineering
IIT Bombay, Powai
Mumbai, India
E-mail: zafarpoly@gmail.com

I. Introduction

In kinetic study of any reaction, once the reaction rate equation is determined based on reaction mechanism, the main challenge in predictions of kinetics of homogeneous reactions is lack of thorough understanding of behavior of rate constant [1],[2]. Strictly speaking, for an elementary reaction, the law of mass action qualitatively states that rate constant (k) is independent of concentration but dependent on catalyst, temperature, and other factors [3]. Whether the overall rate constant derived from reaction mechanism consisting of many elementary steps is independent of concentration of reactants is questionable. The empirical equation of Arrhenius for rate constant is well accepted in study of kinetic parameters from experimental data. Collision and transition state theories are also used for theoretical calculation of rate constant. These theories give an insight into the molecular dynamics of the reactions especially transition state theory provides more details about the mechanistic approach at molecular level for rate constant estimation. However, these theories fail to estimate practical values for rate constants. The theories and Arrhenius equation express the temperature dependency of rate constant clearly but not the influence of the other factors. Therefore, a systematic approach is required to understand reaction kinetics and the effect of reaction parameters on rate constant. Taguchi approachi [5] is adopted to understand the qualitative and quantitative effect of reaction parameters on rate constant and to develop a method to predict reaction kinetics. Taguchi design of experiments is technically advanced and more systematic in approach than the conventional "one factor at a time" way of study. For this study, sulfuric acid catalyzed esterification reactions of oleic acid in sunflower oil with methanol are carried out.

II. Methodology

Taguchi design of experiments (Taguchi DOE) is implemented for this study. $L_9(3^4)$ orthogonal array of experiments (9 experiments, 3 parameters, 3 levels for each parameter) are conducted for sulfuric acid catalyzed esterification of 50 wt% oleic acid (OA) in sunflower with methanol. The L9 array has been selected with the assumption of no interaction between parameters and Table 1 lists the array. Three levels of each reaction parameters are varied: catalyst loading, 0.5-2 wt%; temperature, 40-65^{0}0C; and molar ratio (MR), 3-9.

TABLE I
L_9 (3^4) orthogonal array design of experiment (50% OA in Oil).

Exp. No.	Catalyst Loading	Temperature	Molar Ratio	Empty
1	1	1	1	1
2	1	2	2	2
3	1	3	3	3
4	2	1	2	3
5	2	2	3	1
6	2	3	1	2
7	3	1	3	2
8	3	2	1	3
9	3	3	2	1

⇓

Reaction parameters	Level		
	1	2	3
Catalyst loading (wt%)	0.5	1	2
Temperature (^{o}C)	40	50	65
Molar Ratio (MR)	3	6	9

III. Results and Discussions

The experimental kinetics data are interpreted using power law kinetic model and second order reversible rate equation fitted best. Taguchi analysis (signal-to-noise ratio or SN ratio) of rate constants and analysis of variance (ANOVA) for SN ratio led us to propose a re-defined rate constant **(k')** as **k = k'/(catalyst concentration)** which is found to be absolutely independent of MR and only dependent on catalyst loading and temperature. A change in MR changes reactants concentration and re-defined rate constant (RRC) is found to be independent of reactants concentration. It is also discussed that moles of catalyst (N_{cat}) affects RRC and not catalyst concentration. To examine the above deductions, a method is developed based on RRC to predict kinetics of esterification reaction. In our case, rest of the 18 experiments from full factorial design of 27 experiments (L_27 orthogonal array) are theoretically predicted and few experiments are conducted to compare with predictions. Good agreement is found between experiments and predictions based on RRC as shown in Figure 1. These experiments are also compared with the predictions when conventional rate constant is used in reaction equation and also with predictions when inclusion of the catalyst concentration term is in the numerator of rate equation, as is usually done in heterogeneous catalysis. RRC based predictions are found more accurate than other forms of rate equations. The accuracy in RRC based predictions supports our earlier deductions.

The RRC is independent of MR and therefore, only the interaction between temperature and catalyst loading is stud-

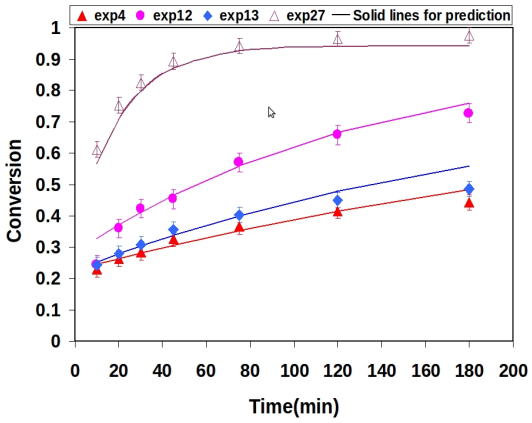

Fig. 1. Kinetic predictions compared with experiments

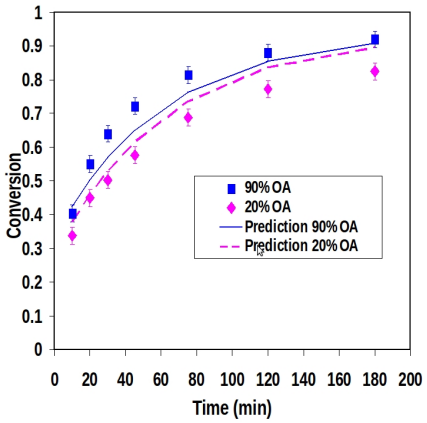

Fig. 2. Kinetic predictions (RRC based on NCat./NOA ratio) for different %OA in oil

ied. From Taguchi analysis, a negligible interaction between temperature and catalyst loading is found. This confirms our assumption of no interaction between parameters when L9 array has been implemented and also corroborates the Arrhenius equation. To further examine the RRC, an overall rate equation based on generalized RRC (GRRC) is derived from esterification reaction mechanism. In acid catalyzed esterification reaction[5], protonation (H^+ from H_2SO_4) of methanol produces an oxonium ion, CH_3OH^{2+}, which reacts with oleic acid to form methyl oleate and hydronium ion (H_3O^+). Proton is regenerated by dissociation of hydronium ion into water and proton. Here, RRC is generalized for different orders of reactions as **k=(k')*(catalyst concentration)**$^{(1-n)}$ where n is order of reaction and the derived rate equation is resulted the same equation as that used for prediction of kinetics of reactions. Inspired by Maxwell-Boltzmann distribution for energies, which gives fractional number of activated particles (N_i/N) occupying state i possessing energy Ei, a relation between Ni/N and RRC is explored. The N_i/N is written as N_{cat}/N_{OA} (where N_{cat} is mole of catalyst and N_{OA} is mole of oleic acid) because according to the mentioned reaction mechanism above, number of moles of activated particles [$CH_3OH^+.OA$] formed would be directly proportional to Ncat when oxonium reacts with OA. In our developed method of kinetic predictions, catalyst loading in wt% is replaced by Ncat/NOA and kinetic predictions are done at 20% and 90% OA in oil using RRC. The predictions are plotted in Figure 2 with experiments. A good agreement is obtained between predictions and experiments within $\pm 7\%$ error, which demonstrates that the mole ratio of catalyst to OA plays key role on RRC. The GRRC is conceptualized for different orders of reactions using sintering reaction mechanism and verified that the generalized RRC is congruent with the existing kinetic models for sintering mechanism. The GRRC for zero order reaction made it possible to device a mechanism for zero-order reaction which is not yet attempted as per our knowledge.

IV. Conclusion

Taguchi approach guided us to re-define the conventional rate constant. The re-defined rate constant (RRC) is found to be absolutely independent of reactants concentration and dependent on catalyst loading and temperature. The mole ratio of sulfuric acid to oleic acid plays key role on RRC. Based on RRC, a method is developed for kinetic predictions for a range of %OA, catalyst loading, temperature, and molar ratio. A generalized concept of RRC is also developed for different order of reactions. Using Generalized RCC (GRRC) a mechanism is proposed for zero-order reaction—which is not yet attempted as per our knowledge. Hence, GRRC is significant for defining the rate law of homogeneous reactions.

References

[1] Jong MC de, Feijt R, Zondervan E, Nijhuis TA, and Haan AB de, Applied Catalysis A: General 365 (2009) 141–147.
[2] Berrios M, Siles J, Martın M.A, and Martın A, Fuel 86 (2007) 2383–2388.
[3] Koudriavtsev A. B, Jameson R. F, and Linert W, The Law of Mass Action, Springer, Berlin, 2000.
[4] Phadke MS, Quality Engineering Using Robust Design, Pearson Education, 1st Low Price Edition, 2008.
[5] Smith, H. A, J. Am. Chem. Soc., 61 (1939) 254.

Mathematical Model Of Viral Kinetics *in vitro* Estimates The Number Of E2-CD81 Complexes Necessary For Hepatitis C Virus Entry

Pranesh Padmanabhan[†], *Narendra M. Dixit*[†‡]
[†]*Department of Chemical Engineering and* [‡]*Bioinformatics Centre*
Indian Institute of Science
Bangalore, India
E-mail: pranesh@chemeng.iisc.ernet.in, narendra@chemeng.iisc.ernet.in

***Abstract*— Interaction between the hepatitis C virus (HCV) envelope protein E2 and the host receptor CD81 is essential for HCV entry into target cells. The number of E2-CD81 complexes necessary for HCV entry remains unknown. We constructed a mathematical model of HCV viral kinetics *in vitro* to analyze recent cell culture studies that examined the dependence of HCV entry and viral kinetics on CD81 expression. Using reaction equilibrium, we determined the dependence of the number of E2-CD81 complexes formed across a virus-cell pair, and hence the susceptibility of cells to infection, on the CD81 expression level. Mimicking cell culture studies, we next constructed dynamical equations to predict the time-evolution of populations of cells with distinct CD81 expression levels collectively exposed to HCV virions. By fitting model predictions to data, we estimated that depending on the E2-CD81 binding affinity, between 1 and 13 E2-CD81 complexes were necessary for HCV entry. Predictions with this estimate described independent observations indicating that the estimate is robust. Our study thus quantifies the molecular requirements of HCV entry and suggests guidelines for intervention strategies targeting the E2-CD81 interaction.**

***Index Terms*—Viral kinetics, protein interactions.**

I. Introduction

HCV entry into target cells is a complex process involving the interactions of the viral envelop proteins E1 and E2 and several cell surface receptors. Several recent studies suggest a central role for CD81, one of the cell surface receptors, in HCV entry. How many E2-CD81 complexes must be formed between a virion and a target cell to enable HCV entry? Knowledge of this threshold would determine the number of E2-CD81 complexes that a drug or a vaccine must prevent from forming in order to block viral entry, thus presenting a quantitative guideline for intervention strategies targeting the E2-CD81 interaction. This threshold is currently unknown. Direct observation of the number of E2-CD81 complexes formed before HCV entry has not been possible. Recent cell culture studies have determined the dependence of viral entry and kinetics *in vitro* on the CD81 expression level on target cells [1]-[3]. In particular, cells expressing higher levels of CD81 were found to be more susceptible to infection [2]. Further, the frequency of cells with low CD81 expression typically increased with time following the exposure of cells to HCV [1]. We reasoned that analysis of these observations using a mathematical model of viral kinetics may allow estimation of the threshold number of E2-CD81 complexes necessary for HCV entry. Here, we constructed a mathematical model of HCV viral kinetics *in vitro* that mimics cell culture studies of the dependence of viral entry and kinetics on CD81 expression. Model predictions captured data from several independent experiments quantitatively and yielded estimates of the threshold number of E2-CD81 complexes necessary for HCV entry.

II. Model Formulation

We considered *in vitro* experiments where a population of target cells with a known distribution of the CD81 expression level across cells is exposed to HCV virions and the progression of infection followed [1]-[3]. We modelled the ensuing viral kinetics as follows. We first considered a single virus-cell pair with the virus attached to the cell by interactions that precede E2-CD81 binding. E2 and CD81 then interact to form E2-CD81 complexes. We computed the mean number of these complexes formed at equilibrium as a function of the CD81 expression level on the cell. Assuming that the number of complexes formed followed a Poisson distribution with the mean as predicted by reaction-equilibrium, we computed the probability that the number of complexes formed was larger than a threshold number. This probability yielded the relative susceptibility to infection of a cell with a given CD81 expression level. We next considered the population of cells exposed to virions. We divided the cells into different subpopulations with distinct CD81 expression levels and hence different susceptibilities. Cells in each subpopulation were assumed to proliferate, die, or be infected at a rate proportional to the susceptibility. The resulting infected cells were lost at

enhanced rates compared to uninfected cells due to virus-induced cytopathicity *in vitro*. Free virions were produced by infected cells and were cleared. With this description, we constructed dynamical equations to predict the time-evolution of each of the uninfected and infected cell subpopulations and the population of free virions and compared our predictions with experiments.

III. Results and Discussions

We considered first the experiments [1], where the kinetics of the growth of Huh-7.5.1 cells with and without exposure to HCV virions were measured. Model predictions provided good fits to the data indicating the ability of our model to capture experimental observations quantitatively (Fig. 1A and 1B). The best-fits, depending on the affinity of E2 for CD81, yielded an estimate between 1 and 13 as the number of E2-CD81 complexes necessary for HCV entry.

To test the robustness of our estimate of the threshold E2-CD81 complexes, we considered an independent experiment [2] where cells with known CD81 expression were exposed to HCV virions and the fractions of cells infected in sub-populations with distinct CD81 expression levels were measured at day 3 post-infection. Model predictions again provided excellent fits to the data (Fig. 1C). Further, the resulting estimates of threshold E2-CD81 complexes were in close agreement with the estimates obtained above indicating the robustness of the best-fit parameter estimates. We considered

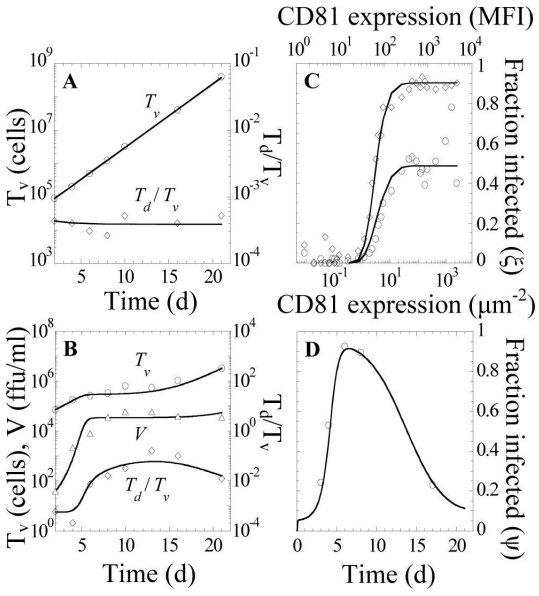

Fig. 1. Comparisons with experiments. Fits of model predictions (lines) to data (symbols) of (A) the time-evolution of viable cells (T_v) and the ratio of dead to viable cells (T_d/T_v) in the absence of infection [1], (B) the time-evolution of T_v, T_d/T_v, and the viral titre (V) during infection [1], and (C) fractions of cells infected in sub-population with distinct CD81 expression levels at day 3 post-infection to data [2]. (D) Model prediction (line) of the time-evolution of the fraction of cells infected compared with data (symbols) [3]

finally the experiments [3] where the fraction of cells infected with HCV was measured as a function of time following the onset of infection. Our model predictions, without any adjustable parameters, were in quantitative agreement with the observations (Fig. 1D).

Our estimate thus provides a quantitative guideline for the optimal usage of drugs and vaccines that target the E2-CD81 interaction: A potent drug or vaccine must ensure that not more than 1-13 E2-CD81 complexes are formed across a virus-cell pair in order to prevent viral entry.

References

[1] J Zhong, P Gastaminza, J Chung, Z Stamataki, M Isogawa, et al., "Persistent hepatitis C virus infection in vitro: coevolution of virus and host", J. Virol., Vol. 80, pp. 11082-11093, 2006.

[2] G Koutsoudakis, E Herrmann, S Kallis, R Bartenschlager, T Pietschmann, "The level of CD81 cell surface expression is a key determinant for productive entry of hepatitis C virus into host cells", J. Virol., vol. 81, pp.588-598, 2007.

[3] DM Tscherne, MJ Evans, T von Hahn, CT Jones, Z Stamataki, et al., "Superinfection exclusion in cells infected with hepatitis C virus", J. Virol. Vol. 81, pp. 3693-3703, 2007.

SESSION-II

Sponsored by

Bristol-Myers Squibb

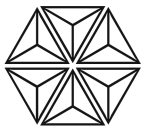

Bristol-Myers Squibb

Conducting Polymers: What Does the Future hold?

S.K. Dhawan CSIR-National Physical Laboratory
Dr. K.S. Krishnan Marg
New Delhi – 110012, India
Email: skdhawan@nplindia.org

Abstract

Electronically conducting polymers are a new class of materials with interesting potential applications in number of technologies like an electrode material in primary and secondary batteries, shielding of electronic equipments from electromagnetic pollution and electrostatic charge dissipation, stealth applications in microwave range, sensors, organic light emitting diodes, super conducting polymers, super capacitors and as corrosion inhibition coatings. Deliberate modification in the chemical and super molecular structure in the polymer matrix can lead to the formation of conducting polymers of high electronic conductivity (p & n type) which can be suitably designed for high tech applications.

The conducting polymer, polyacetylene, discovered by Shiakawa, Heeger and MacDiarmid has electronic conductivity of the order of 105 S/cm whereas the conductivity of copper is 106 S/cm. With the idea that electronic conductivity can be varied with doping has revolutionized the area of research. They acquire importance over inorganic semiconductors in their application because of their high strength to weight ratio, toughness, low cost and ease of processing into film. The prospect of plastic metals has inspired much interest in these materials for technological applications such as antistatic coatings and electromagnetic interference shielding and in other areas where light weight, flexibility and high conductivity materials are required.

Molecular design opportunities in conducting polymers where the electrical and mechanical properties make them outstanding candidate materials for engineered designs and will form a new basis for a new generation of high tech specialty polymers.

Use of a Solar Still for Treatment of Drinking Water, Rainwater Harvesting, and Disposal of Spent Zirconium-SPADNS Solution

*Ravi Sankannavar, K. Kesava Rao**
Department of Chemical Engineering,
Indian Institute of Science,
Bangalore - 560012, India
**Corresponding author E-mail: kesava@chemeng.iisc.ernet.in*

***Abstract*— The aim of the present work is to examine the use a solar still for (i) distillation of water containing excess fluoride (F^-), total dissolved solids, and hardness, (ii) harvesting rainwater, and (iii) disposal of spent zirconium-SPADNS solution. Defluoridation was done using solar distillation for water having high concentration of F^- (c_F) (0.01 - 2 g/L), and the values c_F in the distillates were well below the desirable limit of 1 mg/L for F^-. The water quality parameters such as total dissolved solids (TDS), pH, c_F, and hardness were analysed for water samples collected from Hebbagodi and Lakkihalli villages. These samples had excess c_F, TDS, and hardness. These samples were distilled using a solar still. Rainwater harvesting was done using the upper surface of a solar still. For the distillates and rainwater, the parameters were found to be well below the desirable limit. The SPADNS method is one of the standard method for the estimation of F^- in water. The spent solution was fed to a solar still, resulting in colourless distillate of pH 6.15 - 6.43. It can be disposed in the sewer as the pH of distillate was falls within the accepted range for disposal of waste solutions.**

***Index Terms*—Solar distillation; Defluoridation; Rainwater harvesting; SPADNS method**

I. Introduction

Water is needed for drinking, cooking, cleaning, bathing, irrigating crops and many other tasks. It is important to have ready access to available resources like rivers, lakes, and groundwater. Worldwide, 900 million people do not have to access safe drinking water [3]. So drinking water may have to be treated to improve smell, taste, clarity, or to remove harmful contaminants. In the present work, solar distillation was used to treat and collect drinking water, and to dispose a spent solution that was used to estimate c_F in water.

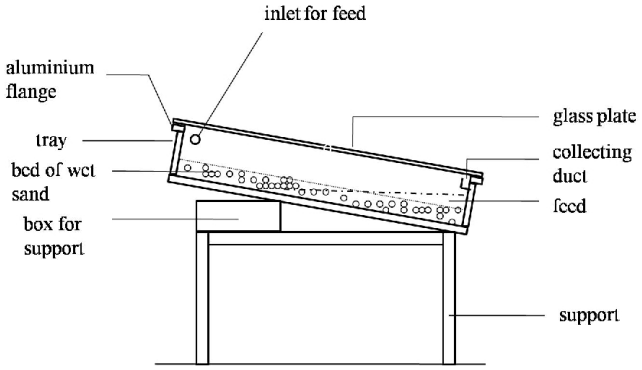

Fig. 1. Elevation of the solar still. The dimensions of the tray are 252 mm X 198 mm.

II. Experiments

Defluoridation was done using solar still containing a bed of sand in the tray (Fig. 1). The feed solution was prepared by dissolving NaF in tap water obtain F^- concentration, $c_F \approx 10$ - 2000 mg/L. The distillate was collected using a polyethylene bottle. The water samples collected from different locations of Hebbagodi and Lakkihalli villages were distilled.

Rainwater harvesting was done by attaching an aluminium L-section (25 mm x 25 mm x 1110 mm) attached to the upper surface of still as suggested by Thomas (http://www.solutionexchange-un.net.in/environment/cr/res20100501.pdf).

Analysis of water quality parameters pH, c_F, total dissolved solids, total hardness, calcium hardness, and magnesium hardness were done for the distillates obtained from water samples, and for rainwater.

One of the standard methods used for the estimation of F^- in water is based on a coloured zirconium-SPADNS solution [1]. The spent solution was distilled in a stainless steel still to obtain a colourless distillate.

III. Results and discussion

The values of the water quality parameters for distillates and rainwater were below the desirable limits, except that the pH of most of the rainwater samples was slightly below the desirable lower limit of 6.5 (Table I) . Distillation from synthetic samples having c_F in the range 10 - 2000 mg/L also had c_F values below 1 mg/L.

The volume of rainwater harvested using solar still in August 2011 varied from 5.12 to 21.12 L/m^2-day.

(a) (b)

Fig. 2. Colours of (a) spent zirconium-SPADNS solution, (b) distillates.

The pH of distillate obtained using spent solution was very low. It was changed to an alkaline pH using about 10% 8 N NaOH solution to the feed. A colourless distillate (Fig. 2) having a pH of 6.15 - 6.43 was obtained, which can be disposed in the sewer.

IV. Conclusion

The solar still can be used to treat water having excess F^-, TDS, and hardness. Alternatively, it can be used to harvest rainwater during rainy season as the output of the distillate will be low during this season. Rainwater can be also used for drinking if a slightly lower pH than the desirable limit can be tolerated.

The spent solutions from analytical methods such as SPADNS method can be distilled using solar still. The cost of the still is about Rs. 2,158 for an area of 0.5 m^2, and the running cost is negligible.

Acknowledgment

We thank Dr. J. R. Mudakavi for his helpful suggestions.

TABLE I

Values of water quality parameters for feed water, distillate, and rainwater. The desirable limits are adapted from [2]. Here c_D denotes the detection limit of 0.01 mg/L. Feed: water from Hebbagodi and Lakkihalli villages.

Parameter	Feed to the still	Distillate	Rainwater	Permissible limit
pH	6.8 - 8.1	6.4 - 7.3	6.3 - 6.7	6.5 - 8.5
c_F	0.33 - 2.02	0.08 - 0.36	$< c_D$ - 0.14	1
total dissolved solids (mg/L)	908 - 1447	13 - 52	9 - 30	500
total hardness (mg $CaCO_3$/L)	297 - 951	5 - 31	5.2 - 7.3	300
calcium hardness (mg Ca/L)	78 - 842	< 9	< 6	75
magnesium hardness (mg Mg/L)	25 - 95	< 4	< 1	30

References

[1] Ervin. Bellack and P. J. Schouboe. Rapid photometric determination of [U+FB02]uoride in water. Analytical Chemistry, 30(12):2032–2034, 1958.

[2] Bureau of Indian Standards. Indian Standards for dinking water quality:10500, 1993.

[3] World Health Organisation. Progress on Sanitation and Drinking-Water. World Health Organization, Geneva, 2010.

Removal of Chromium(VI) Using Anion Exchange Resin TULSION A-23 for Drinking Water Purpose

Dr. Susmita Mishra, Urmi Mullick
Department of Chemical Engineering
National Institute of Technology
Rourkela, Odisha, India
urmi.mullick@gmail.com

***Abstract*— A commercially available anion exchange resin namely, TULSION 23 is an anionic resin form used for the removal of chromium from aqueous solution. It possesses an enhanced chromium sorption capacity (SC) of 1.196 mg/g in a minimum period of 180 min contact time. The sorption experiments were carried out in batch mode to optimize various influencing parameters viz., contact time, initial chromium concentration, pH etc. The mechanism of chromium removal by the resin is by means of electrostatic adsorption coupled reduction and complexation. The adsorption data was fitted with Freundlich and Langmuir isotherms. The dynamic studies demonstrated that the sorption process follows intraparticle diffusion models. The regeneration studies indicated 97% regeneration up to five cycles.**

***Index Terms*—Ion exchange resin, Tulsion A-23, sorption, regeneration**

I. Introduction

Industrial wastewater often contains considerable amounts of heavy metals that would endanger public health and the environment if discharged without adequate treatment. Major sources of heavy metals in the environment include metal extraction, metal fabrication and surface finishing, paints and pigments, battery manufacture etc. Pollution by chromium is of considerable concern as the metal has found widespread use in various industries.

The discharge limit of chromium is 0.2 mg/L for stream and 0.1 mg/L for irrigation. But for drinking purpose, the WHO permissible limit is 0.05 mg/L. Industrial waste that contains very high amount of Cr, needs to be brought down to the permissible discharge limits. Moreover, that water may not be fit for human consumption as the permissible limit for drinking purpose is as low as 0.05 mg/L. Hence Cr removal from such water bodies is essential.

However among these alternatives, ion-exchange method is very attractive with regards to purification for drinking water.

II. Experimental

A. Material

In this study, a commercially available analytical grade anion exchange resin namely, TULSION A-23 (Thermax Limited, Pune) is examined to be used for the removal of chromium from Cr containing waste water and purify it to drinking water purpose

B. Chromium sorption experiments

A stock solution of 200 mg/L of dichromate ion concentration was prepared by dissolving 0.563 g of $K_2Cr_2O_7$ in 1000 mL distilled water.

1) Minimum resin dose: The experiment to find the minimum resin dose was carried out by taking doses of 300 mg/L, 400 mg/L, 500 mg/L, 600 mg/L and 700 mg/L keeping initial Cr concentration and all other parameters constant, agitating at 150 rpm.

2) Average contact time: The average contact time was approximately determined by keeping all other parameters constant and taking samples every 10 minutes.

3) pH: pH was studied by varying pH by of the solution at 6, 6.5, 7, 7.5 and 8.

4) Regeneration studies: The exhausted resin was regenerated using 2% KCl solution for about 1 hour in room temperature with an agitation of 150 rpm. Similarly 5 cycles were carried out.

C. Cr (VI) analysis

As there is only Cr (VI) in the sample, the concentration was determined by diphenyl carbazide method which is nearly specific for chromium.

III. Results and Discussions

A. Effect of contact time

It was found that saturation almost reached after 180 min. Though the contact time is more to reach equilibrium, it gives results very close to 0.05 mg/L Cr in near neutral pH.

B. Influence of solution pH

As the study is specific for water treatment for drinking purpose, pH 8.0 has been selected.

TABLE I
FREUNDLICH AND LANGMUIR ISOTHERMS

	Freundlich			Langmuir		
Temperature (K)	n	ln k_f	R^2	Q^0	b	R^2
303	0.17	15.56	0.953	1.196	8.52	0.979

C. Influence of resin dose

It was found that for an initial Cr concentration of about 10 mg/L, 600 mg/L resin is sufficient for more than 95% removal of Cr.

D. Influence of resin regeneration

In this study of regeneration using 2% KCl, it was found that the resin works with over 96% efficiency for atleast five cycles.

E. Sorption isotherms

To quantify the sorption capacity of TULSION A-23 resin for chromium sorption, two-parameter equations namely Freundlich and Langmuir isotherms have been adopted.

The Freundlich isotherm is represented by

$$lnq_e = lnK_f + 1/n * lnC_e \tag{1}$$

Where q_e = the amount absorbed (mg/gm), C_e = the equilibrium concentration of the adsorbate(mg/L), K_f = the Freundlich constant related to the adsorption capacity, 1/n = the Freundlich constant related to the adsorption intensity. The values of 1/n was found to be 0.17, indicate the conditions favourable for adsorption.

The Langmuir isotherm is represented by

$$C_e/q_e = 1/Q^0 * 1/b + C_e/Q_e \tag{2}$$

Where q_e = the amount of chromium adsorbed per unit weight of the sorbent (mg/g), C_e = the equilibrium concentration of chromium in solution (mg/L), Q^0 = the amount of adsorbate at complete monolayer coverage (mg/g) and gives the maximum sorption capacity of sorbent, b (L/mg) = Langmuir isotherm constant that relates to the energy of adsorption. The Langmuir constants Q^0 and b were calculated from the slope and intercept of the plot C_e/q_e versus C_e as 1.196 mg/g and 8.528 respectively and the values are presented in Table 1

F. Diffusion based models

The intraparticle diffusion model is further investigated here refers to the equation

$$q_t = k_i * t^{1/2} \tag{3}$$

where k_i is the intraparticle rate constant (mg/g min$^{0.5}$). The slope of the plot of q_t against $t^{1/2}$ gives the value of intraparticle rate constant which was found to be 0.731.

IV. CONCLUSION

The following conclusions were drawn based on investigation of chromium removal by TULSION A-23 anion exchange resins that the resin is capable of 20 mg/L chromium from aqueous solution to the extent of 97% at the solution pH of 8.0 with a minimum resin dose required is 600 mg/L at pH 8. The contact time in batch process was about 180 min but the resin works even for very low Cr concentration at drinking water pH. The maximum sorption capacity was found to be 1.196 mg/gm and adsorption intensities (n) 0.17 for this resin. No desorption was reported upto 210 min. The results also demonstrate that an intraparticle diffusion mechanism plays a significant role in the adsorption. The regeneration studies indicated 97% regeneration up to five cycles.

REFERENCES

[1] Dermoua E., Velissarioub A., Xenosa D., Vayenas D.V., Biological removal of hexavalent chromium in trickling filters operating with different filter media types, Desalination 211 (2007) 156163

[2] Muniyappan Rajiv Gandhi, Natrayasamy V., Sankaran M., Adsorption mechanism of hexavalent chromium removal using Amberlite IRA 743 resin, Ion Exchange Letters 3 (2010) 25-35

[3] Pettine M ., Capri S., Removal of humic matter interference in the determination of Cr(VI) in soil extracts by the diphenylcarbazide method, Analytica Chimica Acta 540 (2005) 239246

[4] Rengaraj S., Kyeong-Ho Yeon, Seung-Hyeon Moon, Removal of chromium from water and wastewater by ion exchange resins, Journal of Hazardous Materials B87 (2001) 273287

[5] Sahu S.K. , Meshram P. , Pandey B.D. , Kumar V. ,. Mankhand T.R., Removal of Chromium(III) by cation exchange resin, Indion 790 for tannery waste treatment, Hydrometallurgy 99 (2009) 170174

Removal of Crystal Violet Dye from Wastewater Using H_2SO_4 Modified Sugarcane Bagasse: Equilibrium, Kinetic and Thermodynamic Modeling

Sagnik Chakraborty, Papita Das (Saha)
Department of Biotechnology,
National Institute of Technology-Durgapur,
West Bengal, India
papitasaha@gmail.com

***Abstract*— Batch adsorption studies were carried out using H_2SO_4 modified sugarcane bagasse (HMSB) for removal of hazardous Crystal Violet (CV) dye from aqueous solutions. Effects of different operating parameters such as initial dye concentration, initial solution pH, adsorbent dose and temperature on the sorption process were investigated. The adsorption capacity increased with increasing initial dye concentration (from 10 to 100 mg L^{-1}). The adsorption efficiency increased with increasing solution pH (from 4 to 10), adsorbent dose (from 0.50 to 2.00 g) and temperature (from 298 to 318 K). The Langmuir isotherm model better described the equilibrium dye uptake than the Freundlich and Dubinin-Radushkevich (D-R) isotherm models. Pseudo-second-order kinetic model was found to be in good agreement with the experimental kinetic data. Gibbs free energy (ΔG^0) was spontaneous for all interactions, and the adsorption process exhibited endothermic enthalpy values. The adsorbent exhibits very high monolayer dye binding capacity of 148.24 mg g^{-1} which is comparable to or higher than those of many sorbent materials. These results suggest that HMSB could be effectively used as a low-cost and alternative adsorbent for the removal of CV dye from wastewater.**

***Index Terms*—Adsorption, Modified sugarcane bagasse, Crystal Violet, Equilibrium, Kinetics, Thermodynamics**

I. Introduction

Dyes have become one of the main sources of severe water pollution as a result of rapid industrialization. In this context, the release of Crystal Violet (CV) into our surrounding water bodies has triggered a major concern on the human health and marine lives. CV - a triarylmethane dye, finds extensive use as a purple dye in textile industries for dyeing of silk and cotton. It also finds application in the manufacture of paints and printing inks. CV is a protein dye and hence it is used as an enhancer for bloody fingerprints [1]. As such, a considerable amount of the used dye enters the natural environment through wastes resulting in colored effluents. CV is carcinogenic and has been classified as a recalcitrant molecule since it is poorly metabolized by microbes, is non-biodegradable, and can persist in a variety of environments. Among the existing technologies available for dye removal, adsorption has been globally accepted as the most effective and economic method to treat dye-bearing effluents. If compared with other available technologies, adsorption offers a number of advantages such as simplicity of design, low initial cost, ease of operation, insensitivity to toxic substances and complete removal of pollutants even from dilute solutions. Sugarcane bagasse (SB) is one of the potential adsorbent materials. SB modified with H_2SO_4 was investigated as a new adsorbent for the removal of hazardous CV dye from aqueous solutions; which formed the motivation of the present study. The study includes an evaluation of the effects of various operational parameters such as initial dye concentration, adsorbent dosage, contact time, temperature and pH on the dye adsorption process.

II. Experimental

Sugarcane bagasse (SB) was collected from a local fruit juice centre of Durgapur, West Bengal, India. The bagasse was first thoroughly washed with tap water to remove dust, dirt and any unwanted particles and sun dried. The dried bagasse was grounded into fine particles with the help of an electric grinder and sieved to a constant size (200 μm). Then 100 g of SB was treated with 250 mL concentrated H_2SO_4 and stirred for 30 min and left for overnight. It was then washed with deionized water to remove excess acid and any other soluble substances until neutrality and then oven dried 353 $\pm$ 1 K for 24 h. Stock solution (1000 mg L^{-1}) was prepared by dissolving accurately weighed quantity of the dye in double-distilled water. Experimental dye solution of different concentrations was prepared by diluting the stock solution with suitable volume of double-distilled water. The initial solution pH was adjusted using 0.1 M HCl and 0.1 M NaOH solutions. Batch adsorption experiments were carried out in 250 mL glass-stopperred, Erlenmeyer flasks with 100 mL of working volume, with a concentration of 50 mg L^{-1}. A weighed amount (2 g) of adsorbent was added to the solution.

The flasks were agitated at a constant speed of 150 rpm for 4 h in an incubator shaker (Model Innova 42, New Brunswick Scientific, Canada) at 308 $\pm$ 1 K. The influence of pH (2.0, 3.0, 4.0, 5.0, 6.0, 7.0, 8.0, 9.0, 10.0), initial dye concentration (10, 20, 40, 50, 60, 80, 100 mg L^{-1}), adsorbent dosage (1, 2, 3, 4, 5 g) and temperature (298, 308, 318 K) were evaluated during the present study. Samples were collected from the flasks at predetermined time intervals for analyzing the residual dye concentration in the solution. The residual amount of dye in each flask was investigated using UV/VIS spectrophotometer (Model Hitachi - 2800).

A. *Effect of pH*

The adsorption of CV onto HMSB was studied over a pH range of 2–10. The percentage removal of CV by HMSB increases with the increase in pH of the dye solution, appreciably up to pH 6.0. With further increase in pH from 6.0 to 10.0 the percentage CV removal increases but the difference in the percentage increase is not very significant. Since maximum removal is obtained at pH 9.0, all further experiments were carried out at pH 9.0.

B. *Effect of Adsorbent Dose and Contact Time*

Adsorbent dose is an important parameter influencing the sorption processes since it determines the sorption capacity of an adsorbent for a given initial concentration of the adsorbate under the operating conditions. The adsorption efficiency increased from 90.24 % to 98.08 % as the adsorbent dose increased from 0.5 to 2 g. The increase in the percentage of dye removal with adsorbent dosage could be attributed to an increase in the adsorbent surface area, augmenting the number of adsorption sites available for adsorption.

C. *Effect of Temperature*

Batch adsorption experiments were carried out at different temperatures ranging from 298 to 318 K. Data obtained from the experiments. The percent dye removal increases with rise in temperature from 298 to 318 K at the same dye concentration. The increase in percentage removal of dye at increasing temperatures could be explained by the increased affinity of binding sites for dye molecules. Increased dye removal capacity with increasing temperature suggests that biosorption of CV by HMSB is kinetically controlled by an endothermic process.

D. *Effect of Initial Dye Concentration*

The adsorption capacity at equilibrium increased from 83.23 to 166.48 mg g^{-1} with increase in initial dye concentration from 10 to100 mg L^{-1}. This behaviour is a result of the increase in the driving force from the concentration gradient.

III. Adsorption Isotherm and Kinetic Studies

Freundlich, Langmuir and Dubinin-Radushkevich (D-R) isotherm were applied to describe the equilibrium relationships between sorbent and sorbate in solution. The adsorption isotherm was described by Langmuir isotherm . The maximum monolayer adsorption capacity of HMSB for CV as obtained from the Langmuir isotherm at 318 K was found to be 148.24 mg g^{-1}. Pseudo -first- order and Pseudo- second-order were used to explain the kinetics of adsorption to investigate the adsorption mechanism. The kinetics of adsorption followed Pseudo-second-order Model. The rate constant increased with increase in temperature indicating endothermic nature of adsorption.

IV. Thermodynamic Studies

Gibb's free energy for adsorption of Crystal Violet onto HMSA SCB at all temperature was obtained from Van't Hoff equation. The negative value of (ΔG^0) at all temperatures confirms the spontaneous nature of the adsorption process. Positive value of (ΔH^0) implies that the adsorption process is endothermic.

V. Conclusion

The present study reveals that Modified SB was an effective adsorbent for the sorption of CV from aqueous solution.

References

[1] R Ahmad. "Studies on adsorption of crystal violet dye from aqueous solution onto coniferous pinus bark powder (CPBP)," J. Hazard. Mater., Vol.171, pp.767-773, 2009.

Solar Photo Catalytic Degradation of Pesticides in Wastewaters using Floating Photo Catalyst

K. Sivagami , R. Ravi Krishna and T. Swaminathan
Department of Chemical Engineering/EMRL
Indian Institute of Technology Madras
Chennai, India
tswami@iitm.ac.in

***Abstract*— Solar Photo Catalytic Degradation of Pesticides in Wastewaters was studied using polymeric TiO_2 bead as floating photo catalyst. The effects of parameters such as the initial concentration of pesticide and aeration on the photocatalytic degradation of the organophosphorus pesticides are also studied.**

***Index Terms*—Chlorpyrifos, Endosulfan and floating photo catalyst**

I. Introduction

Large scale, indiscriminate use of pesticides to accelerate food production, particularly in developing countries, has resulted in pesticide contamination of natural waters in many parts of the world. The concentrations of pesticides have exceeded frequently the permissible concentrations in surface water and ground water. Among the techniques for their removal, heterogeneous Photo catalytic oxidation is emerging to be the most effective technique. A recent development in this area is the use of floating catalyst which facilitates high efficiency with ease of separation. Chen's group [1],[2] have studied the solar photo catalytic degradation of organo phosphorus pesticides using floating photo catalyst $TiO_2 \cdot SiO_2$ hollow glass beads. In the present study, photo catalytic degradation of three pesticides, widely used in India, viz. Endosulfan (ES) and Chlorpyriphos (CPS), was investigated using polymeric beads coated with TiO_2 under solar irradiation.

II. Experimental

The floating polymeric beads were prepared by coating polystyrene beads (6 millimeter) with commercial grade TiO_2 (CDH, 99 % Anatase) using silica based adhesive solution as the binder. The coated beads were dried in oven for 1 hour. The dried beads were stirred in 500 millilitre of water to remove the loosely bound TiO_2. Batch degradation experiments were carried out in well stirred glass beakers exposed to sunlight at initial concentrations of pesticides ranging from 5 to 50 parts per million and at a catalyst loading of 1 gram per litre. Experiments were performed during daytime (10 am - 4 pm). Samples were collected from the beaker at specific time intervals and analyzed for residual pesticide by gradient HPLC (Jasco Pu-2089 plus, Japan) using PDA detector (Agilent Eclipse PAH 5 micro meter). The samples were filtered using syringe filter to remove titania particles.

III. Results and discussions

The results indicate good removals of both the pesticides (70 - 90 %) depending on the initial pesticide concentration. Figures 1 and 3 show that increasing initial pesticide concentration decreases the removal. Figures 2 and 4 show that

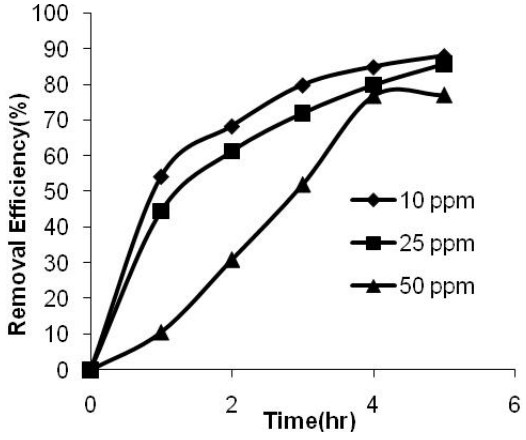

Fig. 1. Effect of initial concentration in CPS degradation

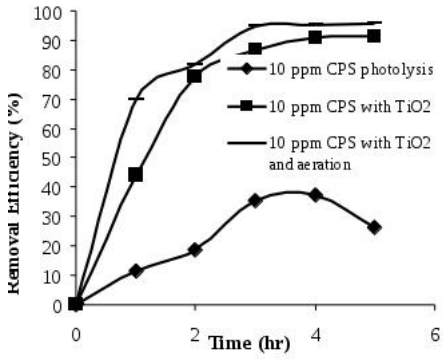

Fig. 2. Effect of aeration in CPS degradation

photo catalysis significantly enhances the pesticide removal over photolysis alone. Aeration enhances the photo catalytic removal. It is observed from figure 5 that ES degradation followed the first order kinetics. SEM image of coated TiO_2 (Fig.6) shows the uniform distribution of TiO_2 on the bead.

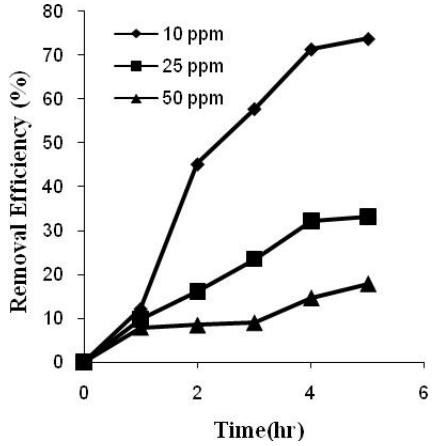

Fig. 3. Effect of initial concentration in ES degradation

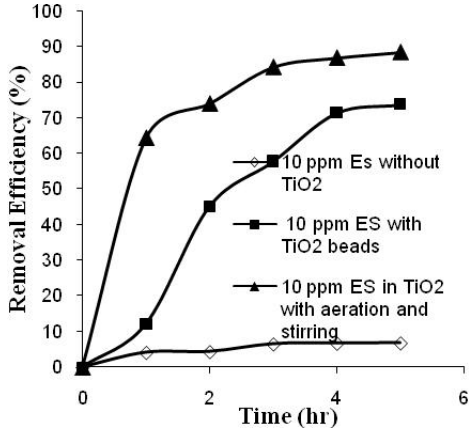

Fig. 4. Effect of aeration in ES degradation

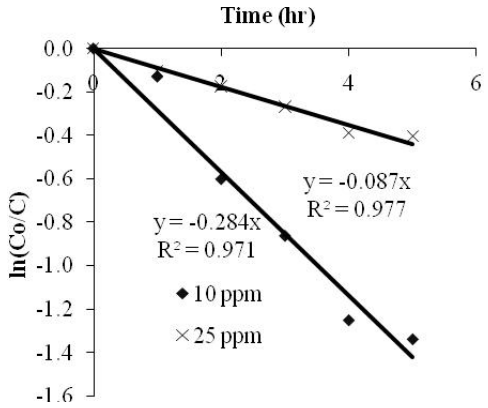

Fig. 5. Order kinetics fit for ES degradation

IV. Conclusion

The study indicates that the floating polymeric TiO_2 coated beads can be effectively used for the photo catalytic degradation of Endosulfan and Chlorpyrifos in sunlight. As the density of polymeric beads is lower than 1.0 gram per cubic centi meter, they can float on wastewater and use sunlight directly. At the same time, it also avoids the filtration and resuspension of the photocatalyst powders. After 60 h illumination by sunlight there is no significant loss of photocatalytic activity

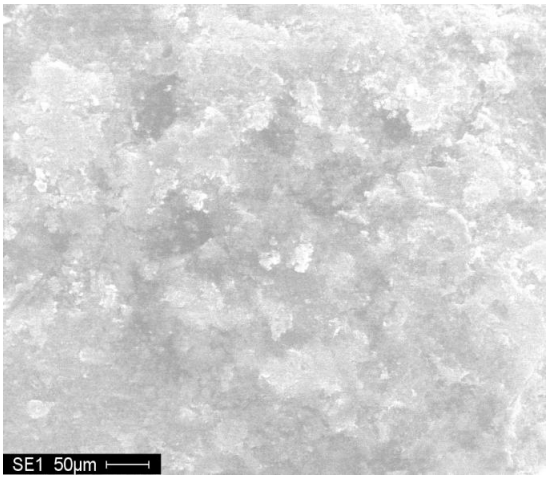

Fig. 6. SEM image of TiO_2 coated polymeric bead

of the TiO_2 beads. Initial concentration of pesticide and aeration has significant impacts on removal efficiency. The relatively high removals obtained with solar radiation indicated the effectiveness of this process and its potential for practical application.

References

[1] S. Chen, X. Liang and M. Zhao, "Photocatalytic degradation of organophosphorus pesticides by TiO_2 supported on hollow glass microbeads", Photographic Science and Photochemistry, 17 pp. 85–91,1999

[2] S.Chen and Cao Gengyu , "Photocatalytic degradation of organophosphorus pesticides using floating photocatalyst $TiO_2 \cdot SiO_2$/beads by sunlight", Solar energy, 79(1), pp. 1-9, 2005.

SESSION-III

Sponsored by

Shell, India

A Stick in a Haystack: Identifying the Root Cause for Oscillations in a Process Plant

Raghunathan Rengaswamy
Department of Chemical Engineering,
Indian Insititute of Technology Madras
Chennai, India
Email: raghur@iitm.ac.in

Abstract

In this talk, we will introduce the problem of root cause diagnosis of oscillating control loops. In a single-input single-output (SISO) closed-loop chemical process system, under constant or non-oscillatory set-point, oscillations in the output can occur mainly due to one or a combination of the following reasons: aggressively tuned controllers, presence of stiction in control valves and disturbances external to the loop. The presence of these oscillations can propagate plant-wide and force plants to back off from optimal operating conditions. Therefore, it is essential to develop techniques that can diagnose the source of oscillation in control loops. In recent years, several methods have been developed to address this diagnosis problem by focusing on only one of the causes for oscillation. In this talk, a data driven approach combining both parametric (Hammerstein model based analysis) and non-parametric (Hilbert-Huang spectrum analysis) schemes for identifying the root causes of oscillation will be discussed. Unlike the existing techniques, our approach identifies and distinguishes between the three causes of oscillation in linear closed loop process systems with minimal assumptions. Simulation and industrial chemical process case studies that demonstrate the utility of the proposed method will be discussed.

Development of Porous Titania Electrodes as Catalyst Supports for PEM Fuel Cell

Manoj Krishna[†], *Christina Roth*[‡], *Raghuram Chetty*[†]
[†]*Dept of Chemical Engineering, Indian Institute of Technology Madras, Chennai 600036*
[‡]*Erneuerbare Energien, Dept of Material Sciences, Technical University Darmstadt, D-64287, Germany*
Email: manojkrishnakn@gmail.com, raghuc@iitm.ac.in, c_roth@tu-darmstadt.de

***Abstract*— An improved performance and higher electrocatalyst utilization equipped with stable titania electrodes is achieved by exploiting pore forming additives in the electrode recipe formulation in proton-exchange membrane fuel cells. Membrane electrode assembly is prepared by hot spraying procedure. Additional porosity is obtained by adding pore former to the electrocatalyst slurry which is used for the hot spraying process. This allows for a better access of gases to the depth of the electrode. An increase of 28 $\%$ current density can be obtained with such electrodes.**

I. Introduction

Numerous studies have been devoted to the development of low temperature fuel cells. However, the costs associated with high noble metal (e.g. platinum-based) catalysts limit their practical application. An efficient way to decrease the precious metal loadings and to achieve higher utilization of the catalyst is by better dispersion on a suitable inert support. The most widely used catalyst supports are highly conductive carbon materials [1]. However, carbon as catalyst support could be corroded chemically and/or electrochemically under the fuel cell operation environment, which could lead to the detachment and loss of the noble metal particles and thus decrease the electrochemical activity and durability. In the search for novel and stable supports for the noble metal catalysts, ceramic oxide supports like TiO_2 have shown excellent physical and chemical properties and high stability in acidic and alkaline solutions [2, 3]. In addition to their high stability in fuel cell environment, ceramic oxide supports act as co-catalysts. These favourable features have attracted researchers to use ceramic oxides as support materials; however few challenges need to be overcome to make this feasible. The electrical conductivity of the ceramic oxide is generally low and proper electrode modification is required to make the catalyst layer conducting. Also oxide supports often form dense layers, not allowing efficient gas and water transport. Fischer et al. [4] suggested a method for Pt/C to enhance the porosity by adding pore formers to the electrocatalyst slurry prepared for the hot spraying process. Up to 65 $\%$ porosity was achieved using different pore forming agents. This concept however was not applied for ceramic oxides till now, where structural porosity of the ceramic oxide composites is a bigger issue. In this work, titania, a typical ceramic oxide, is studied as a catalyst support material for low temperature polymer electrolyte membrane (PEM) fuel cells. The fuel cell electrode structure is modified using pore forming agents and their performances are studied.

II. Experiments

A. Catalyst Preparations

Pt on TiO_2 of different ratios was synthesized using polyol method [5]. TiO_2 (P25) obtained from Aeroxide, was first suspended in ethylene glycol solution by ultrasonication. 0.1M NaOH was added to adjust the pH of the solution to 10 and heated to 160 ^{o}C in an oil bath. Appropriate amount of K_2PtCl_6 was added to the solution and refluxed for 3 hours, then cooled to room temperature and kept overnight for settling. The catalyst was obtained by filtration of the solution.

B. MEA Preparation

MEAs were manufactured using a standard method, which is a slightly modified airbrush technique, which was first published by Wilson et al. [6]. In order to remove organic impurities and to switch the polymer electrolyte membrane to the required H^+ form before spraying, the Nafion 112 membrane (Ion Power Inc.) was boiled in 50 vol.% HNO_3 and DI water for 1 hr, rinsed in boiling DI water for 30 min, boiled in 0.5 M H_2SO_4 solution for 30 min and boiled twice in MilliQ water for 30 min, respectively. For airbrushing, an optimized amount of ink of MilliQ water, isopropanol, and Nafion 117 (Aldrich) homogenized by an ultrasonic disintegrator was sprayed onto the membrane at 120 ^{o}C using a conventional airbrush pistol. Depending on the MEA manufacturing technique, slight modifications of the ink recipe was made.

III. Results and Discussions

The polyol process was used to obtain high metal dispersion on the titania support. Figure 1 shows a transmission electron microscope (TEM) image of 20 wt.% Pt dispersed on TiO_2. The particle size of Pt obtained from image analysis was around 5 nm.

To enhance the electrical conductivity of catalyst layer, weight percentage of Pt was increased, by decreasing the TiO_2 content. Increasing the Pt concentration and keeping

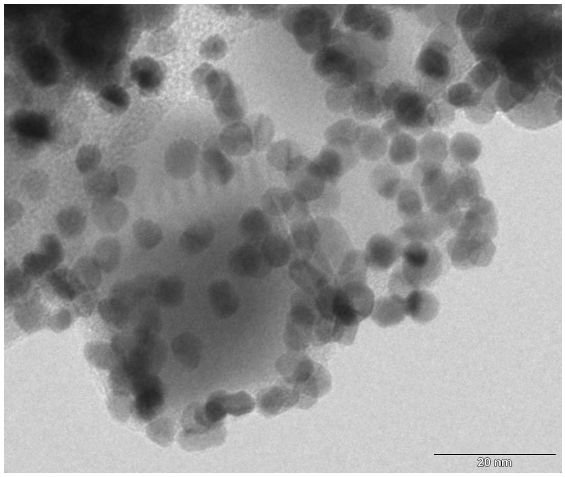

Fig. 1. TEM image of 20 wt% Pt/TiO_2

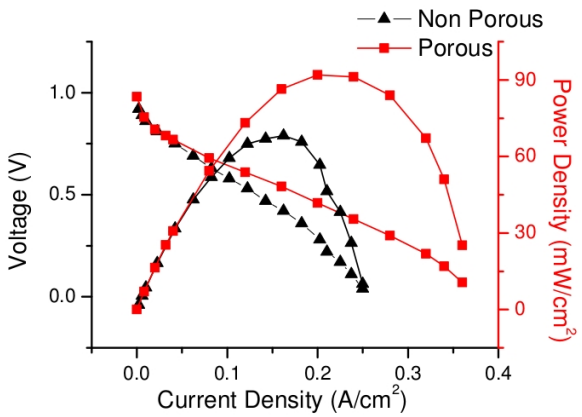

Fig. 2. Polarisation curves for porous and non porous electrodes. Operating Conditions: Temp 70 ^{o}C, Flow rates: H_2 150 ml/min and O_2 75 ml/min

the overall content constant served two purposes. Pt itself can act as high electrical conducting medium, increasing the overall conductivity of the system. Secondly it can decrease the catalyst layer thickness decreasing the mass transfer resistance. Keeping overall Pt loading constant at 1.6 mg cm^{-2} and increasing Pt content from 20 wt % to 60 wt% enhanced the overall performance and increased the current density and power density from 0.12 A cm^{-2} to 0.21 A cm^{-2} and 33.51 mW cm^{-2} to 66.1 mW cm^{-2}, for 20 wt% Pt/TiO_2 and 60 wt% Pt/TiO_2, respectively.

Apart from the electrical conductivity of the support, porosity of the electrode structure plays vital role in fuel cell performance. Porous structures enable proper gas diffusion and effective water management. Unfortunately, porosity of ceramic oxides like TiO_2 particles is low. In order to increase the porosity, $(NH_3)_2CO_3$ was used as pore forming additive. $(NH_3)_2CO_3$ was added after preparing Pt/TiO_2 catalyst slurry just before hot spraying on the membrane. $(NH_3)_2CO_3$ decomposes at around 58 ^{o}C releasing NH_3 and CO_2 creating pores. To minimize the rapid decomposition, the hot spraying temperature was performed at 80 ^{o}C. As a result of porosity enhancement, about 28 % increase in current densities was observed as shown in Figure 2. The power density increased from 66.1 mW cm^{-2} to 92 mW cm^{-2} on changing the Pt/ TiO_2 electrode from normal to porous structure.

IV. Conclusion

The introduction of additional porosity into electrodes enhances the performance of the cell. The enhanced porosity of the electrodes provides better access to the gases to the inner surface and improved catalyst utilization is achieved. Finally, with TiO_2 as an alternative support for PEM fuel cells, a maximum current density of 0.36 A cm^{-2} and power density of 92 mW cm^{-2} was obtained. The activity of the performance was mediocre compared to the Pt/C catalysts. This may be due to the following reasons:

- Standard electrode preparation procedures used nowadays are optimized for carbon-supported materials and fail for the novel materials.
- There is only limited experience in the preparation of electrodes made of new non-carbon supported materials.
- The electron conductivity in most of the oxide supports.

While ceramic oxide demonstrated their suitability from a chemical point of view, their unsuitable structural features and electrical conductivity hinders their successful application, hence, further work is needed to achieve power densities comparable with the carbon supported catalysts.

References

[1] E. Antolini, "Carbon supports for low-temperature fuel cell catalysts," Appl. Catal. B, vol. 88, no. 1-2, pp. 1–24, Apr. 2009.

[2] S.-y. Huang, P. Ganesan, S. Park, and B. N. Popov, "Development of a titanium dioxide-supported platinum catalyst with ultrahigh stability for polymer electrolyte membrane fuel cell applications." J. Am. Chem. Soc., vol. 131, no. 39, pp. 13 898–9, Oct. 2009.

[3] E. Antolini and E. Gonzalez, "Ceramic materials as supports for low-temperature fuel cell catalysts," Solid State Ionics, vol. 180, no. 9-10, pp. 746–763, May 2009.

[4] A. Fischer, J. Jindra, and H. Wendt, "Porosity and catalyst utilization of thin layer cathodes in air operated pem-fuel cells," J. Appl. Electrochem., vol. 28, pp. 277–282, 1998.

[5] H.-s. Oh, J.-g. Oh, and H. Kim, "Modi[U+FB01]cation of polyol process for synthesis of highly platinum loaded platinum carbon catalysts for fuel cells," J. Power Sources, vol. 183, pp. 600–603, 2008.

[6] M. S. Wilson and S. Gottesfeld, "Thin-[U+FB01]lm catalyst layers for polymer electrolyte fuel cell electrodes," J. Appl. Electrochem., vol. 22, no. 1, pp. 1–7, Jan. 1992.

Synthesis of Pd Nanostructures by Potentiostatic Deposition for Oxygen Reduction Reaction

Kranthi Kumar Maniam, Raghuram Chetty Department of Chemical Engineering
Indian Institute of Technology Madras
Chennai, India
Email: m.kraanthi@gmail.com, raghuc@iitm.ac.in

I. Introduction

Oxygen reduction reaction (ORR) is a multi-electron reaction which includes a number of elementary steps involving different reaction intermediates [1]. It plays a key role in metal-air batteries, corrosion and electrochemical energy converters like polymer electrolyte membrane (PEM) fuel cells. PEM fuel cells are one of the key enabling technologies for future economy thereby providing power in stationary and portable power applications. However, crucial issues such as cost, durability and operation flexibility, deter their widespread applications. The high price and the limited resources of Pt-based catalysts are among the main challenges hindering their further commercialization. Reduction of oxygen (ORR) is a key electrochemical reaction, and an improved understanding of its mechanism and the development of more efficient electrocatalysts underlie much of fuel cell research . An ambitious approach towards improving ORR catalysis is to completely remove Pt from these systems and replace it with less expensive materials. Since palladium-based catalysts in nano-particle form display increased activity and feature superior methanol tolerance, researchers have devoted to develop palladium-based catalysts as promising catalysts for oxygen reduction reaction in PEM fuel cells and direct methanol fuel cells [2]. In this work, synthesis of Pd nanostructures by electrochemical deposition on Vulcan coated graphite (VCG) substrate using constant voltage/ potentiostatic techniques is discussed, and their activities towards the ORR are compared.

II. Experimental

Graphite electrodes (4 mm) were coated with a thin layer of carbon black (Vulcan XC-72R). Carbon black dispersed in a mixture of Nafion® and iso-propanol was ultrasonically blended for 30 min, and 2.5 μL of the ink was dropped on the surface of a polished graphite electrode and air dried. The VCG substrate was subjected to an electrochemical activation process to increase the hydrophilic character of carbon black surface. The resulting carbon coated and electrochemically activated substrate was used for the deposition of Pd. All the current densities are normalized to the geometric area (0.125 cm2) of the electrode surface. Potentiostatic technique was employed in the potential range 0.2-0.5 V for the deposition of Pd from 2 mM $PdCl_2$ in 10 mM $HClO_4$($PdCl_2$, Aldrich) solution for 1800, 2700 and 3600 s respectively. The deposited Pd catalysts were physically characterized by Hitachi S4800 high resolution scanning electron microscopy interfaced with an energy dispersive X-ray analysis. The catalysts were electrochemically characterized by cyclic voltammetry (CV) and linear sweep voltammetry (LSV) using a CHI 1100A electrochemical workstation (CH Instruments, Inc.) in a three electrodes cell housed in a BASi C3 cell stand. Electrodeposited Pd substrate was used as the working electrode, Pt wire electrode, and $Ag/AgCl_{(3MNaCl)}$ were used as counter and reference electrodes, respectively. All electrochemical tests were carried out at room temperature (23 $\pm$ 1oC) in 0.5 M H_2SO_4 solution saturated and blanketed with either nitrogen or oxygen.

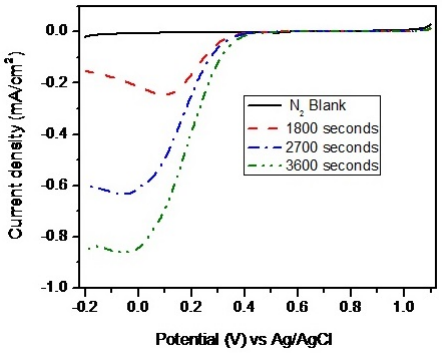

Fig. 1. Cyclic voltammograms of the Pd deposited on Vulcan coated graphite electrode at 0.2 V for 1800 s (dashed line), 2700 s (dashed dotted line) and 3600 s (dashed dot dotted line) in 0.5 M H_2SO_4 saturated with N_2 at a scan rate of 100 mV^{s-1}.Blank represents the Vulcan coated graphite electrode before the deposition of Pd. Electrodeposition bath consists of 2 mM $PdCl_2$ in 10 mM $HClO_4$.

III. Results and Discussions

Prior to electrodeposition, the substrate is submitted to an electrochemical activation process to increase the hydrophilic character of carbon black surface [3]. Pd catalysts were electrochemically deposited by potentiostatic technique on VCG substrate. From the cyclic voltammogram of $PdCl_2$ in an acidic electrolyte, suitable deposition potentials were selected for the deposition. The deposition potentials were in the range of 0.2-0.5 V. Cyclic voltammograms of the Pd catalyst deposited at 0.2 V for different time intervals : 1800, 2700 and 3600 s in 0.5 M H2SO4 saturated with N_2 are shown in Figure 1. As can be seen, typical H^+ adsorption/desorption, oxide formation/stripping peaks are well observed in all the cases, indicative of Pd surface electrochemistry.

Figure 2 represents the analogous LSVs in 0.5 M H_2SO_4 saturated with O_2. As can be seen, an increasing trend in ORR activity was observed with increasing deposition time.

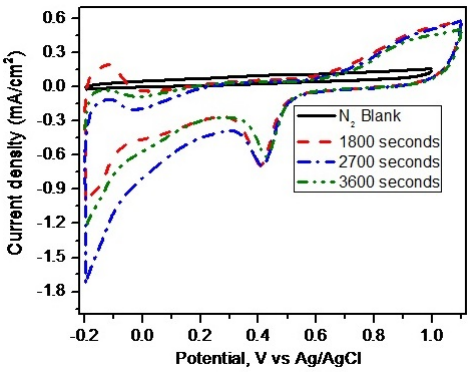

Fig. 2. Linear sweep voltammograms of the Pd deposited on Vulcan coated graphite electrode at 0.2 V for 1800 s (dashed lines), 2700 s (dashed dotted lines) and 3600 s (dashed dot dotted lines) in an oxygen saturated 0.5 M H_2SO_4 solution at a scan rate of 5 mV^{s-1}. Blank represents the activity of the Pd catalyst in N_2 atmosphere. Electrodeposition bath consists of 2 mM $PdCl_2$ in 10 mM $HClO_4$.

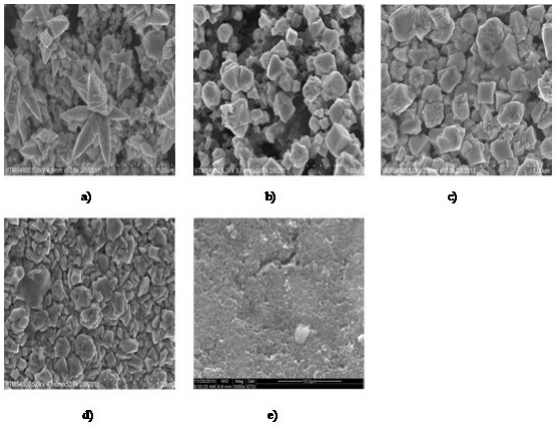

Fig. 3. Scanning electron micrographs of Pd on Vulcan coated graphite electrode deposited at different potentials for 1800 s: a) 0.2 V, b) 0.3 V, c) 0.4 V and d) 0.5 V and e) SEM image of the Vulcan coated graphite (bare electrode) before Pd deposition. Electrodeposition bath consists of 2 mM $PdCl_2$ in 10 mM $HClO_4$.

Similar trend of Pd surface electrochemistry and increase in cathodic current for the oxygen saturated solution was also observed for the Pd catalysts deposited at 0.3, 0.4 and 0.5 V respectively. Pd deposited at 0.2 V for 3600 s showed the highest ORR activity with a shift of 20 mV in terms of onset potential towards positive direction. Scanning electron micrographs (SEM) of the Pd catalyst deposited for 1800 s at different potentials are shown in Figure 3. As can be seen, Pd deposited at 0.2 V for 1800 s display a dendritic flower like morphology. On the contrary, Pd spherical agglomerates are formed when deposited at other potentials. Deposition potential has a strong influence on the morphology, structure and composition of the catalyst. Morphology strongly depends on the distance of formation condition of nuclei from thermo dynamic equilibrium. This distance of formation is large when Pd is deposited away from its deposition peak potential i.e.; at a potential of 0.2 V, and resulted in a dendritic flower like nano crystals, on the VCG substrate. With increase in time, the size and strength of the crystallites formed at 0.2 V increased, evocative of increased metal-support interaction and deposition. On the other hand, the distance of formation of nuclei for the Pd deposited at 0.3, 0.4 and 0.5 V is not so large and therefore resulted in an isolated palladium nano particles on the Vulcan coated graphite substrate. n such cases, the formation of nuclei will be faster and crystal growth becomes slower thereby changing the morphology to spherical [4].

IV. Conclusion

Pd catalysts were deposited on an electrochemically activated Vulcan coated graphite electrodes using potentiostatic technique at different time intervals and tested for oxygen reduction. Cyclic voltammograms of the deposited Pd catalysts showed the typical features of Pd surface electrochemistry thereby confirming the presence of Pd metal on VCG electrode surface. LSVs for ORR showed an increase in cathodic current with time for the oxygen saturated solution, confirming the reduction of oxygen. In accordance with the SEM images and LSVs, Pd catalyst deposited at 0.2 V displayed a dendritic flower like morphology whose size and strength increase with increasing time and resulted in an enhanced ORR activity with a shift of 20 mV in terms of onset potential. On the other hand, Pd deposited at other potentials showed a spherical morphology. The conditions for the deposition of palladium were further optimized by changing the support, precursor concentration in the acidic electrolyte.

Acknowledgement

We thank the Department of Science and Technology (DST), Government of India for the financial assistance under SERC FAST Track Scheme.

References

[1] References G. Wu, K.L. More, C.M. Johnston and P. Zelenay. “High-performance electrocatalysts for oxygen reduction derived from polyaniline, iron, and cobalt.” Science, vol. 332, pp.443-447, Apr. 2011.

[2] E. Antolini. “Palladium in fuel cell catalysis.” Energy and Environmental Science, vol. 2, pp.915-931, May. 2009.

[3] A.J. Martin, A.M. Chapparro, B. Gallardo, M.A. Folgado and L.Daza. “Characterization and single cell testing of Pt/C electrodes prepared by electrodeposition.” Journal of Power Sources, vol. 192, pp.14-20, Nov. 2008.

[4] J.Yu, T. Fujita, A. Inoue, T.Sakurai and M.Chen. “Electrochemical synthesis of palladium nanostructures with controllable morphology.” Nanotechnology, vol. 21, pp.85601-85607, Jan.2010.

Characterization of Carbon Films Prepared at Different Temperature: A Basic Study for Carbon based MEMS

Manohar Kakunuri[†], *Chandra S. Sharma*[†], *Ashutosh Sharma*[*]
[†]*Department of Chemical Engineering Department of Chemical Engineering, IIT - Hyderabad, India.*
[*]*Department of Chemical Engineering, IIT - Kanpur, India.*
cssharma@iith.ac.in

***Abstract*— This study aims towards studying the properties of photoresist derived carbon films prepared under different pyrolysis conditions. SU-8 is an epoxy based negative photoresist widely used for micromachining applications including Carbon based MEMS and Bio-MEMS. Upon pyrolysis, SU-8 yields glassy carbon which is characterized by Raman spectroscopy, EDAX, XRD and FTIR analysis. Efforts are being made to study the transformation of glassy carbon into graphitic carbon at higher pyrolysis temperatures.**

***Index Terms*—C-MEMS; SU-8; Pyrolysis, Graphite, Glassy Carbon**

I. Introduction

Fabrication of graphitic carbon for MEMS specifically for battery application is a challenge in nanofabrication. Among the secondary batteries, lithium (Li) ion batteries have significantly higher density and lighter weight. Most often, Li ion cell consists of carbon anode and lithium metal oxide such as $LiCoO_2$, $LiNiO_2$ or $LiMnO_4$ cathode. As carbon exists in many allotropic forms including graphitic, amorphous etc., there are not many references available in literature to distinguish between graphitic and non-graphitic carbon anode for Li-ion intercalation. This study aims towards studying the properties of carbon films prepared at different synthesis conditions. SU-8 is a high contrast; epoxy based negative photoresist designed for micromachining applications where chemically and thermally stable image desired.

II. Experimental

In present work SU-8 2015 is used as a polymer precursor for carbon film preparation. SU-8 2015 was spin coated on silicon wafer, used as a substrate. After coating, the resist film was soft baked to evaporate the solvent and densify the film followed by exposure to UV light and post expose baking. This SU-8 film was subsequently carbonized in inert atmosphere maintained at 0.3 lpm flow rate of nitrogen. Before we start pyrolysis, furnce chamber was purged with nitrogen at flow rate 0.9 lpm for 20 min to remove any traces of oxygen. Pyrolysis temperature was varoed from 600^0C to 1000^0C. Carbon films thus prepared were analyzed using RAMAN, XRD, SEM and FTIR characterization tools.

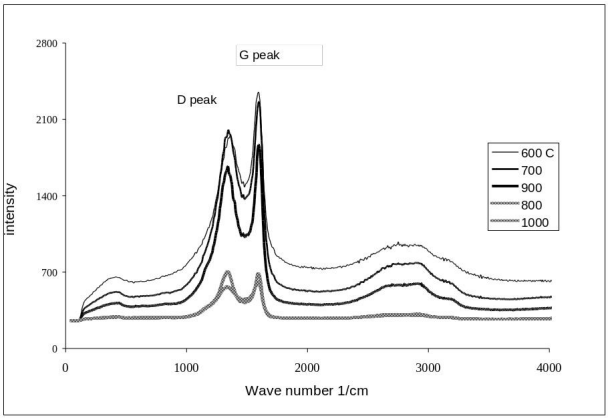

Fig. 1. RAMAN spectra for carbon films carbonized at various temperatures

TABLE I
Variation of D-peak and G-peak positions with temperature

Powers	Peak position (2 theta)			
	D-peak position	G-peak position	Intensity of peaks	
			D	G
600	1360	1590	1950	2350
700	1350	1590	2000	2260
900	1340	1590	1670	1870
800	1340	1590	563	607
1000	1340	1590	699	680

III. Results and Discussions

A. RAMAN analysis

RAMAN analysis used to study the graphitic nature of the carbon film prepared. The peak at around 1350 cm-1 is identified as D-band while the other at around 1530 cm-1 as G-band. The ratio of peak intensity of D-band over that of G-band or I_d/I_g provides signature of the atomic bonding structure of carbon film. Fig.1 shows RAMAN spectrums of carbon films carbonized at various temperatures.

B. XRD analysis

XRD spectra analysis was used to study the crystalline structure of carbon film prepared. Distance between layers at various 2-theta calculated and compared from spectra data and studied peak position variation with temperature. Fig.2 presents x-ray diffraction spectrums at various temperatures, and variation of intensity with 2-theta.

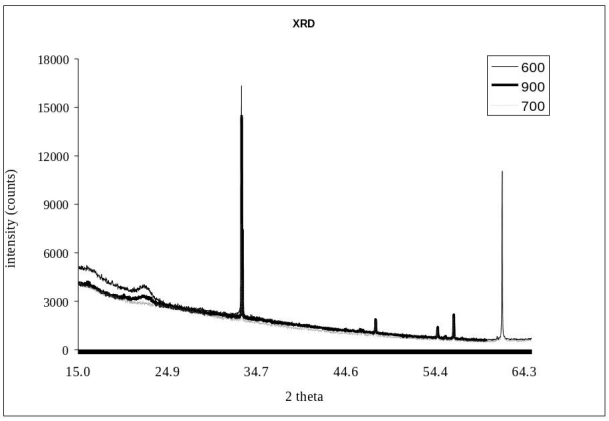

Fig. 2. XRD spectra for SU-8 films carbonized at various temperatures

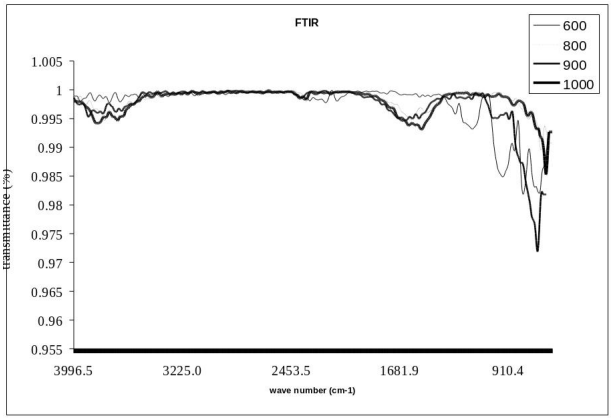

Fig. 3. Variation of transmittance with the wavenumber

C. FTIR analysis

FTIR analysis was used to find out the functional groups present in thin film carbonized at various temperatures with the help of IR chart. Fig. 3 presents the transmittance variation with wave number.

D. EDAX analysis

EDAX analysis was used for elemental analysis, and it was observed that weight percentage of carbon increased with temperature.

IV. Conclusion

We studied variation of graphitic nature, carbon composition and crystal structure with temperature. It was observed that graphitic nature, carbon composition and spacing between layer increases with temperature.

References

[1] Amit singh, Jaishankar Jayaram, Marc Madou, Sheikh Akbar. "Pyrolysis of negative photoresists to fabricate carbon structures for micro mechanical Systems and electrochemical applications" Journal of the Electrochemical Society 2002, 149, E78-E83.

[2] J.S. Park, A. Reina, R. Saito, J. Kong, G. Dresselhaus, M.S. Dresselhaus, "G'band Raman spectra of single, double and triple layer graphene" Carbon. 2009, 47, 1303-1310

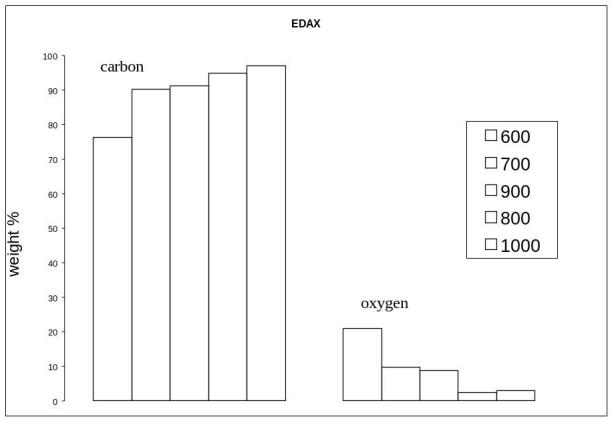

Fig. 4. Graphical representation on carbon content in films prepared at different pyrolysis temperatures

[3] Benjamin Y. Park, Lili Taherabadi, Chunlei Wang, Jim Zoval, Marc J. Madoud. "Electrical properties and shrinkage of carbonized photoresist films and the implications for carbon microelectrochamical systems and devices in conductive media" Journal of the Electrochemical Society. 2005, 152, J136-J143.

[4] Chandra S. Sharma, Rajesh Vasita, Devendra K. Upadhya, Ashutosh Sharma, Devendra S. Katti, Venkataraghavan, R. "Photoresist derived electrospun carbon nanofiber with tunable morphology and surface properties" Ind. Eng. Chem. Res. 2010, 152, 2731-2739.

[5] Endo M., Kim C., Nishimura K, Fujino T., Miyashita K."Recent development of carbon materials for Li ion batteries" Carbon. 2000, 38, 183–197.

CO_2 Reforming of CH_4 To Produce Sythesis Gas Over Modified And Unmodified Ni/Al_2O_3 Catalysts

Siddhartha Sengupta, Goutam Deo
Department of Chemical Engineering
Indian Institute of Technology Kanpur
Kanpur-208016, India
E-mail: sidsen@iitk.ac.in

***Abstract*— Conventional Ni/Al_2O_3 and Ni based modified catalysts for CO_2 reforming of CH_4 was studied and carbon deposition was observed. Appropriate proportions of Co and/or a basic oxide CaO were added to modify Ni/Al_2O_3 catalysts. The Raman spectra assisted in understanding the nature of deposited carbon on the spent catalysts. In case of the conventional Ni/Al_2O_3; the selectivity, activity and carbon deposition is a function of metal loading. At a constant total metal loading, introduction of appropriate amount of Co into Ni/Al_2O_3 system improves its activity and selectivity. Furthermore, the amount of carbon deposition also went down at a specific Ni:Co combination. Basic oxide addition to Ni/Al_2O_3 also enhanced the activity and selectivity but the amount of carbon formation also increased. Incorporation of cobalt and the basic oxide to conventional Ni/Al_2O_3 improved the activity and selectivity, however, the amount of coking also simultaneously increased with increasing the amount of basic oxide addition.**

***Index Terms*—CO_2 reforming of CH_4, Ni/Al_2O_3 catalyst, Carbon deposition, Synthesis gas**

I. Introduction

Increase in the concentration of Green House Gases (GHGs) like CO_2 and CH_4, in the atmosphere is believed to be responsible for the major changes in global climate. Consequently, there is an increased interest in improving the understanding of CH_4 and CO_2 removal, disposal, and utilization, as well as the influence of these gases in the atmosphere [1]. Catalytic CO_2 reforming of CH_4 to synthesis gas (i.e., CO + H_2), which can be used in chemical energy transmission systems or utilized in the Fischer-Tropsch reaction to produce liquids; has been proposed as one of the most promising technologies for simultaneous utilization of these two greenhouse gases. The main problems of this reaction, like requirement of a high reaction temperature and catalyst deactivation by inactive carbon deposition, necessitate the presence of a catalyst that can accelerate the reaction at an industrially feasible temperature and kinetically inhibit carbon formation [1]. Ni based catalysts and noble metal-supported catalysts were found to have promising catalytic performance for the CO_2 reforming reaction. Although the noble metal catalysts are reported to be less sensitive to coking compared to the Ni based catalysts, the high cost and limited availability of noble metals prevent the industrial application of this reaction [2],[3].Thus, it is worthwhile to develop an economical, stable and efficient Ni based catalyst for the reforming reaction of CO_2 and CH_4.

II. Experimental

Conventional Ni/Al_2O_3 and Ni based modified catalysts for CO_2 reforming was studied; problem of carbon deposition on catalytic surface was also encountered. We have tried to develop economical Ni based catalysts that can resist coking and exhibit high activity for the reforming reaction. Conventional Ni/Al_2O_3 catalysts were modified by adding appropriate proportions of cobalt (Co) and a basic oxide. Typical impregnation method was employed during the catalyst preparation. Prior to reaction, the catalysts were reduced in H_2 at 823 K. Catalysts were evaluated by conducting the reforming reaction in a fixed bed quartz reactor operating at atmospheric pressure and at a low contact time. Quartz particles were used as diluents and were well mixed to prevent channeling of gas within the catalyst bed. The temperature of the reactor was measured by a thermocouple located just above the catalyst bed and was controlled by a PID temperature controller (CYSCON, REX c-100). Separate mass flow controllers were used for controlling the flow rates of CO_2, CH_4 and N_2. Nitrogen was used as an inert and also for cooling the reactor after reduction of the catalyst before reaction studies. The exit gases were analyzed in a gas chromatograph containing a Carbosphere column, using a thermal conductivity detector (TCD). The process variables, including volumetric flow rates of the different reactant gases, amount of catalyst and reaction temperature were varied depending on the purpose of the study. Coke content of spent catalysts was measured by a CE-440 Elemental Analyzer, EAI. Jobin Yvon RMS-550 micro-Raman system was used to study the nature of deposited carbon on the spent catalysts.

III. Observations

In case of the conventional Ni/Al_2O_3 catalyst; activity and selectivity were found to be functions of metal loadings

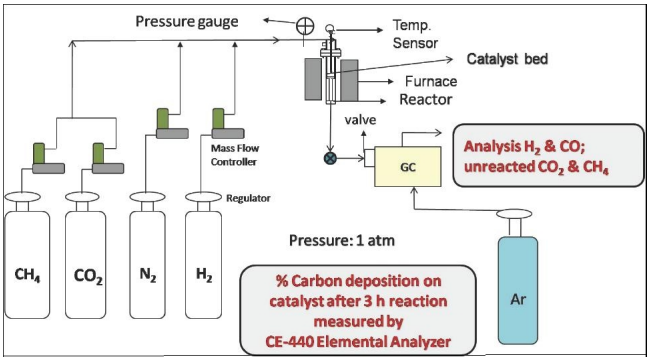

Fig. 1. Experimental Setup

and contact time. From micro-Raman analysis of the spent Ni/Al_2O_3 catalysts (after reaction) during the contact time study, it was evident that both hexagonal crystalline (G band) and disordered (D band) graphite were present. At a constant total metal loading, introduction of appropriate amount of cobalt into Ni/Al_2O_3 system improves its activity and selectivity, consequently the amount of carbon deposition also went down at a specific combination.

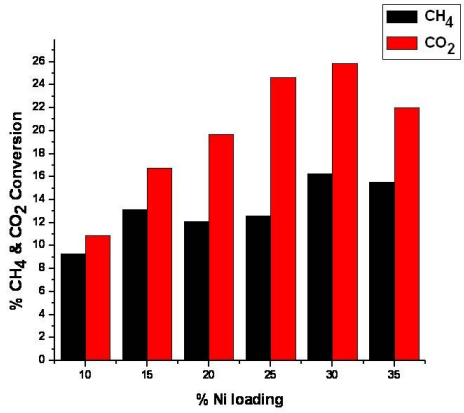

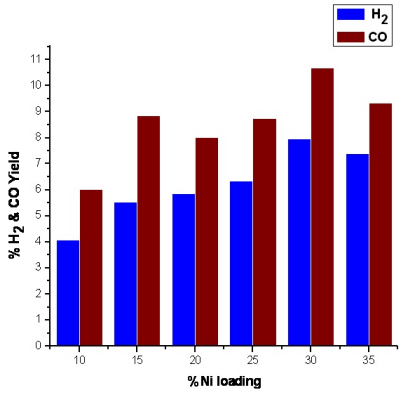

Fig. 2. Optimum performance obtained with 30-35% metal loading

Furthermore, basic oxide addition to Ni/Al_2O_3 also enhanced activity and selectivity but amount of carbon formation

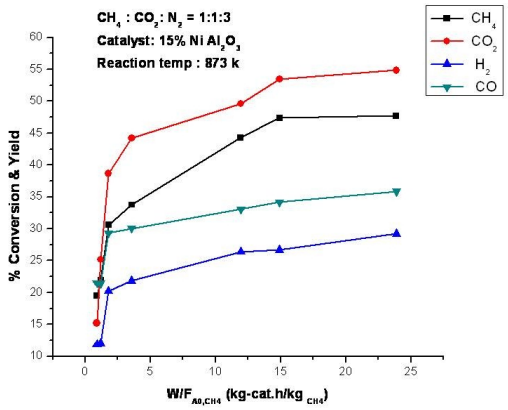

Fig. 3. Contact time study with Ni/Al_2O_3 catalyst

increased. Although incorporation of both the modifiers to conventional Ni/Al_2O_3 improved the activity and selectivity but amount of coking also increased simultaneously with increasing amount of basic oxide addition.

IV. Conclusion

Conventional Ni/Al_2O_3 catalyst modified by appropriate Cobalt addition, demonstrate better performance for CO_2 reforming of CH_4; not only in terms of high activity and selectivity but also in carbon resistance. Further work is to be done to improve catalyst performance by basic oxide addition.

References

[1] M.C.J.Bradford and M.A.Vannice, "CO_2 Refroming of CH_4", Catalysis Reviews 1999,41(1): p. 1-42.
[2] E.Verykios, X., "Catalytic dry reforming of natural gas for the production of chemicals and hydrogen", Hydrogen Energy, 2003. 23: p. 1045-1063.
[3] Wang, S. and G.Q.M. Lu, "Carbon Dioxide Reforming of Methane To Produce Synthesis Gas over Metal-Supported Catalysts: State of the Art", Energy & Fuels, 1996. 10: p. 896-904.

SESSION-IV

Sponsored by

Tata Research Development and Design Centre

Instability of a Moving Liquid Sheet in the Presence of Acoustic Forcing

Mahesh Tirumkudulu
Department of Chemical Engineering,
Indian Institute of Technology Bombay, Powai
Mumbai, India
Email: mahesh@che.iitb.ac.in

Abstract

A fundamental understanding of the break-up and subsequent drop formation is important in areas as diverse as spray coating, combustion, biomedical devices such nebulizers etc. One such route of atomization involves radial liquid sheets generated by laminar jet impingement which eventually break-up into fine droplets. We focus on sheet break-up subjected to acoustic forcing of controlled sound intensity and frequency to identify regimes of accelerated and more violent sheet break-up. Experiments show that for a given frequency, there was a threshold value of sound pressure level below which the sheet was unaffected. The droplet sizes formed by the disintegration of the sheet reduced with an increase of the measured response and the drop-shedding frequency was near the imposed frequency. Model equations accounting for the varying pressure field across the moving liquid sheet of constant thickness was solved to determine the linear stability of the system. The model calculations suggest that the parametric resonance involving the dilatational mode are responsible for the observed instability.

Power-Law Flow Over Two Square Cylinders in Tandem Arrangement

Radhe Shyam, R.P. Chhabra
Department of Chemical Engineering
Indian Institute of Technology Kanpur
Kanpur, India
rshyam@iitk.ac.in

***Abstract*—The steady flow over two square cylinders in tandem arrangement is simulated numerically using FLUENT by solving the continuity and momentum balance equations. Extensive numerical results spanning wide ranges of parameters as $1 \leq$ Re ≤ 30, $0.2 \leq$ n ≤ 1.9 and L/d=2, 5 and 8 (L is the center-to-center spacing and d is the side of cylinder) are presented. The detailed flow visualization is done with the help of streamline contours. The pressure and drag coefficients show classical inverse dependence on the Reynolds number for the whole power-law index range. The drag coefficient is always higher for the upstream cylinder than that for downstream one due to the negative pressure on the latter.**

***Index Terms*—Tandem square cylinders, power-law, Reynolds number, friction and pressure drag.**

I. Introduction

Flow across bluff bodies has been studied extensively in the past due to their wide applications in electronic component cooling, heat exchanger system design, flow dividers in process industries, design of vortex flow meters, etc. The analogous flow over multiple bluff bodies like tandem square cylinders has been studied by only a few researchers [1], especially at low Reynolds numbers in the steady flow regime. On the other hand, many workers have explored the unsteady flow regime [2],[3],[4],[5],[6]. As of now, there appears to be no prior study on the power-law flow over tandem square cylinders and is the main motivation for the present study. In particular the detailed flow field and drag behaviour of two square cylinders in tandem arrangement submerged in an infinite sea of power-law fluids are examined

II. Problem Statement and Numerical Formulation

A schematic of the flow geometry is shown in Fig. 1. An incompressible power-law fluid with an uniform velocity u=1 enters the inlet. Upstream and downstream distances are fixed as X_u and X_d respectively and L/d is varied as 2, 5 and 8. The unconfined flow domain is approximated here by an artificial box whose top and bottom walls are treated as slip boundaries so that these are tractionless. Inlet velocity and outflow boundary conditions are used at the inlet and outlet respectively. Above flow is governed by Continuity (1) and momentum balance (2) equations, which are solved simultaneously using CFD solver FLUENT.

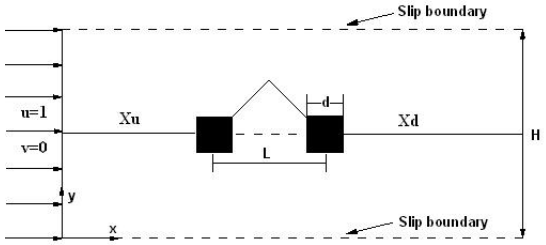

Fig. 1. Schematic of geometry for the flow over tandem square cylinders

$$\frac{\partial u_i}{\partial x_j} = 0; j = 1, 2 \tag{1}$$

$$\sum \frac{\partial (u_j u_k)}{\partial x_k} = -\frac{\partial p}{\partial x_j} + \sum \frac{\partial \tau_{kj}}{Re \partial x_k} \tag{2}$$

Where, p is pressure, u is velocity and Reynolds number is defined based on free stream velocity and the side of cylinder.

III. Results and Discussions

A domain with upstream distance, X_u=60, downstream distance, X_d=70 and domain height, H=70, obtained after a detailed domain study, is used in this study.

As shown in Fig. 2, drag coefficient decreases with the Reynolds number under all conditions spanned here. It is also deduced that drag coefficient increases as L/d is varied from 2 to 8, this is presumably so due to the varying mutual interaction between the two cylinders. The pressure drag coefficient for the upstream cylinder is nearly independent of the power-law index whereas the friction drag coefficient increases consistently and appreciably (Fig. 3). In the case of downstream cylinder, decrease in pressure drag (due to high negative pressure on the cylinder) is too significant as compared to the friction drag, hence there is a decrease in the overall drag coefficient with power-law index. Variation of streamline pattern with L/d ratio is also shown in Fig. 4. At L/d=2, inter-cylinder space is filled with a pair of common

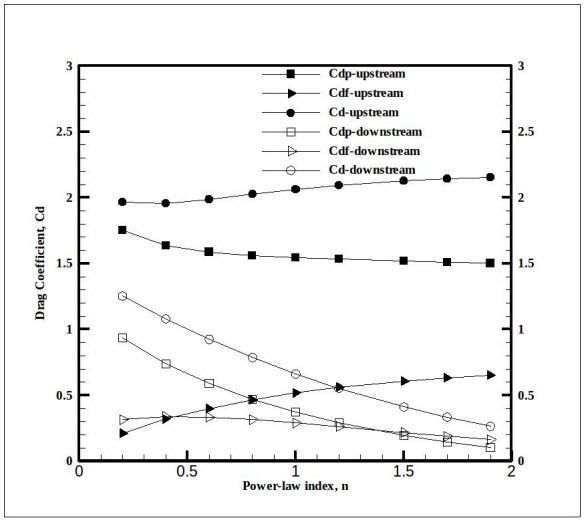

Fig. 2. C_d vs Re at different L/d ratio, n=1

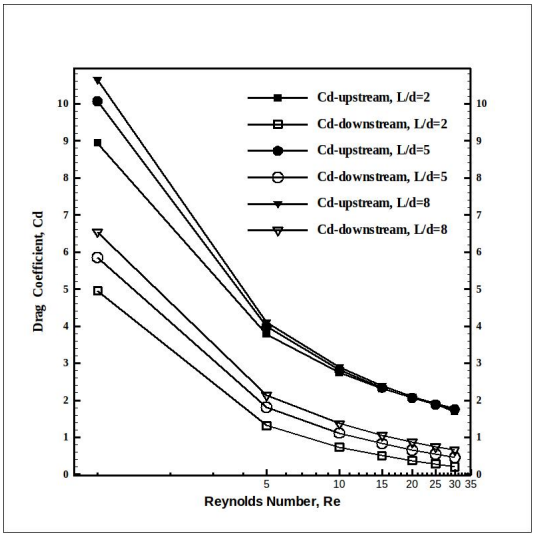

Fig. 3. C_d Vs n at Re=20 and L/d=5.

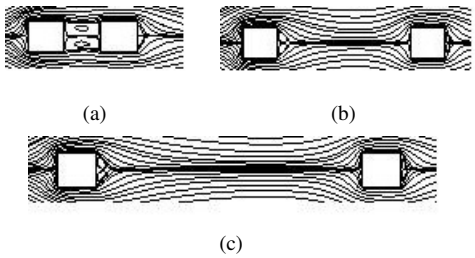

Fig. 4. Effect of L/d ratio on streamline pattern, Re=5, n=1, (a) L/d=2, (b) L/d=5, (c) L/d=8.

wakes implying highest interaction between cylinders. Wakes tend to be independent for higher L/d ratios, but interaction is not yet decayed, hence, wake length of upstream cylinder is larger for L/d=5 (L_r=0.3374) than L/d=8 (L_r=0.3033).

IV. Conclusion

In the range of parameters embraced here, the drag coefficient always decreases with Reynolds number, whereas it increases with inter-cylinder spacing due to reduction in the negative pressure. Overall drag on the upstream cylinder increases with power-law index because pressure component of drag changes very little, whereas friction component changes significantly with power-law index. On the other hand, for the downstream cylinder, pressure drag shows stronger inverse dependence on power-law index than the frictional component due to high negative pressure, thereby leading to a net decrease in overall drag.

References

[1] A.Sohankar, and A. Etminan,"Forced-convection heat transfer from tandem square cylinders in cross flow at low Reynolds numbers", Int. J. Numer. Meth. Fluids, vol. 60, pp. 733-751, September 2008.

[2] S.C. Yen, K.C. San, and T.H. Chaung, "Interaction of tandem cylinders at low Reynolds numbers", Exper. Therm. Fluid Sci., vol. 32, pp. 927-938, February 2008.

[3] C.H. Liu and J.M. Chen,"Observation of hysteresis in flow around two square cylinders in a tandem arrangement", J. Wind Eng. Ind. Aerodyn., vol. 90, pp. 1019-1050, September 2002.

[4] J.L. Rosales, A. Ortega, and J.A.C. Humphrey, "A numerical simulation of the convective heat transfer in confined channel flow past square cylinders: comparison of inline and offset tandem pairs", Int. J. Heat Mass Transfer, vol. 44, pp. 587-603, February 2001.

[5] S. Bhattacharya, and S. Dhinkaran,"Vortex shedding in shear flow past tandem square cylinders in the vicinity of a plane wall", J. Fluids Struct., vol. 24, pp. 400-417 April 2008.

[6] Lankadasu, and S. Vengadesan, "Interference effect of two equal-sized square cylinders in tandem arrangement: With planar shear flow", Int. J. Numer. Meth. Fluids, vol. 57, pp. 1005-1021, November 2007.

Photocatalytic Degradation of Reactive Red Dye Using a Titania-Carbon Mixture in Batch Slurry and Fixed Film Reactors

Abhilasha Krishnamurthy, R. Ravikrishna
Department of Chemical Engineering
Indian Institute of Technology Madras
Chennai, India
abhilasha.krishnamurthy@gmail.com

***Abstract*— This study examines the effect of carbon mixed with titania for the degradation of organic chemicals. The motivation and the overall goal for this is to explore the possibility of the photocatalytic remediation of carbon-containing solid matrices (such as activated carbon or soils/sediments/sludge) contaminated with organic chemicals. Photocatalytic degradation experiments on reactive red dye were performed using titania (Degussa P25) and titania-activated carbon mixture as catalyst in slurry and fixed film type reactors. In experiments conducted in slurry type reactor, mixture of titania and carbon show faster decolourization rates than those conducted with only titania. In the case of fixed film reactor, titania coated films show better photocatalytic rates than films obtained with a mixture of carbon and titania.**

***Index Terms*—photocatalysis; titania; activated carbon; remediation**

I. Introduction

Chemical accumulation in heterogeneous solid phases can be found in several scenarios. These include natural environmental compartments such as contaminated bed sediments in rivers, lakes and coastal areas; contaminated soil and disposal facilities for contaminated solids such as industrial sludge. In addition, there are spent adsorbents such as activated carbon, which are present at different scales (industrial to domestic). In both the systems mentioned above, the common factor is the presence of an organic pollutant adsorbed primarily on a carbon phase.

Photocatalytic degradation of organic chemicals in water and air is widely practiced at the laboratory and field scale using a photocatalyst (primarily titania) illuminated by UV radiation. There have been several studies that report the use of carbon and other supports to titania to enhance photocatalysis in mostly batch systems [1],[2] with the expectation that carbon has a higher capacity to adsorb organic molecules. There have been very few studies using a fixed film of titania and carbon [3]. The results from these studies have been mixed for a variety of target organic molecules. These studies have been designed from a perspective of treatment of liquid wastes and not from that of treatment of solid wastes. The primary objective of this study is to investigate the efficiency of photocatalysis of organic molecules adsorbed on carbonaceous surfaces. The studies described here represent the approach to this final objective. Two important factors influence the photocatalysis process – kinetics of the reaction and mass transfer of the target analyte to the reactive surface. This study describes the first part – the kinetics of photocatalysis in system with a mixture of titania and carbon.

II. Experimental

The photocatalyst used in this study is Degussa P25 TiO_2. Powdered activated carbon (AC) from Rankem® has been used in the experiments of AC-TiO_2 mixture. Reactive Red dye (commercial grade) was used as the model pollutant. The experimental set up comprises of a cylindrical glass reactor bottle with a hollow quartz cylinder (sleeve) inserted at the center of the reactor and it houses the UV source (Phillips UV-C 11W, 254 nm). In the slurry experiments, slurry of titania and the aqueous solution of the organic are introduced in the reactor in the annular space around the quartz sleeve. A stirrer at the bottom of the reactor keeps the entire contents of the reactor in suspension. In a fixed film experiment, the photocatalyst is coated on the outer surface of the quartz cylinder. The quartz cylinder is dip coated in 10 g/l slurry of TiO_2 or TiO_2-AC mixture. The drying temperature was increased in steps from 105 to 150°C during the coating cycle.

Adsorption or dark experiments were carried out for 1-2 hrs, after which the UV source was turned on for the photocatalysis experiments. Batch slurry experiment had a run time of 3-5 hrs, depending on the catalyst loading and initial concentration of the dye. The run time of the fixed film experiments varied between 10-20 hrs depending on the initial concentration of the dye solution. Samples drawn from the slurry reactor were filtered through 0.2μm Nylon 6, 6 filter membrane using an SS syringe filter before chemical analysis using a UV-Vis spectrophotometer (Shimadzu UV1800). Initial concentration of the dye solution used was in the range 10–60 mg/l in slurry experiments, and 15–80 mg/l in the fixed film experiments. All experiments were conducted at room temperature (32 °C).

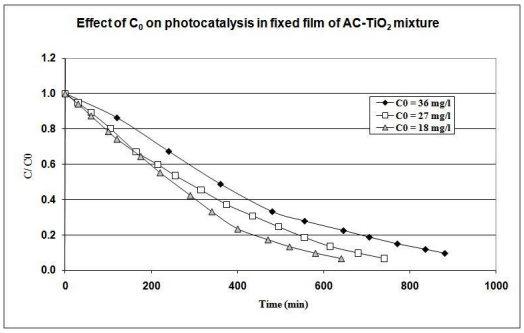

Fig. 1. Effect of initial concentration on photocatalysis in $AC - TiO_2$ fixed film

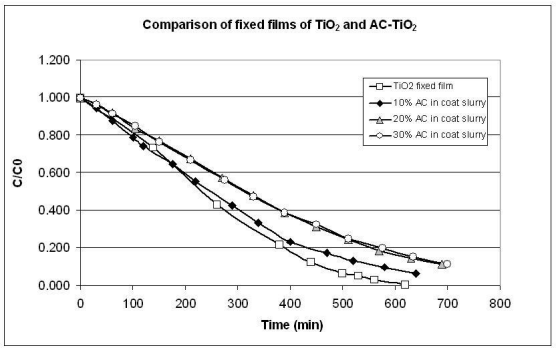

Fig. 2. Effect of carbon on photocatalysis in fixed film containing TiO_2-activated carbon mixture

III. Results and Discussions

A. Batch studies – Slurry Reactor

Slurry experiments were carried out with TiO_2 and $AC - TiO_2$ mixtures (5 & 10 % of total solids). Removal of dye due to adsorption on TiO_2 surface was not significant, but at lower concentration of dye and high titania loading some adsorption was observed. In AC-TiO_2 mixtures, even 5 % AC shows considerable reduction in concentration during the dark/ adsorption experiments. At low catalyst loading (0.05 g/l), 5 % AC-TiO_2 mixture had nearly the same adsorption capacity as TiO_2 alone but, at 10 % AC the mixture showed better removal capacity. At a given catalyst load, dye solutions with higher initial concentrations showed slower reaction rates. Adsorption of reactive red on the catalyst increases with increasing AC %, predictably.

B. Batch studies - Fixed film

As in the case of the slurry reactors, there is a decrease in the degradation rate with increasing initial concentration of reactive red on a thin film of titania. Figure 1 shows the effect of initial concentration on photocatalytic degradation on a TiO_2-AC film on quartz. The trend is very similar to that of a titania film. Figure 2 shows the effect of AC on titania. It gives a comparison of fixed film of titania and of those with TiO_2-activated carbon mixtures with 10, 20 and 30 % of total solids as AC in the coat slurry. The AC-titania composite has a lower degradation rate than the titania catalyst. The lower degradation indicates that there is some effect of availability of the target molecule to the titania surface from the AC sites.

Fixed film experiments with TiO_2 coating and those carried out by coating quartz sleeve with AC-TiO_2 coat slurry of different compositions show no observable reduction in concentration due to adsorption; since the total mass of catalyst in the film is estimated to be roughly 6-8 mg, no apparent variation in concentration may be measurable. This doesn't however preclude the effect of adsorption in photocatalytic degradation. This implies that the analyte is not coming in contact with the AC. It is important to ascertain the correlation between the AC in the slurry used for the coating and the actual percentage of AC in the coating. This correlation was attempted by measuring the coat using EDS-SEM. However the results were not conclusive and accurate. The coating must be analyzed using an alternative technique such as X-Ray fluorescence. Similar observations in slurry experiments with low catalyst loading may be cited here to show that photocatalytic degradation is faster and effective, than adsorption. In fixed film studies too the degradation of reactive red dye confirms to pseudo first order kinetics.

IV. Conclusion

Experiments with the slurry show some effect of the presence of AC in the catalyst mixture. The normalized kinetic curves show that the rate of degradation is higher showing some positive effect of carbon on the photocatalytic process. However the fixed film studies do not show any conclusive results possibly as a result of the uncertainties in the coating. Further studies to correlate the amount of carbon in the coating slurry and the actual coat must be made to conclude anything further in this direction.

References

[1] Yoneyama H., Torimoto T.,"Titanium dioxide/adsorbent hybrid photocatalysts for photo destruction of organic substances of dilute concentrations", Catalysis Today, vol. 58, pp. 133-140, May 2000.

[2] El-Sheikh A. H., Al-Degs Y. S., Newman A. P., Lynch D. E., "Oxidized activated carbon as support for titanium dioxide in UV-assisted degradation of 3-chlorophenol", Separation and Purification Technology, vol. 54, pp. 117-123, March 2007.

[3] Ao Y., Xu J., Fu D., Shen X., Yuan C., "Low temperature preparation of anatase TiO_2-activated carbon composite film", Applied Surface Science, vol. 254, pp. 4001-4006, April 2008.

Prediction of Vapour-Liquid Equilibria of polymerization system viz. LDPE using molecular simulation

Parul Sahu, Jhumpa Adhikari
Department of Chemical Engineering
Indian Institute of Technology Bombay, Mumbai, India
Email: sahu.parul14@gmail.com

***Abstract*— Molecular simulations are used to generate the vapour-liquid equilibria (VLE) data and to determine other thermo-physical properties for pure ethylene and ethylene-polyethylene binary system to improve the design of industrial LDPE reactors. High temperature and pressure operating conditions for LDPE manufacture prevent the determination of VLE by experiments and hence, Monte Carlo simulations have been conducted using the TraPPE-UA (Transferable Potential for Phase Equilibrium-United Atom) and NERD force-fields. The coexistence densities for pure ethylene are determined using Monte Carlo simulation and a reasonable agreement is observed with the results reported in literature. Solubility of ethylene in polyethylene and densities of polyethylene have been determined using Gibbs ensemble Monte Carlo simulations.**

***Index Terms*—LDPE; Monte Carlo Simulation; Vapour-liquid equilibria; solubility.**

I. Introduction

Knowledge of thermo-physical properties, such as vapour–liquid equilibria (VLE), of individual components and of mixtures is required for the design and optimization of process equipment. Low density polyethylene (LDPE) is a widely used polymer. Accurate modelling and simulation of LDPE reactors is an important problem with enormous economic impact. LDPE is commercially synthesized at pressures in the range of 2000-3000 bar and temperature near 473-573 K [1] by free radical polymerization in supercritical ethylene (CH_2=CH_2). Since only 20 % to 35 % monomers convert to polymer, unreacted ethylene must be recovered by separation unit. Process design for ethylene recovery separators requires optimum conditions of temperature and pressure. Thus, the information about the phase equilibria of the ethylene-polyethylene system is required for design of industrial reactors and separators. Luft and Linder [2] measured the solubility curve for ethylene-polyethylene mixtures at a constant temperature of 403 K through flash experiments in the pressure range of 100-2000 bar. They investigated the effect of average molecular weight as well as molecular weight distribution on the solubility of polymer. Loos et al., [3] measured cloud point curves and critical curves in fluid systems of linear polyethylene and ethylene, in an optical high-pressure autoclave with sapphire windows and magnetic stirring, in the temperature range 380-445 K and pressure range from 900 to 2000 bar for a number of polyethylene samples with known average molecular weights and known molecular weight distributions. Maloney and Prausnitz [4] predicted phase equilibrium with Prigogine-Flory theory of polymer solutions, which is valid only for a dense solution and gives unsatisfactory results below 300 bar. Liu and Prausnitz [1] applied perturbed-hard-chain theory with two binary parameters and investigated the effect of molecular weight distribution on phase diagram only for two temperatures of 403 and 533 K, at ambient to 2000 bar. Application of equation of state for modelling and simulation, of phase equilibrium and flash operations, in LDPE production process have been investigated by Orbey et al., [5]. The authors used Sanchez-Lacombe, Polymer-Soave-Redlich-Kwong and statistical associating fluid theory (SAFT) models in the temperature range 399 K to 428 K and for pressures up to 80 bar. Molecular simulations (Monte Carlo simulations with expanded Gibbs ensemble method) have been performed by Nath and de Pablo [6] to determine the solubility of small molecules (nitrogen, ethylene) at 298 K and a pressure range of 40-90 bar in polyethylene using a self-developed NERD force field.

The detailed information on the composition of the phases at equilibrium is still inadequate which leads to overdesign of reactors. Experimental studies of VLE at reactor conditions (high pressures and temperatures) are expensive and time consuming, and with safety considerations, the cost increases significantly. Molecular simulations with a suitable force-field prove to be a valuable predictive tool for such calculations.

II. Potential Energy Functions

Two different potential models are considered i.e. TraPPE-UA and NERD. In these potential models the total potential energy is divided into bonded and non-bonded parts. The non-bonded potentials are used only for the interactions of pseudo-atoms (united atoms) belonging to different molecules and described by pair wise-additive Lennard-Jones (L-J) 12-6 potentials. The intramolecular bonded potentials include: fixed bond lengths for neighboring pseudo-atoms (1-2 interactions), harmonic bond bending potentials for pseudo-atoms separated by two bonds (1-3 interactions), and dihedral potentials for

pseudo-atoms separated by three bonds (1-4 interactions). The general potential function of both force fields is a sum of all the above contributions:

$$u(total) = \sum_{molecules} u_{NB}(r_{ij}) + \sum_{stretch} \frac{k_r}{2}(r - r_{eq})^2 + \sum_{bends} \frac{k_\theta}{2}(\theta - \theta_{eq})^2 + \sum_{torsions} u_{dih}(\varphi) \quad (1)$$

TraPPE-UA is a semi-flexible model and the parameters are transferable between different species [7], [8]. The TraPPE-UA parameters for ethylene and n-alkanes were taken from [8], which list the bonded and non-bonded interaction parameters for linear alkenes and alkanes. Five different types of interaction potentials are used to describe the complete NERD force field.

III. Simulation Details

All simulations have been performed using Monte Carlo (MC) simulation VLE of pure ethylene has been predicted using both TraPPE-UA and NERD model for temperature range 140-240. For these simulations, 25000 Monte Carlo cycles were carried out as equilibration runs and 50000 cycles were carried out for production runs. The properties of the two phases have been averaged over five 'blocks' in the production run.

Since at the reactor conditions ethylene is supercritical, one box NPT simulations for the temperature range 280 K to 550 K and for pressures up to 3000 bar are performed using both TraPPE-UA and NERD model. The total number of molecules used is 200. The equilibration and production runs consist of 25000 and 50000 MC cycles, respectively. To determine solubility of ethylene in polyethylene all phase equilibria simulations are conducted using the Equilibria module in molecular simulation software Materials Studio®. 20 chains of 70 carbon units are used to represent polyethylene.

IV. Results and Discussion

A. Vapour-liquid coexistence curve for ethylene

The TraPPE-UA and NERD model parameters are verified by performing GEMC-NVT simulations to determine the coexistence liquid and vapour densities of ethylene over the temperature range 140 $\leq$ T $\leq$ 250K. Fig. 1 shows the simulation results for the saturated liquid and vapour lines obtained.

The coexistence density data from our simulations using TraPPE-UA model are found to be in an excellent agreement (less than 2.0 % deviation) with literature [8]. While the vapour phase coexistence density predicted by NERD is well matched with literature; the liquid coexistence density with NERD are underestimated by almost 7.0 %.

B. Densities of supercritical ethylene

At reactor operating conditions, one box NPT simulations for the temperature range 280 K to 550 K and for pressures up to 3000 bar are performed using both TraPPE-UA and NERD models. The results with the TraPPE-UA model are accurate (less than 3.0 % deviation) as compared to PC-SAFT [9] predicted densities for ethylene. The simulation results with NERD model are in good agreement (¡ 2.0 %) with literature data [9] up to pressure 500 bar.

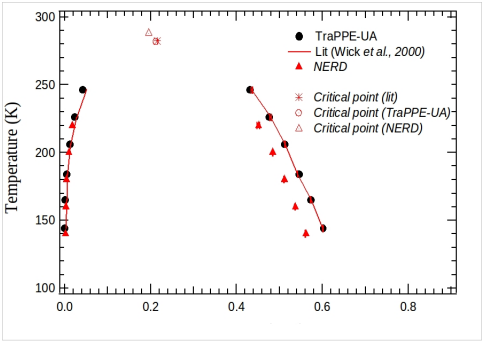

Fig. 1. VLE generated for pure ethylene using TraPPE-UA and NERD model. Comparison with simulation data from Siepmann group [8].

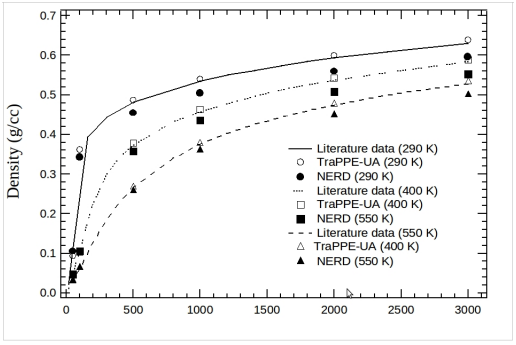

Fig. 2. Supercritical density data of ethylene using TraPPE-UA and NERD model, compared with literature data [9].

C. Polyethylene-ethylene mixture at LDPE flash separator conditions

1) VLE at high pressure separator (HPS): For HPS, solubility of ethylene in polyethylene in the pressure range 100-200 bar and the temperature range 430-500 K have been calculated. Fig. 3 shows the solubility measured in gms of ethylene per 100 gms of polyethylene.

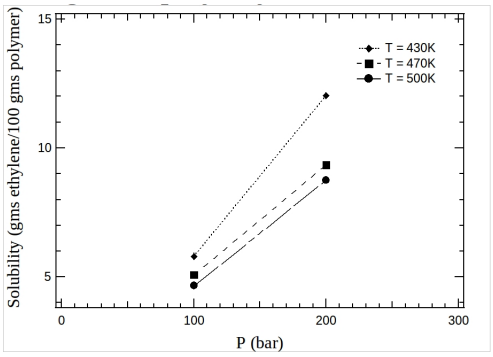

Fig. 3. Solubility of ethylene in polyethylene (C_{70}) as a function of pressure for a temperature range 430-500 K.

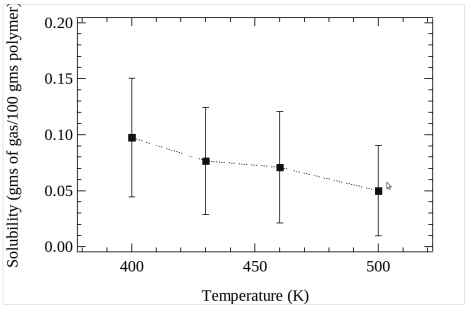

Fig. 4. Solubility of ethylene in the polymer-rich phase at low pressure separation condition.

The simulation results show that the solubility of ethylene in polyethylene increases with increasing pressure at all three temperatures. However, on increasing the temperature, the solubility of ethylene tends to decrease. The density results from simulations at HPS conditions are in range of 0.6-0.7 g/cc, which are lower than that of pure polymer densities (0.75-0.80 g/cc) reported in literature [10] at the same operating conditions. The difference in density may be explained by the fact that in the liquid phase the concentration of ethylene in polymer varies from 60 to 80 mole $\%$. Ethylene has much lower density as compare to polymer which leads to an overall decrease in the mass density of the mixture.

2) VLE at low pressure separator (LPS): After the HPS, the remaining monomer present in the polymer-rich phase, is separated in the next separation vessel, the LPS.

The operating conditions for phase separation in the LPS are a pressure of 1.5 bar and a temperature ranging from 400 K to 500 K. Using the GEMC-NVT simulation method, the compositions of the ethylene in the polymer rich phase have been obtained. The predicted values are shown in Fig. 4.

The liquid phase consists of the polymer with a low weight fraction of unreacted ethylene molecules. The change in predicted densities of polyethylene rich phase with temperature have been plotted in Fig. 5

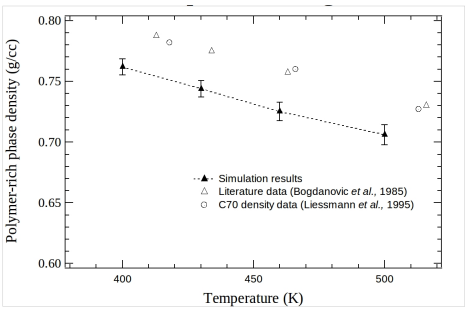

Fig. 5. Polymer rich phase density data compared with literature data.

From the above plot, the first observation is that the density of liquid polymer at atmospheric pressure [10] is comparable with C_{70} alkane (heptacontane) density data [11] as has also been assumed by Nath and de Pablo [6]. The simulation results are within (4.4 $\%$) of the literature values. The difference can be explained by the presence of ethylene in the polymer-rich phase which reduces the liquid phase density.

V. Conclusion

In this study, we have predicted the VLE data for pure ethylene to compare and validate two force-fields. After validation we have used the same simulation technique to predict the ethylene-polyethylene binary VLE data at the operating conditions. The simulation results have been found to be in excellent agreement with those in literature and also with values obtained from PC-SAFT. In this study, we have predicted the VLE data for pure ethylene to compare and validate two force-fields. After validation we have used the same simulation technique to predict the ethylene-polyethylene binary VLE data at the operating conditions. The simulation results have been found to be in excellent agreement with those in literature and also with values obtained from PC-SAFT.

Acknowledgement

The authors thank Prof. Santosh K. Gupta for valuable discussions and suggestions. Computational resources have been provided by Computer Centre at Indian Institute of Technology, Bombay.

References

[1] D. D. Liu and J. M. Prausnitz, Calculation of Phase Equilibria for Mixtures of Ethylene and Low-Density Polyethylene at High Pressures. Ind. Eng. Chem. Process Des. Dev., vol. 19, pp. 205-211, 1980.

[2] G. Luft and A. Linder, On the influence of polymer molecular weight on the phase behavior of polymer-gas systems under high pressure. Angew. Akromol. Chem., vol. 56, pp . 99-114, 1976.

[3] T. Loos, W. Poot and G. Dlepen, Fluid phase equilibriums in the system polyethylene + ethylene. 1. Systems of linear polyethylene + ethylene at high pressure. Macromolecules, vol. 16, pp.111-117, 1983.

[4] D. Maloney and J. Prausnitz, Solubilities of ethylene and other organic solutes in liquid, low-density polyethylene in the region 124 ^oC to 300 ^oC. AIChE J., vol. 22, pp. 74-82, 1976.

[5] H. Orbey, C. P. Bokis, and C. C. Chen, Equation of State Modeling of Phase Equilibrium in the Low-Density Polyethylene Process: The Sancheza Lacombe, Statistical Associating Fluid Theory, and Polymer-Soavea Redlicha Kwong Equations of State. Ind. Eng. Chem. Res., vol. 37, pp.4481-449, 1998.

[6] S. K. Nath and J. J. de Pablo, Solubility of Small Molecules and Their Mixtures in Polyethylene. J. Phys. Chem. B, vol. 103, pp. 3539-3544, 1999.

[7] M. H. Ketko, J. Rafferty, J. I. Siepmann, and J. J. Potoff, Development of the TraPPE-UA force field for ethylene oxide. Fluid Phase Equilibr, vol. 274, pp. 44-49, 2008.

[8] C. D. Wick, M. G. Martin, and J. I. Siepmann, Transferable Potentials for Phase Equilibria. 4. United-Atom Description of Linear and Branched Alkenes and Alkylbenzenes. J. Phys. Chem. B, vol. 104, pp. 8008-8016, 2000.

[9] A. Buchelli, M. L.Call, A. L.Brown, C. P.Bokis, S. Ramanathan, and J. Franjione, Nonequilibrium Behavior in Ethylene/Polyethylene Flash Separators. Ind. Eng. Chem. Res., vol. 43, pp. 1768-1778, 2004.

[10] V. Bogdanovic, A. Tasic and B. Djordjevic Industrial aspects of phase separation in ethylene-polyethylene system at pressures of 15-30 MPa. Ind. Eng. Chem. Process Des. Dev., vol. 24, 576-581, 1985.

[11] G. Liessmann, W. Schmidt, and S. Reiffarth, Data Compilation of the Saechsische Olefinwerke Boehlen, Germany.

Effect of Blend Composition and Mixing Shear on Nanoclay Modified PP/HDPE Blends by Response Surface Methodology

R. Anjana[†], *Dr. K.E. George*[†], *Anil Kumar K.R*[‡]
[†]*Dept. Of Polymer Science and Rubber Technology, Cochin University of Science and Technology, Kochi, India*
[‡]*Dept. of Electronics and Communication Engg. NSS College of Engg, Palakkad, India*
Email: anjan.rnair@gmail.com,
kegeorge@cusat.ac.in, akkr77@rediffmail.com

***Abstract*—Polypropylene (PP) and high density polyethylene (HDPE) are two widely used commodity plastics which can be upgraded by blending and nanoclay addition for enhanced mechanical properties. In this work basic mathematical models, response surface and contour graphs have been used to illustrate the effects of blending, nanoclay content, and mixing torque on the mechanical properties of PP/HDPE/nanoclay composites. Box-Behnken statistical design experiment methodology is used to optimize the parameters for the enhancement of the mechanical properties like tensile strength, flexural strength, impact strength, tensile modulus, flexural modulus and break strain. The study shows that PP/HDPE blends can be upgraded by addition of nanoclay.**

***Index Terms*—Box-Behnken design, blending, nanokaolinite clay, polymer nanocomposites.**

I. Introduction

Polymer nanocomposites (PNC) emerged as potential materials of 21st century. Blending of two or more polymers offers a good possibility to modify thermoplastic material so as to improve their properties [1],[2],[3],[4],[5]. PNC are a class of hybrid materials composed of an organic polymer matrix that is embedded with inorganic particles which have at least one dimension in the range of 1 to 100nm. On this scale they can strongly impact the macroscopic properties of the polymer even at low weight (1-6) percentages [6],[7],[8]. The effect of shear field on the morphology of nanocomposite has been reported by Homminga et. al[9]. They found the shear forces can facilitate the breakup of large-sized agglomerates. Similar results were reported by Dennis et. al [10].Response surface methodology is a modelling and optimising technique which can be used to find the effect and inter-relationship between the testing parameters on desired responses. Similar studies were carried out by a few researchers [11],[12].The purpose of the present work is to investigate the effect of blend composition and mixing shear on the mechanical properties of nanoclay modified PP/HDPE blends using response surface methodogy.

II. Experimental

A. Materials

Polypropylene-MFI-25(230 ^{o}C/2.16kg) and HDPE -MFI-20 (190 ^{o}C/2.16 kg) are supplied by Reliance polymers LTD., Mumbai. Nanokaolinite clay- Nanocaliber 100 supplied by English India Clays Ltd. India.

B. Method of preparation

60/40 and 80/20 blends and pure PP, containing 1,2 & 3 wt % nanoclay were prepared in a Themo Haake rheocord at a temperature of 150 ^{o}C using different rotor speeds of 30, 50 and 70 rpm according to the runs suggested in the design table. The mixing was done for a uniform time of 8 minutes. The resulting compound were hot pressed into sheets and cut into pieces. The material was then injection moulded using a plunger type laboratory injection moulding machine with a barrel temperature of 160 ^{o}C.

C. Measurement of mechanical properties

Tensile and flexural properties were evaluated using Schimadzu Autograph AG-I series Universal testing machine with a load cell capacity of 10KN according to ASTM D 638 and ASTM D 790 respectively. Izod impact test on un notched rectangular bar samples were carried out following ASTM D 256 test method on a pendulum type RESIL IMPACT JUNIOR (CEAST). Thermal analysis is done in TA-Q 500 series instrument in nitrogen atmosphere for a temperature range of 40 ^{o}C to 1020 ^{o}C at 20 ^{o}C/min. SEM images were taken with JSM 6390 with an accelerator voltage 20 kV on a vacuum atmosphere.

D. Experimental Design

A three level- three factor Box-Behnken design containing 27 experiments under response surface methodology was chosen as experimental method to evaluate the effect of blending, shear rate and nanoclay addition on the mechanical properties of the nanocomposite. The levels in coded and uncoded form are given in Table 1.

TABLE I
THREE LEVELS IN BOX-BEHNKEN DESIGN

Variables	Low(-1)	Medium(0)	High(1)
Wt %PP(X_1)	60	80	100
Wt % nanoclay(X_2)	1	2	3
Mix shear(rpm)(X_3)	30	50	70

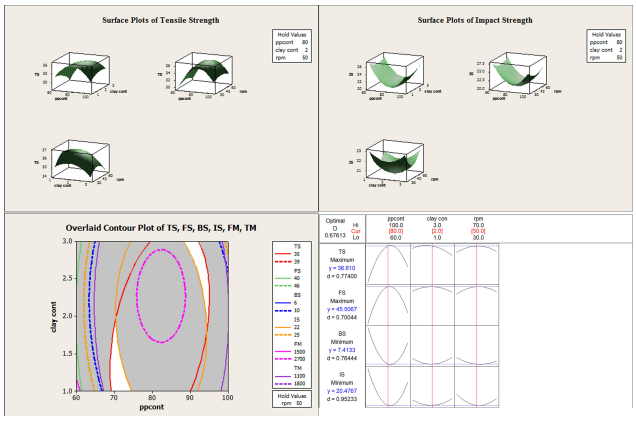

Fig. 1. Response surface plots, overlaid contour plot and optimisation plot for the mechanical properties of nanocomposite

III. RESULTS AND DISCUSSIONS

The model equation for tensile strength is given by Equation (1).Similar model equations are obtained for all the responses. The R2 value which is the degree of agreement between the experimental results with those predicted by the model are obtained in the range of 0.85-0.99 for all the responses The range achieved for R2 in this study is an indication of very good fitting of experimental data by the model equations.

$$\begin{aligned} TS &= 36.6 + 1.19X_1 - 0.5725X_2 + 0.0775X_3 \\ &\quad -4.5213X_1^2 - 0.9413X_2^2 - 0.9263X_3^2 \\ &\quad +1.3925X_1X_2 - 0.1175X_1X_3 - 0.2275X_2X_3 \end{aligned} \quad (1)$$

Response surface plots and contour plots are based on the model equations obtained in the regression analysis. Figure 1 shows the response surface plots of tensile strength and impact strength. Overlaid contour plot and response optimization plot. The response surface plots of the mechanical properties indicate that the response passes through a maximum and then decreases for tensile strength, flexural strength, tensile modulus and flexural modulus For impact strength the reverse trend is observed. The overlaid contour plot is drawn with all the responses taken into account and the central portion where the responses encircle is the best operating condition for optimum performance of nanocomposite. The response optimizer indicates that there exists an optimum processing condition for all the responses. The optimization is done using MINITAB software. From the figure it can be clearly stated that the optimum parameters for maximum mechanical properties blend composition are 80 wt% PP and 20 wt% HDPE, nanoclay loading is 2wt% clay and a mixing shear of 50 rpm.

IV. CONCLUSION

Effect of blend composition and mixing shear on the mechanical properties of nanoclay modified PP/HDPE blend were studied and optimized using design of experiments. The optimum values obtained were –Tensile strength-36.61 MPa, Tensile Modulus- 1217.33 MPa, Flexural strength- 45.5 MPa, Flexural modulus- 2758.66 MPa, Impact strength- 20.48 kJ/m^2 and break strain- 7.41% Model equations were developed for the mechanical properties like tensile strength, tensile modulus, flexural strength, flexural modulus, impact strength and break strain using response surface methodology. These model equations are capable of predicting the property value at points other than the experimental points that are in the selected range of study. About 25-35% increase in tensile and flexural properties are obtained for the nanocomposite compared to pure PP and HDPE. Although impact strength is marginally decreased, improvement in mechanical strength and thermal stability counteracts this defect. The SEM images reveal that clay layers are maximum exfoliated in composites contain 2 wt% nanoclay. Hence it can be concluded that modification of PP/HDPE blends using nanokaolinite clay is a very attractive method to upgrade the commodity plastics PP and HDPE.

ACKNOWLEDGEMENT

The authors are extremely thankful for the financial support extended by Centre for Engineering Research and Development, Govt. of Kerala under the Research Seed Money Scheme. Project No. CERD/RSM/32.

REFERENCES

[1] Jeffrey Jordan; Karl, I, Jacob; Rina Tennenbaum; Mohammed, A, Sharaf; and Iwona Jaisu; Material Science and Engineering. A 393(2005) 1-11
[2] K, Masenelli-Varlet; E, Reynaudm; G, Vigier; and Varlet; J. Polymer Science B; Polym. Phy., 40(2002) 272-2835
[3] D,H.t, Vollenberg; and D, Heikens; Polymer, 30(1989), 1656-1662
[4] Min Zhi Rong; Ming Qui Zhang; Yong Xiang Zeng; Han Min Zeng; and K, Friedrich; Polymer 42(2001), 3301-3304.
[5] Chirawithayaboon, A; and Kiatkamjornwong, S; (2004). J Appl. Polym Sci., 91(2) 742-755
[6] Kawasumi, M; Hasegawa, N; Kato, M; Usuki, A; Okada, A; Macromolecules (1997), 30: 6333.
[7] Oya, A; Kurokawa, Y; Yasuda, H; J Mater Sci. (2000); 35:104,
[8] A, Pegoretti; A, Dorigato; A, Penati; eXpress Polymer Letters Vol.1,No.3(2007),123-131
[9] Homminga D., Goderis B., Hoffman H., Reynaers H., Groeninckx G.: Polymer, 46, 9941-9957 (2005)
[10] Dennis, H.R; Hunter, D, L; Chang, D; Kim, S; White, J, L; Cho, J, W; Paul, D, R;, Polymer (2001), 42, 9513-9522
[11] Meera Balachandran; Lisha P, Stanly; Muraleekrishnan, R; Bhagawan, S, S; J Appl. Polym. Sci., 118 (2010) 3300-3310
[12] I, Ghasemi., M, Karrabi., M, Mohammadi., H, Azizi.: e XPRESS Polymer Latters Vol 4, No.2 (2010), 62-70

SESSION ON ENTREPRENEURSHIP

Microfluidic Technology as a New Frontier for Chemical Engineers: Experiences of a Start-up Company

Dhananjaya Dendukuri
CEO & Co-Founder,
Achira Labs Pvt. Ltd.
Bangalore, India
Email: d.dendukuri@achiralabs.com

Abstract

Microfluidic technologies are an exciting set of new platform technologies that can be used to enable the miniaturization of fluid flow and analysis in a number of areas such as medical diagnostics, food and environment testing and drug screening. Achira Labs is a start-up company in Bangalore focused on the development of microfluidic technologies that can serve as a platform to perform rapid, affordable and multi-analyte testing in the medical diagnostics space. I will talk about some of our experiences in this regard and the technology portfolio that Achira Labs has built. The talk will focus on two different platform technologies that we have created – one involves methods to load micron sized reagent blocks into a microfluidic device and the other is a novel fabric-based platform to perform ultra low-cost testing.

Entrepreneurial Ventures of a Research Scientist: Conceiving, Founding, Running & Letting it Fly

Vivek V. Ranade
Founder & Chairman,
Tridiagonal Solutions
Pune, India
Email: vv.ranade@tridiagonal.co.in

Abstract

In this talk I will provide personal reflections of a first generation entrepreneur on science/ technology based entrepreneurship. At the end of this talk I will also briefly touch upon eco system we have created at NCL to encourage and support such science based entrepreneurship as well as importance of 'intrapreneurship'.

POSTER SESSION

Sponsored by

Hindustan Petroleum Corporation Limited

Removal of Nitrate from Water Using a Fluidized Bed Ion Exchange Column

Ammar Arab Beddai , V.V.Basava Rao and Basma A. Badday
University College of Technology,
Osmania University
Hyderabad, India
Email: ammararab77@yahoo.com,

***Abstract*— Experimental and theoretical studies were carried out to investigate the performance of a fluidized bed ion exchange system to remove nitrate. The exchange of nitrate on strong anion exchange resin (TULSION A-27) was studied in the flow rate range of 1.59 to 3.53 L/h. Nitrate removal was done at four conditions of the flow rate. The results showed that the experimental data can be fitted to Richardson and Zaki equation, and the comparison between the experimental and calculated terminal velocities showed low relative error.**

***Index Terms*—component; nitrate; ion exchange; fluidized bed.**

I. Introduction

Increased levels of nitrate in ground water have made many wells unsuitable as sources for drinking water. Nitrate is so toxic, especially to pregnant women and infants, that the USEPA (United States Environmental Protection Agency) standard of 10 mg NO3—N/L or less in drinking water was established for human health Taekyung et al [1]; Kavita et al [2]; Lucija et al [3]. Ion exchange is a chemical treatment process used to remove unwanted ionic species from wastewater [M. Matosic et al [4]; Robert Kunin [5]; Ammar Arab [6]

Solid-liquid fluidized beds (SLFB) are used in industry for hydrometallurgical operations, catalytic cracking, chromatographic separation, ion exchange, adsorption, crystallization and sedimentation, etc Prakash and Jyeshtharaj [7]; Srikuma et al [8]. However, the packed bed ion exchange process has some disadvantages such as high pressure drop and bed clogging. These disadvantages can be eliminated if the packed bed is replaced by a fluidized bed Shyh-Jye and Wen-Jang [9]; Hideaki et al [10]; Seung-Jai et al [11]. The purpose of this study was to investigate nitrate removal in a liquid-solid fluidized bed ion-exchange system. The effects of operating parameters including liquid flow rate and height of the bed on the removal rate of nitrate were studied. The experimental data of voidage versus superficial velocity were successfully correlated using the Richardson-Zaki Equation.

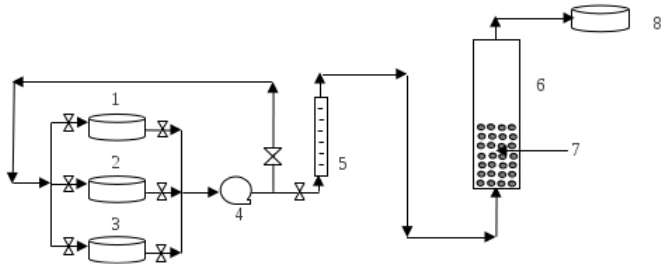

Fig. 1. Experimental system: (1) $NaNO_3$, (2) H_2O,(3) NaOH ,(4) Pump, (5) Rotameter, (6) Column, (7) Resin, and (8) Effluent.

II. Materials and Methods

A. Resin Material

The ion-exchange resin employed was the OH-1 type TULSION A-27 which was a strong base anion exchange resin. TULSION A-27 (OH-1) was obtained from the Thermax Company. The particles are in the shape of almost perfect spheres with an average diameter 0.7 mm (700 μm) and a wet density of 1.08 g/mL. The capacity of the resin was measured from the breakthrough curve of the OH-/NO-3 exchange experiments. The total exchange capacity was about 1.2 meq/ml of resin.

B. Fluidized Bed System

The overall experimental apparatus is depicted in Figure 1. The column was filled with resin and washed with distilled water. Experiments were carried out in a glass column having 1 cm diameter and 100 cm high. To obtain the hydroxide, the resins were regenerated in downflow with four bed volumes of 4% NaOH solution and washed with distilled water. The temperature was maintained at 31 ± 1^0C. As the fluidized bed showed a quiescent behavior, the height of the bed could be determined visually.

III. Chemical Analysis

Nitrates were measured by a UV-Vis spectrophotometer. The absorbance was measured at 220 nm and a second reading was taken at 275 nm. This allowed correction for the interference due to dissolved organic matter. The difference between the two absorbance measurements was then calculated by the formula , Andre [12]:

REFERENCES

[1] Taekyung Yoon, Zang HoShon, Gangchoon Lee, Byunghyun Moon, Byeongil Noh and Nakchang Sung, Korean J. Chem. Eng., 18(2), 170-177 (2001).

[2] Kavita Batheja, A.K. Sinha and Gita Seth, Asian J. Exp. Sci., Vol. 23, No. 1, 2009; 61-66.

[3] Lucija Foglar, Laszlo Sipos, Nenad Bolf, World J Microbiol Biotechnol (2007) 23:1595-1603.

[4] M. Matosic, Mijatovic, and E. Hodzic, Chem. Biochem. Eng. Q. 14 (4) 141-146 (2000).

[5] Robert Kunin, "Ion Exchange Resins", Rohm and hass company, Philadelphia, Pennsylvania, 1958.

[6] Ammar Arab Beddai, "Water treatment of Cooling Towers Blowdown from Dissolved salts ", M.Sc. Thesis, Baghdad University, 2002.

[7] Prakash V. Chavan and Jyeshtharaj B. Joshi, Ind. Eng. Chem. Res., Vol. 47, No. 21, 8458-8470, 2008.

[8] Srikuma V. Murli, Prakash V. Chavan and Jyeshtharaj B. Joshi, Ind. Eng. Chem. Res., Vol. 46, No. 6, 1836-1842, 2007.

[9] Shyh-Jye Hwang and Wen-Jang Lu, Ind. Eng. Chem. Res., Vol. 34, No. 4, 1434-1439, 2008.

[10] Hideaki Tokuyama, Susumu Nii, Fumio Kawaizumi, and Katsuroku Takahashi, Ind. Eng. Chem. Res., Vol. 41, 3447-3453, 2002.

[11] Seung-Jai Kim, Kyung-Ran Hwang,Sung-YongCho and Hee Moon, Korean J. chem.. Eng., 16(5), 664-669, (1999).

[12] Andre D. Eaton, Leonore S. Clesceri, Eugene W. Rice and Arnold E. Greenberg, "Standared Methods for the Examination of Water and Wastewater", American Public Health Association (APHA), American Water Works Association (AWWA) & Water Environment Federation (WEF), 2005.

Solar Energy with Nano-Technology

Chandra Shekhar Besta[†], *Shashidhar Besta*[‡] , *VK Naveen Kumar*[*]
[†]*Department of Chemical Engineering, University College of Technology – OU Hyderabad*
[‡]*Department of Electronics and Communication Engineering, DVR College of Engineering, JNTU – Hyderabad*
Andhra Pradesh, INDIA
Email: krushiratna@gmail.com, shashi.2346@gmail.com, naveen04730@gmail.com

***Abstract*— The world is facing the threat of depleting fossil fuel (petroleum) resources. This could case a major setback to the world. Researches show that the fossil fuels will get depleted completely in about 15-20 years. The world needs an alternative source of fuels that could keep the world running on its wheels. Alternatives in the form of solar energy, wind energy, bio-fuels, hydrogen fuels etc have been found, but they need more study and experimentation before they could be launched commercially.**

The energy that reaches earth from sunlight in one hour is more than that used by all human activities in one year. The dream of generating electricity from sunlight in large scale at low cost may not be that far from reality in this century. Rapidly emerging solar energy technology using low cost dye sensitized photovoltaic cells on plastics would be a real boost for the third world countries.

This paper discusses the convert sunlight into electricity by using nanotechnology. Though the conventional silicon solar cells are efficient in converting solar energy into electricity until now, the non conventional solar cells based on molecular photosensitization by colored materials in wide band gap semiconductors is a fast growing field of basic scientific and industrial research. Present state-of-the-art cells using molecular dyes shows energy conversion efficiencies of 10-11 %.

Generating electricity from sunlight by highly efficient sensitization of titanium dioxide (TiO_2) is new revolutionary technology, that using nanotechnology to develop a better solar cell is to convert as much sunlight to electricity as possible. TiO_2 is the best suited semiconductor for chemisorbing the dyes for efficient light harvesting and energy conversion. This approach of generating electricity from sunlight has many advantages over silicon solar cell technology. This paper consists of process that formation of nanocrystalline TiO_2 based solar cell.

Growth Mechanism of Eu doped LaF_3 Nanoparticle

Debadrita Bhattacharya[†], *Sri Sivakumar*[†], *Venkataramanan Mahalingam*[‡]
[†]*Chemical Engineering, IIT Kanpur, India*
[‡]*Chemistry, IISER Kolkata, India*
debadrbh@iitk.ac.in, srisiva@iitk.ac.in, mvenkataramanan@yahoo.com

***Abstract*— Our aim is to investigate the growth mechanism of Eu doped LaF_3 nanoparticles. It is synthesized in aqueous solution, stabilised with citrate ligand. Eu is doped as the probe in LaF_3 nanoparticles which enables us to use fluoremetric analysis for estimating the change in size of the nanoparticles. The samples were characterized by XRD, DLS and fluorescence study. The results indicate that initially particle size increases with growth time. However with further increase in growth time the particle size decreases.**

***Index Terms*—Growth mechanism; LaF_3 nanoparticles; Eu doping**

I. Introduction

Lanthanide doped nanoparticles have several applications such as biolabels, lasers, optical-display and optical amplifiers due to their high photo stability and relatively sharp, non overlapping emission and excitation peaks. LaF_3 nanoparticles are of great importance due to their low phonon energy and minimum quenching of emissive Ln^{3+} ions. Water soluble LaF_3 nanoparticles are synthesised by Sudarshan et.al [2]. Further results by Anatoly Safronikhin et al. [1] indicate that citrate ions bond chemically with EuF_3 particle. Therefore a layer is formed onto the surface which stabilizes nanoparticle colloids and imparts high solubility in polar solvent like water. Our nanoparticles are also highly dispersible in water. D.D.Sharma et al. [3] has observed ZnO growth mechanism that is intermediate between the two limits of diffusion control and kinetic control. We have also tried to resolve the mechanism of LaF_3 nanoparticles but it is still not decided completely. To know the exact mechanism is of great importance so that it can facilitate the control of the size and can lead to a wide range of applications where a specific particle size is needed. Eu is doped as the probe in LaF_3 nanoparticles so that average lifetime value obtained from fluorescence study can be correlated to different LaF_3 nanoparticle size.

II. Experiments

A set of LaF_3:Eu nanoparticle samples was made with varying growth time.

A. Preparation of stock solution

Around ∼6 gm of Citric acid is dissolved in 70 ml of water taken in a beaker. The pH of the solution was adjusted to 6 by adding NH_4OH (stock solution-1). Stoichiometric amount of the nitrate salts of lanthanide ions $La(NO_3)_3.6H_2O$ and $Eu(NO_3)_3.5H_2O$ (95:5) (1.33 mmol total) were dissolved in 6 ml methanol (stock solution-2). They were taken in the amount of 1.092 gm and 0.0624 gm respectively. 0.532 gm of NaF is dissolved in 6 ml of water (stock solution-3).

B. Synthesis of LaF_3 nanoparticles

10.4 ml of stock solution-1 and 0.88ml stock solution-2 were added in a beaker followed by addition of stock solution-3 at room temperature. The nanoparticles were allowed to growth. Time of growth was varied from sample to sample. Quantitative amount of ethanol (10ml) was added to precipitate the nanoparticles. These particles were collected by centrifugation, washed with ethanol(10ml) thrice and later dispersed in water in ultrasonicator for ∼20 minutes.

III. Results and Discussion

XRD of LaF_3 : Eu (95:5) nanoparticles with different growth time is compared in Figure 1. Sharp peak in XRD is observed for the sample with growth time 1 minute. With increase in time upto 2 minutes the crystallite size seems to increases. However, with further increase in growth time it appears that the size decreases and remains almost same for the rest of the samples. Further investigation is needed to draw any definite conclusion. Average lifetime value at 591 nm from the decay analysis is shown in the Figure 2. It also shows that upto 2 minutes of growth time the average lifetime increases followed by sudden decrease. From 3 minute onwards average lifetime remains almost same with change in growth time. Emission spectra of LaF_3:Eu (95:5) nanoparticles is shown in Figure 3 and area ratio of peaks at 591 nm and 612 nm wavelength obtained from this spectra is shown in Table I. It further shows that asymmetry increases with decrease in crystallite size. Average diameter obtained form DLS data is compared in Table II. It also proves the same concept that particle size is larger at the beginning and afterwards it decreases. After a certain time, the partciles size remains almost unchanged. So, there is a possibility that at first nucleation of particles and simultaneous growth leads to bigger sized particles. Then formation of smaller particles takes place.

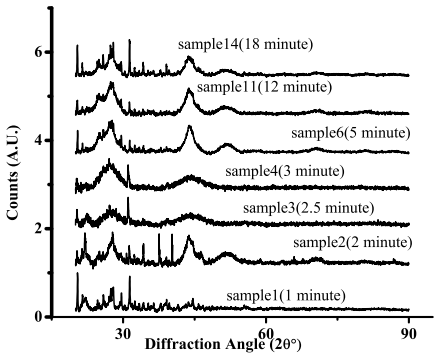

Fig. 1. XRD pattern of LaF_3 nanoparticles with different growth time

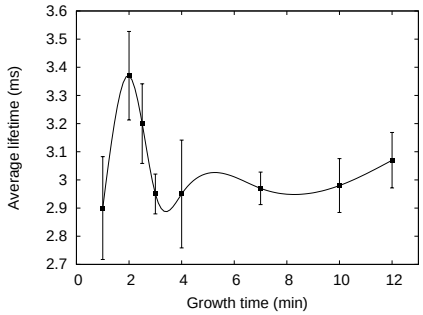

Fig. 2. Average lifetime at 591 nm emission

IV. Conclusion

We have investigated the growth mechanism of LaF_3 nanoparticles. Though it requires more study still we can conclude that the bigger LaF_3 nanoparticles are forming in the beginning and later smaller particles are formed.

Acknowledgement

The authors are thankful to IIT Kanpur for funding the project.

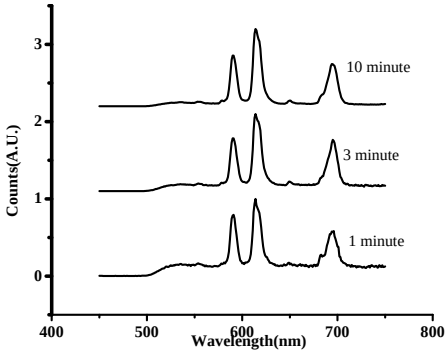

Fig. 3. Emission spectra of LaF_3 nanoparticles with different growth time

TABLE I
Area ratio of characteristic peaks at 591 nm and 612 nm in emission spectra at different growth time

Growth Time (min)	Area Ratio
1	1.49
3	1.69
10	1.80

TABLE II
Average Diameter obtained from DLS data at different growth time

Growth Time (min)	Average Diameter (nm)
1	25.3
2	9.8
2.5	9.3
3	1.2
7	3.4
10	1.2
12	4.1

References

[1] Anatoly Safronikhin, Tatyana Shcherba, Heinrich Ehrlich, and Georgy Lisichkin. Applied Surface Science, 255(18):7990 – 7994, 2009.

[2] V. Sudarsan, Sri Sivakumar, Frank C. J. M. van Veggel, and Mati Raudsepp. Chem. Mater., 17(18):4736–4742, 2005.

[3] Ranjani Viswanatha, Pralay K. Santra, Chandan Dasgupta, and D. D. Sarma. Phys. Rev. Lett., 98(25):255501, Jun 2007.

Modeling and Comparative Analysis of Flat Turbine Impeller with Perpendicular and Angel Holed Impeller

Deepak Ojha
Department of Chemical Engineering
Birla Institute of Technology & Science, Pilani
Goa Campus, Zuari nagar
Goa (India)
Email: deepakojha@bits-goa.ac.in

I. Introduction

The way a liquid moves in an agitated vessel depends on many things 1) The type of impeller, 2) The characteristics of the liquid specially its viscosity and 3) The size and proportion of the tank, baffles and impellor. The liquid velocity at any point in the tank has three different components and the overall flow pattern in the tank depends on the variation in these three velocity components from point to point. The first velocity component is radial and acts in the direction perpendicular to the shaft of the impellor. The second component is longitudinal and acts in a direction parallel with the shaft. The third component is tangential or rotational and acts in a direction tangent to a circular path around the shaft. In the usual case of vertical shaft, the radial and tangential components are in horizontal plane and the longitudinal component is vertical. The radial and longitudinal components are useful and provide the flow necessary for the mixing action. When the shaft is vertical and centrally located in the tank the tangential component is generally disadvantageous. The tangential flow follows a circular path around the shaft and creates a vortex in the liquid. Flat blade turbine gives good radial flow in the plane of the impellor with the flow dividing at the wall, to form two circular patterns. One portion flows downward along the wall and back to the center of the impeller from below and the other flows upward toward the surface and back to the impeller from above. In an unbaffled tank there are strong tangential flows and vortex formation at moderate stirrer speed. With baffles present the vertical flows are increased and there is more rapid mixing of the liquid. In a vertical cylindrical tank, the depth of the liquid should be equal to or somewhat greater then the diameter of the tank. If greater depth is desired two or more impellers are mounted on the same shaft. The lowest impellor is commonly a radial flow unit such as a straight blade turbine, the upper ones are usually axial flow impellers. The lowest impeller is mounted about one impellor diameter above the bottom of the tank. The study is using Navier-Stoke and Moving Mesh module of Comsole Multiphysics 3.4 to model the three type of 4 turbine impellor.

The modeling and analysis has done for three different type of impellors 1) Flat turbine, 2) Flat turbine with the circular holed drilled on the impellor surface perpendicular to the surface and 3) Flat plate turbine with the circular holed drilled at some with the surface. The modeling has also included baffled and un-baffled tank and the generated result shows the velocity and Reynolds number distribution across the tank.

References

[1] R.M. Hockey and J.M. Nouri 'Turbulent flow in a baffled vessel stirred by a 60 degree pitched blade impeller' , Mechanical engineering department, Imperial college of science technology and medicine, Thermo fluids section, Exhibition road, London, UK.

[2] Z.D. Chen and J.J.J. Chen, 'Comparison of mass transfer performance for various single and twin impellers', Department of Chemicals and Materials Engineering, The university of Auckland , Auckland, New Zealand.

[3] Andrej Bombac and Iztok Zun 'Individual impeller flooding in aerated vessel stirred by multiple- Rushton impellers', Laboratory for fluid dynamics and Thermo dyanamics, Faculty of Mechanical Engineering, University of Ljubljana, Slovenia.

[4] B.N. murthy, N.A. Deshmukh 'Hollow self-inducing impellers: Flow visualization and CFD simulation', Department of chemical engineering, Institute of chemical technology, University of Mumbai, India.

An Off-Lattice, Self-Learning Kinetic Monte - Carlo Method Using Local Environments

Dhrubajit Konwar, Dr. Abhijit Chatterjee
Department of Chemical Engineering
Indian Institute of Technology Kanpur
Kanpur, India
achatter@iitk.ac.in

***Abstract*— We present a method called local environment kinetic Monte Carlo (LE-KMC) for efficiently performing off-lattice, self-learning kinetic Monte Carlo (KMC) simulations of activated processes in material systems. Like other off-lattice KMC schemes, new atomic processes can be found on-the-fly in LE-KMC. However, a unique feature of LE-KMC is that as long as the assumption that all processes and rates depend only on the local environment is satisfied, LE-KMC provides a general algorithm for i) unambiguously describing a process in terms of its local atomic environments, ii) storing new processes and environments in a catalog for later use with standard KMC, and iii) updating the system based on the local information once a process has been selected for a KMC move. Search, classification, storage and retrieval steps needed while employing local environments and processes in the LE-KMC method are discussed. The advantages and computational cost of LE-KMC are discussed.**

***Index Terms*—multiscale simulation, rare event dynamics, kinetic Monte Carlo, non-equilibrium phenomenon, materials modelling.**

I. Introduction

The recent development of MD-based accelerated dynamics methods[1-5] has helped in extending the MD time scales to microseconds and longer with that of accuracy to MD but these methods still are computationally expensive to large class of important problems such as diffusion, nucleation and growth, crystallization, defect evolution and chemical reactions. Consequently the kinetic Monte Carlo(KMC) method [6-9] is attractive when milliseconds to hours time scales need to be reached. Despite the higher computational efficiency of standard KMC over MD, KMC has many shortcomings and approximation limitations. To overcome those limitations, many off-lattice and self-learning KMC algorithms [10-15] have been recently developed. We present here a new off-lattice, self-learning KMC algorithm; the underlying principle being the process mechanisms and their rates are dependent on the atomic environments, i.e., arrangements of atoms in a local region of the system.

II. Algorithm

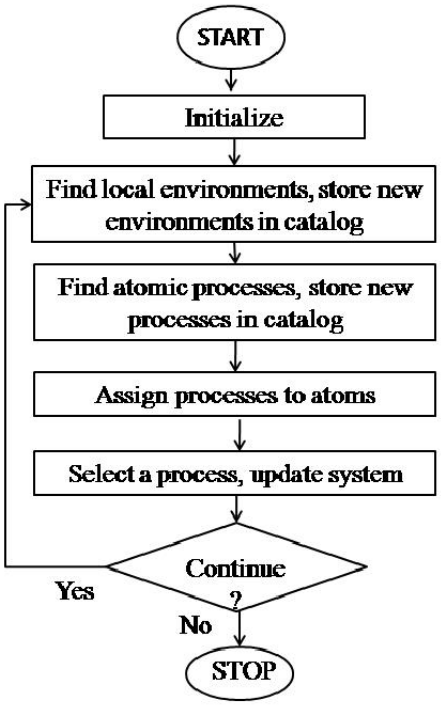

Fig. 1. Flowchart for the LE-KMC algorithm in learning mode.

Fig. 1 shows the flowchart of LE-KMC method. During the initialization step, the starting atomic coordinates, process catalog from previous calculations, and the inter-atomic potential information is read. The next step entails the finding the environments of all atoms in the current state, classifying these environments and storing the unique ones in an environment catalog. Typically, the system is partitioned into domains and atoms in the each domain are searched in parallel using multiple processors for processes.

Rate 'r' of the processes is computed out assuming that the Arrhenius rate expression[11]

$$r = \nu e^{\frac{E_a}{k_B T}} \quad (1)$$

is valid. Here ν is the prefactor, which is set to 10^{13} s^{-1} in this work, E_a is the activation barrier from the process, which is obtained using climbing-image nudged elastic band(CI-NEB) method[16], k_B is the Boltzmann constant and T is the system temperature. Once the process search is complete and process catalog is updated, processes from the catalog are assigned to the atoms in the system. Eventually, a process is randomly selected from a list of processes that are possible and the system is updated.

A. Building Environment Catalog

The local environment for atom *i* is obtained by considering the atoms inside an environment cut-off radius , r_{env}. Positions $r_{ij} = r_j - r_i$ of atom *j* relative to *i* for all atoms *j* within local environment cut-off radius r_{env} is stored. The choice of r_{env}, as a minimum requirement should be greater than the average spacing between two neighboring atoms. Although the inter-atomic potential cut-off distance can also be a possible choice for r_{env}, to account for the off-lattice atomic position, a variable δr_{tol} is introduced. The atoms inside r_{env} are distributed among number of shells with atom *i* as the center. Environments are compared by performing the following sequence of comparisons: chemical species type, total number of atoms of each chemical species in r_{env}, and the number of each chemical species in each shell A modified hash search process is performed to remove false-negatives by adding a buffer layer of thickness Δr_{tol} to r_{env} and considering the atoms residing inside radius, $r_{env} + \Delta r_{tol}$ to be part of environment atoms. Atoms residing inside the buffer layer are called buffer atoms. Comparison of the number of atoms of a chemical species in each shell is started from the inner-most shell. Atoms are borrowed from the adjoining outer shell to obtain the required match for the number of atoms in the current shell. If a match is found the comparison of shells continue. The number of atoms in the adjoining shell is lowered appropriately when atoms have been borrowed from it. After the comparison is over, the distribution of atoms in each shell is reset to the value prior to the comparison. The modified hash search algorithm provides an effective procedure for filtering most environments from the catalog while remaining computationally less expensive than the brute-force comparison.

B. Building Process Catalog And Assigning Processes to Atoms

A process is said to occur when an atom is displaced from its initial position. The displaced atoms form part of the process atoms. An NEB-based analysis is performed to guide the identification of process atoms. We introduce a minimum movement variable, Δx_{NEB} which takes into account the energy relaxation, ΔE_{NEB} performed during NEB relaxation. Atoms that move more than Δx_{NEB} are tagged as process atoms. Processes are compared in the following steps. First the environment type of the processes are compared. Next, it is checked whether the difference in activation energy for the processes is less than ΔE_{NEB} (chosen to be 0.01 eV in our calculations) when the atom is not allowed to move during NEB. Finally it is checked whether the relative initial, transition and final position of the process atoms in the processes lie within distance Δr_{tol}. If match is found in all the three steps, then the processes are said to be identical. Processes found are stored in the process catalog. The relevant local environment information about the process atoms are stored in process index catalog. The next step entails assigning process to atoms which is akin to pattern recognition problem. A process is assigned to an atom *i* by first comparing the environment type of the process and the atom *i*. When the environment types match, it is checked whether all other process atoms needed by the process are present around atom *i* given the relative initial positions are within a tolerance Δr_{tol}. Processes from the catalog that are assigned to one or more atoms are termed active, otherwise they are inactive. One active process is then chosen for a move using the n-fold algorithm [6]. A change in the list of active processes and local environments of atoms near the selected process atom is executed eventually. New processes are searched and atoms are assigned new processes from the catalog in the affected region before the next KMC process selection step is performed. The algorithm continues till the end of KMC iteration.

III. Conclusion

LE-KMC algorithm described above is computationally more efficient than standard off-lattice KMC algorithm as only the local information is stored which make the method size independent. Moreover the catalogs generated can be retrieved and reused with the KMC for further calculations involving the same material system. As a demonstration of the method, we have studied the evolution of sub-monolayer Ag on Ag(001) for hop and exchange mechanisms, and the environment dependence of processes are reliably captured with LE-KMC. It is also observed that although the number of environments and processes stored can be large, the memory requirements comparatively are smaller than the memory typically available in present-day personal computers.

References

[1] A. F. Voter, Phys. Rev. Lett., 78, 3908 (1997)
[2] A. F. Voter, Phys. Rev. B, 57, 13985 (1998)
[3] M. R. Sorensen and A. F. Voter, J. Chem. Phys. 112, 9599 (2000)
[4] R. A Miron and K. A. Fichthorn, J. Chem. Phys. 119, 6210 (2003)
[5] A. F. Voter, F. Montalenti and T. C. Germann, Ann. Rev. Mat. Res. 32, 321-346 (2002)
[6] A. Bortz, M. Kalos, and J. Lebowitz, J. Comp. Phys. 17, 10 (1975).
[7] D. Gillespie, J. Comp. Phys. 22, 403 (1976).
[8] A. F. Voter, in Radiation Effects in Solids, pages 1-23, Springer Netherlands, 2007.
[9] A. Chatterjee and D. G. Vlachos, J. Comput. Aided Mater. Des. 14 (2007).
[10] G. Henkelman and H. Jonsson, J. Chem. Phys. 115, 9657 (2001).
[11] O. Trushin, A. Karim, A. Kara and T. S. Rahman, Phys. Rev. B, 72, 115401 (2005).
[12] F. El-Mellouhi, N. Mosseau and L. J. Lewis, Phys. Rev. B 78, 153202 (2008).
[13] K. Reuter and M. Scheffler, Phys. Rev. B 73, 045433 (2006).
[14] K. Honkala, et al., Science 307, 555 (2005)
[15] L. Xu and G. Henkelman, J. Chem. Phys. 129, 114104 (2008).
[16] G. Henkelman, B. P. Uberuaga and H. Jonsson, J. Chem. Phys. 113, 9901 (2000).

Review on Sonochemical Methods for Treatment of Organic Pollutants in Wastewater

Nikhil Gharat and Dinesh Thakare
Institute of Chemical Technology, ICT (formerly UDCT)
Mumbai, India
Email: gharatnikhil@gmail.com, dinesh10thakare593@gmail.com

***Abstract*— Wastewater treatment has become the need of the hour because of rapid industrial growth. The use of conventional wastewater treatment processes has become increasingly challenged with the identification of more and more organic and non-biodegradable contaminants, rapid growth of population and industrial activities, and diminishing availability of water resources. Recently, 'Advanced Oxidation Processes' (AOP's) are gaining huge importance as they help in complete removal of organic waste. Ultrasonication is an emerging and very effective method to enhance the biodegradability of the organic compounds by disrupting their physical, chemical and biological properties. Heterogeneous sonocatalytic degradation process involving different types of catalyst particularly titanium dioxide (TiO_2) appears to be the most promising technology. Some researchers focus on the enhancement of the degradation efficiency by use of chemical additives e.g. hydrogen peroxide, Fenton reagent, various types of salts and ozone. This paper critically reviews up-to-date technologies to be applied in conjunction with sonochemical degradation process for enhancing degradation of recalcitrant organic compounds.**

***Index Terms*—Recalcitrant organic, Sonocatalytic, Hydrogen peroxide, Fenton's reagent, Oxidation.**

Fenton Process for the Degradation of Neonicotinoid Insecticide

Fasnabi P.A, Dr. G.Madhu
Chemical Engineering Group, School of Engineering
Cochin University of science and Technology
Kochi, India
fasnasalah@gmail.com

***Abstract*— The use of Fenton reagent for the degradation of Acetamiprid- a neonicotinoid insecticide has been investigated. The effect of operating variables such as pH, concentration of H_2O_2 and Fe^{2+} has been studied.. Optimum conditions for the maximum % COD removal is observed as pH-3, COD/ H_2O_2-0.2 and Fe^{2+}/ H_2O_2-2 .**

***Index Terms*—Fenton process, Acetamiprid.**

I. Introduction

Water quality regulations are becoming more stringent all over the world due to an increasing social concern for environment. A wide range of organic compounds are detected in industrial and municipal wastewater. Some of these compounds pose severe problems in biological treatment systems due to their resistance to biodegradation and/or toxic effects on microbial processes. A chemical wastewater treatment using advanced oxidation process (AOPs) can produce the complete mineralization of pollutants to carbon dioxide, water or at least their transformation into more innocuous products. Furthermore, the partial decomposition can lead to biodegradable intermediates.

Among the AOPs, the Fenton's process is quite well known and has been successfully applied for the treatment various recalcitrant compounds [1]-[5]. In the Fenton process, the organic substances are reacted with hydrogen peroxide in the presence of ferrous sulphate. It has been extensively used for the removal of COD, TOC, dyes, pigments, phenolic compounds etc. Fenton's reagent is a mixture of ferrous iron, a catalyst and Hydrogen peroxide, oxidizing agent .The mechanism of Fenton process is given below [1]-[3].

$Fe^{2+} + H_2O_2 \longrightarrow Fe^{3+} + OH^- + HO$ (1)

$Fe^{2+} + HO. \longrightarrow Fe^{3+} + OH^-$ (2)

Fe^{3+} catalytically decomposes H_2O_2 by the following equation

$Fe^{3+} + H_2O_2 \longrightarrow Fe\text{-}OOH^{2+} + H^+$ (3)

$Fe\text{-}OOH^{2+} \longrightarrow HO2. + Fe^{2+}$ (4)

$Fe^{2+} + HO_2. \longrightarrow Fe^{3+} + HO_2^-$ (5)

$Fe^{3+} + HO_2. \longrightarrow Fe^{2+} + H^+ + O_2$ (6)

The reaction of H_2O_2 with ferric ions is referred to as Fenton like reaction [3]

$H_2O_2 + HO. \longrightarrow H_2O + HO_2.$ (7)

Hydroxyl radicals can oxidize organics (RH) by abstraction of protons producing organic chemicals (R.) which are highly reactive and can be further oxidized [4],[5].

$RH + HO. \longrightarrow H_2O + R.$ (8)

Reaction (1) is modified by Walling et.al [6] by accounting for the dissociation of water

$2Fe^{2+} + H_2O_2 + 2\ H+ \longrightarrow 2Fe^{3+} + 2H_2O$ (9)

The equation suggests the need for an acidic environment to produce the maximum hydroxyl radical Pesticides and insecticides are major problem creators in the biological treatment plants because of their nature of inhibiting the growth of organisms. Neonicotinoid insecticides represent the fastest growing class of insecticide. As per EPA (USA), this class of insecticide will be a significant replacement for organophophates for labeled use. The major parameters affecting Fenton process are solution pH, amount of ferrous ions, concentration of H_2O_2, initial concentration of pollutant and presence of other ions [7],[8] .

II. Experimental

A. Model substrates

A commercial grade acetamiprid (MANIK) manufactured by Rallis India was used for the study. The properties and application of the acetamiprid is given in Table 1 . Ferrous sulphate heptahydrate ($FeSO_4.7H_2O$) was used as the source of $\%Fe^{2+}$ .The reagents were not subjected to any further purification. Sulphuric acid, sodium Hydroxide and hydrogen peroxide solution (30% w/w) used are from Merck. Distilled water was used throughout.

B. Procedures

Synthetic solution of the insecticide was prepared using distilled water. 500ml of the sample is taken in a beaker for the treatment. The desired pH was adjusted with sulphuric acid and then the required amount of iron salt was added. The iron salt was mixed very well with the solution of insecticide. Then the required amount of H_2O_2 was added. The reaction mixture was kept stirred throughout the reaction time. As the Fenton reaction cannot proceed above pH 10, the reaction was stopped after 2 hours by increasing the pH above 10 using NaOH. One drop of 0.1 N $Na_2S_2O_3$ was also added to each sample to decompose any residual H_2O_2 and preventing from reacting with organic substrates during the analysis. The solution is allowed to settle and the supernatant solution is used for analysis. Experiments are conducted at room temperature. COD of the samples after and before Fenton treatment were

TABLE I
PROPERTIES AND APPLICATION OF ACETAMIPRID

Name	Acetamiprid
Chemical formula	$C_{10}H_{11}ClN_4$
IUPAC name	$(E) - N^1 - [(6 - chloro - 3 - pyridyl)methyl] - N^2 - cyano - N^1 - methylacetamidine$
Chemical structure	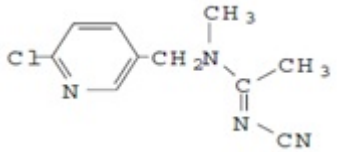
Molecular weight	222.68
Chemical family	Neonicotinoid insecticide
Application sites	Control of sucking type insects on leafy vegetables, Fruiting vegetables, Cole crops, Citrus Fruits, Pome Fruits, Grapes, Cotton and ornamental flowers and plants

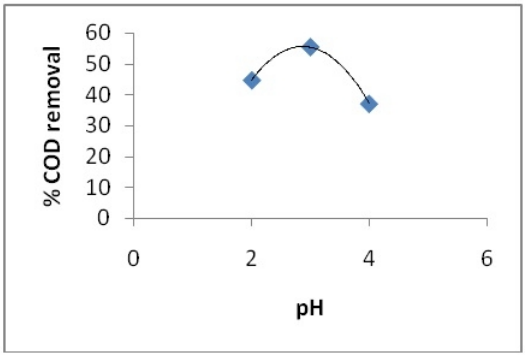

Fig. 1. The effect of pH on % COD removal

found out using open reflux dichromate method. Residual H_2O_2 present in the samples were determined using modified iodometric method. Absorbance of samples at 245nm was measured using UV-VIS spectrophotometer.

III. Results and Discussions

The results of main experimental runs are shown in the Figs 1-3.

IV. Conclusion

A study on Fenton Process for the degradation of acetamiprid, a neonicotinoid pesticide has been carried out. Optimum conditions for the process was found to be pH-3, COD/ H_2O_2-0.2, Fe^{2+}/ H_2O2.-2

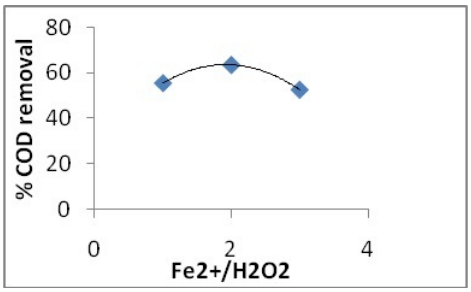

Fig. 2. The effect of Fe^{2+}/H_2O_2 on % COD removal

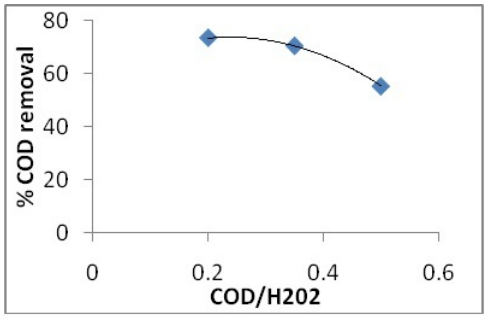

Fig. 3. THE EFFECT OF COD/H_2O_2 ON % COD REMOVAL

V. Acknowledgment

The authors are grateful to the Centre for Engineering Research and Development (CERD), Government of Kerala for the financial support.

References

[1] E.Neyens J.Baeyens, " A review of classic Fenton's peroxidation as an advanced oxidation techn'ique", J.Haz.Mater. B98, 2003, pp 33-50.
[2] E.Chammaro, A.Marco ans S.Esplugas, "Use of Fenton reagent to improve organic chemical biodegradability", Wat.Res. Vol 35, 2001, pp 1047-1051.
[3] C. Walling, A.Goosen, " Mechanism of the ferric ion catalysed decomposition of hydrogen peroxide : efcets of organic substrate", J.Am.Chem.Soc. 95(9) 1973, pp 2987-2991.
[4] Sheng H.Lin and Cho C. Lo, " Fenton process for treatment of desizing waste water", Wat.Res. Vol 31, no:8, 1997, pp 2050-2056.
[5] Yung Whan Kang,and Kyung-Yub Hwang, " Effcets of Reaction Conditions on the oxidation efficiency in the Fenton process,", Wat.Res. Vol 34 No:10, 2000, pp 2786-2790.
[6] Cheves Walling "Fenton's Reagent Revisited", Acc.Chem Res, 8 , 1975, 125.
[7] Gogate P.R and Pandit A.B, " A review of imperative technologies for wastewater treatment I: oxidation technologies at ambient conditions", Adv.Environ.Res, 8, 2004a, pp 501-551.
[8] A.S.Stansinakis "Use eof selected advanced oxidation proceesses (AOPs) for wastewater treatment – A mini Review", Global NEST Journal, Vol 10, N0:3 2008, pp 376-385

Electrochemical Reduction of Carbon Dioxide at Copper Electrodes

G. Keerthiga†, B. Viswanathan‡, C. Alex Pulikottil, Raghuram chetty†*
†Chemical Engineering Department, Indian Institute of Technology Madras, Chennai
‡National Centre for Catalysis Research (NCCR), Indian Institute of Technology Madras, Chennai
**R & D centre, Indian Oil Corporation Limited (IOCL) Faridabad, Delhi*
E-mail: keerthigagopal@gmail.com

***Abstract*— Conversion of CO_2 by electrochemical process has been achieved using copper electrodes in potassium chloride as supporting electrolyte. Cyclic voltammograms confirmed the reduction of CO_2 and the product analysis shows methane, ethane as major product while methanol, ethanol and acetaldehyde were observed in trace. Results suggest a reaction mechanism in the solid /liquid two phase configuration where the presence of Cu-Cl as the catalytic layer facilitates the electron transfer from the electrode to CO_2.**

***Index Terms*—Electro reduction, Carbon dioxide, Copper, Potassium chloride**

I. Introduction

As of current estimation, CO_2 is present in the atmosphere with a volumetric concentration of 0.0391 % (391 ppmv). Apart from being one of the reasons for global warming, CO_2 can also be considered as a possible C1 feedstock for the production of many useful products [1]. The transformation of CO_2 into organic substrates is a promising long term objective. However, the thermodynamic stability and the relative kinetic inertness of CO_2 pose a great challenge to recycle or to reuse carbon dioxide. Electrochemical method for the reduction of CO_2 appears to be one of the promising methods for the conversion and reduction of CO_2. The reaction rate and product distribution depends on the nature of the electrocatalysts, the reaction conditions, kinetics of electron transfer, adsorption/desorption at the electrode surface, and diffusion of CO_2 to the cathode [2]. Though various metal electrodes like Au, Ag, Zn, Pd, and Pt were employed for the reduction CO_2 to CO, copper is unique among the metals investigated. Cu belongs to the electrode material with medium hydrogen overvoltage with a weak CO adsorption, and catalyses the carbon–oxygen bond breakage in CO_2, and also allow the CO to desorbs [3]. The aim of this work is to optimize suitable conditions for maximum efficiency of the electrochemical reduction of carbon dioxide on copper electrode.

II. Experimental

The metal electrodes used in the present study are Cu sheet of 4 cm^2 where electrical connection is established through the same strip. The electrodes were polished with fine emery paper, electrolytically treated in 1M phosphoric acid and sulphuric acid, cleaned with acetone to remove grease and washed subsequently with ethanol and water. The electrochemical measurements were conducted with an EC Epsilon potentiostat. The experiments were performed in a homemade H-cell with $Ag/AgCl$ saturated KCl as reference electrode. Platinum foil was used as the counter electrode, while the supporting electrolyte was 1 mol dm^-3 KCl. The supporting electrolyte was purged with CO_2 gas for about 1 hr, and the CO_2-saturated solution was reduced electrolytically at the cathodic potential ranges determined from cyclic voltammograms. Gaseous products obtained during the electro reduction were analysed at regular intervals by gas chromatography for the presence of hydrocarbons by Porapak Q column through FID detector with N_2 as carrier gas.

III. Results and Discussions

A. Voltammetric studies

Cyclic voltammograms (CVs) were performed at room temperature at the Cu electrode in KCl electrolyte to determine the reduction potential. Fig. 1 shows the current–potential curves with the Cu electrode in CO_2 saturated and N_2 saturated (blank) KCl solution. The steep peak at -0.3 V could be due to the initial adsorption of Cl^- ions on the electrode surface. The reduction peak at potential greater than -0.9 V (vs. Ag/AgCl) for the CO_2 saturated solution compared with that of nitrogen saturated solution signifies the reduction of CO_2.

B. Electro reduction of CO_2

From the increase in reduction current seen in CV studies at potentials greater than -0.9 V for the CO_2 saturated KCl solution, three different potentials were chosen in the range from -0.9 to -2 V for electrolysis and the products were analyzed by gas chromatography. Figure 2 illustrates methane and ethane to be the major products formed during reduction while acetaldehyde and acetone have been observed in traces.

In this system, electron-transfer to CO_2 may occur via the $X_ad-(Cl^-)$–C bond, which is formed by the electron flow from the specifically adsorbed chloride anion to the vacant orbital of CO_2. Furthermore, it is believed that specifically adsorbed chloride anions could suppress the adsorption of protons, leading to a higher hydrogen overvoltage. Hence, the strongly restrained CO_2 leads to higher hydrocarbons. Maximum products formation was observed within the first

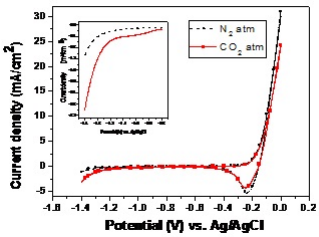

Fig. 1. Cyclic voltammograms of CO_2 reduction on Cu electrode in 1 M KCl at room temperature at a scan rate of 10 mV s^-1. Inset: Enlarged voltammogram showing the forward scan in the potential range -0.8V to -1.4V

2 hours. This may be due to scarcity of CO_2 in the system at longer time and the deposition of poisoning species on electrode surafce. Among the three different potentials chosen for KCl medium, -2.0 V showed the highest Faradic efficiency for ethane near to 7%.

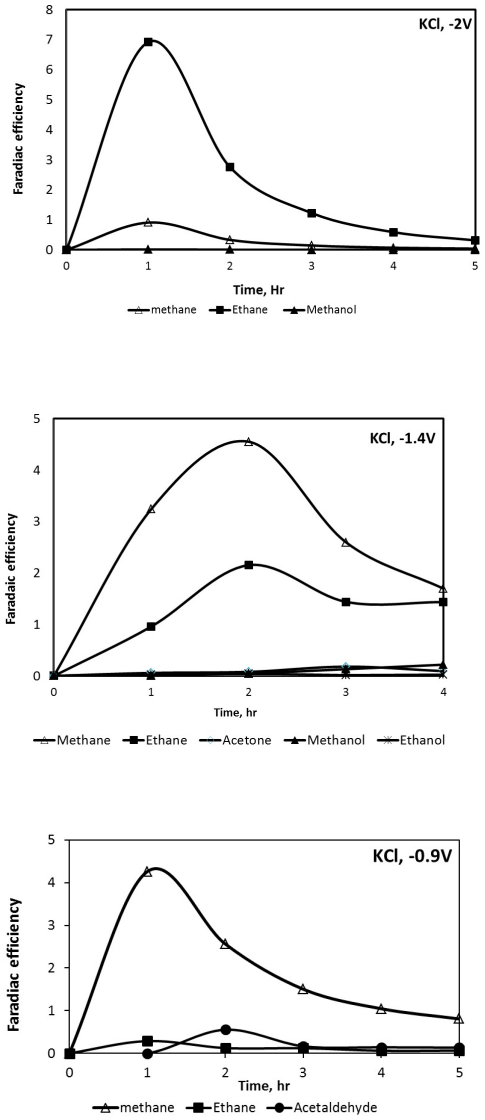

Fig. 2. Effect of time on Faradaic efficiency for the products formed by electroreduction of CO_2 with Cu electrode in KCl at room temperature at three different potentials

The formation of methane and ethane ought to have occured by a series of simultaneous or consecutive electronation /protonation steps which is coherent with the literature [4]. CO is expected to be formed as key intermediate which follows four electronation: protonation steps to get a reactive methylene group and this may either stabilize as a methane molecule or dimerize to form ethylene and ethane

IV. Conclusion

The electro reduction of CO_2 was performed with Cu as the working electrode in KCl electrolyte and the products were analyzed using gas chromatography. The reduction performed at three different potentials showed methane and ethane as the major products formed by the electronation and protonation.

Acknowledgment

We would like to thank Indian Oil Corporation Limited (IOCL), R&D centre, Faridabad for its fellowship, Department of Science and Technology (DST) for its funding, National Centre for Catalysis Research (NCCR) for its facilities.

References

[1] M. Aulice Scibioh and B. Viswanathan, "Photo-/photo electro-catalytic pathways for carbon dioxide reduction," Proc. Indn. Natl. Acad. Sci, vol. 70 A3, pp. 407-462, 2004.

[2] S. Ohya, S. Kaneco, H. Katsumata, T. Suzuki and K. Ohta,"Electrochemical reduction of CO_2 in methanol with aid of CuO and Cu2O," Catal. Today vol. 148, pp. 329–334, 2009.

[3] K. Ogura, R. Ferrell, V. Cuginic, S. Smotkin and S. Villalpando, "CO_2 attraction by specifically adsorbed anions and subsequent accelerated electrochemical reduction," Electrochim. Acta vol. 56, pp. 381–386. 2010.

[4] S. Kaneco, K. Iiba, N. Hiei, K. Ohta and T. Mizuno, T. Suzuki, "Electrochemical reduction of carbon dioxide to ethylene with high Faradaic efficiency at a Cu electrode in CsOH: methanol," Electrochim. Acta, vol. 44, pp. 4701–4706, 1999.

Water Dispersible Polymer Encapsulated Nanoparticles for Biological Applications

J Jaishree and Sri Sivakumar
Department of Chemical Engineering
Indian Institute of Technology Kanpur,
Kanpur, India
jaishree@iitk.ac.in, srisiva@iitk.ac.in

***Abstract*— Optical imaging by labeling or staining agents has greatly assisted the study of complex biological interactions in the field of biomedicine. In particular, fluorescent labeling of biomolecules has been demonstrated as an indispensable tool in many in-vivo and in-vitro studies. Types of fluorescent labeling agents that are commonly used include conventional classes of organic fluorophores such as fluorescein and cyanine dyes. This work focuses on lanthanides as upconversion fluorescent labels which are gaining increasing popularity in place of their predecessors due to their better optical properties such as possessing an enhanced photostability, low toxicity, lesser auto-fluorescence of tissues, sharp emission lines in the visible spectrum and a larger Stokes shift over conventional organic fluorophores. Core-shell nanoparticles are prepared by Pechini sol-gel method. Zeta potential measurement confirms the layer-by-layer assembly with oppositely charged polymers carried out on core-shell particles. Removal of template leads to encapsulation of nanoparticles inside polymer shell which is revealed by SEM and TEM images. Photoluminescence spectrum shows that the emission peaks remain same before and after template removal. MTT assay suggests that these particles are non-toxic to the cells.**

***Index Terms*—Fluorescent labeling; up conversion; lanthanides; core-shell; layer-by-layer assembly; encapsulation**

I. Introduction

Bio-imaging using nanoparticle has created new vistas in the field of nanomedicine, specifically nanodiagnostics. Though labeling of cells with organic dyes as fluorescent markers is widely used for various studies, it suffers from drawbacks such as broad overlapping absorption and emission spectrum, low photostablity and high autofluorescence from tissues. Lanthanide based fluorescent labels have their unique properties which arises due to shielding of 4f electrons leading to forbidden 4f-5d transition. They follow two mechanisms of fluorescence which includes down-conversion which generates low energy photons (ultra violet) from high energy photons (visible) and up-conversion which involves simultaneous excitation of two lower energy photons (near infra red) to produce high energy photons (visible) [1]. As autofluorescence of tissue is reduced by NIR excitation, labeling of biomolecules with up-converting phosphors leads to higher sensitivity. In this work, lanthanides with both down-converting (Eu^{3+}) and up-converting (Yb^{3+}/Er^{3+}, Yb^{3+}/Tm^{3+}, Yb^{3+}/Ho^{3+}) nanoparticles were prepared by sol-gel method to form lanthanide shell on silica template. Layer by layer (LbL) assembly on these core-shell structures followed by removal of template leads to encapsulation of nanoparticles inside polymer shell.

II. Experimental

Core-shell structures are formed by the coating of $LaVO_4$ doped Eu^{3+}, (Yb^{3+}/Er^{3+}, Yb^{3+}/Tm^{3+}, Yb^{3+}/Ho^{3+}) ions on silica core by Pechini sol-gel method with citric acid as chelating agent and polyethylene glycol as pegylating agent[2]. Fabrication of polyelectrolyte multilayers on core-shell particles is carried out by layer-by-layer (LbL) assembly with the deposition of oppositely charged polymers Poly(ethylene imine), Poly (Styrene Sodium sulfonate) and poly(allylamine hydrochloride). Removal of silica core is carried out with buffer oxide etchant which leads to nanoparticle encapsulation inside polymer shell.

III. Results and Discussions

TEM images show LbL assembly on $LaVO_4$:Eu^{3+}@silica core-shell structure (Fig. 1).Figure 2 shows TEM images of polymer encapsulated nanoparticles after removal of silica core (Inset: SEM image after core removal). XRD pattern (Fig.3) shows the tetragonal phase of $LaVO_4$.

IV. CONCLUSION

Lanthanide based core shell structures coated with polymers were successfully prepared using LbL assembly. Removal of silica template leads to nanoparticle encapsulated inside polymer layers which finds potential application in bio-imaging.

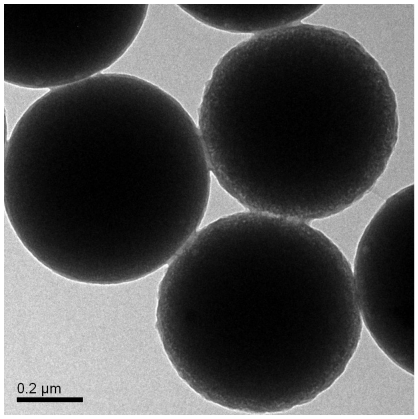

Fig. 1. LbL assembled core-shell structure

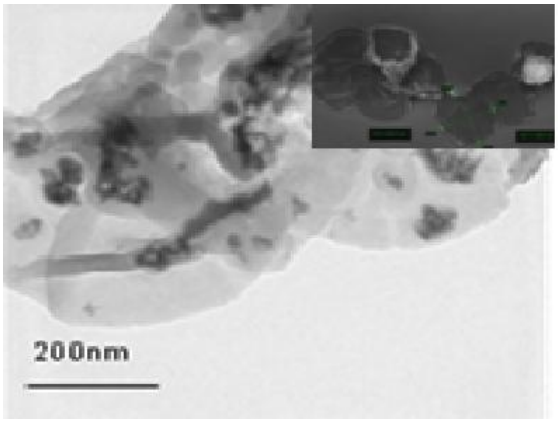

Fig. 2. TEM image of nanoparticles encapsulated inside polymer shells after core removal (Inset:SEM image)

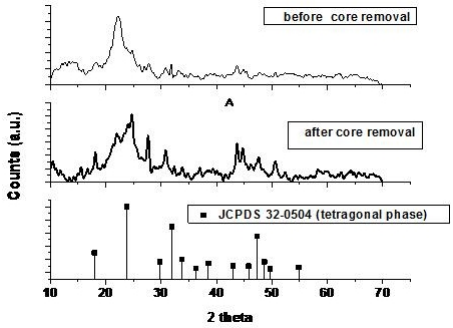

Fig. 3. XRD pattern of LbL assembled $LaVO_4$:Eu^{3+}@silica

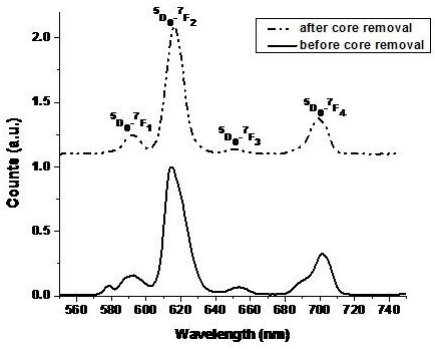

Fig. 4. Emission spectrum of LbL assembled $LaVO_4$:Eu^{3+}@silica

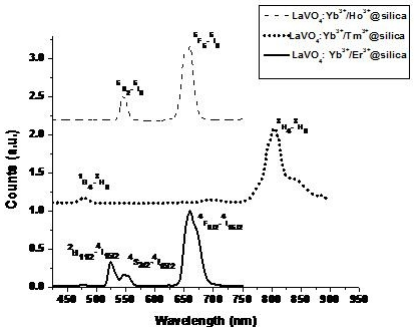

Fig. 5. Emission spectrum of up-converting lanthanides doped in $LaVO_4$ matrix

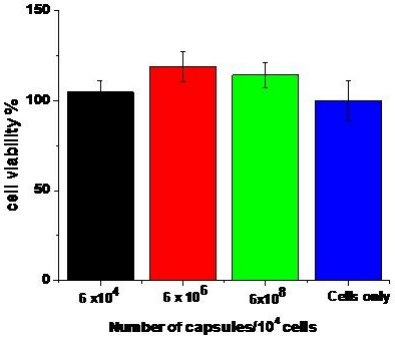

Fig. 6. MTT assay of polymer encapsulated nanoparticles in H460 lung cancer cell line. It is observed that these particles are non-toxic to the cells.

ACKNOWLEDGMENT

The authors are thankful to Dr. Venkataramanan M, IISER Kolkata, Dr. Ashok kumar, IITK and Nanoscience centre IITK for the characterization facilities offered by them.

REFERENCES

[1] Sivakumar, S.; Diamente, P. R.; van Veggel, F. C. Chemistry-a European Journal 2006, 12, 587.
[2] Yu, M.; Lin, J.; Fang, J. Chemistry of Materials 2005,17,1783.

Evaluation of Various Techniques for Extraction of Natural Blue Dye from Butterfly Pea-Aqueous Extraction, Microwave Irradiation and Magnetic Stirring Process

Keka Sinha, Sagnik Chakraborty, Papita Das (Saha)
National Institute of Technology - Durgapur
West Bengal, India
papitasaha@gmail.com

***Abstract*— Due to environmental awareness about synthetic dye pollution, it necessitated to work about the dyes extracted from natural sources and can be used in textiles industry, food industry etc. Magnetic stirring process, Microwave irradiation method and Aqueous extraction method have been used for extraction of dye from Butterfly Pea and then a comparative study is done among previous mentioned methods with aqueous extraction method as control. Analytical studies such as UV-VIS spectrophotometry and TDS analysis are performed on the extract sample. Traditionally, extraction of natural dyes with aqueous extraction method involved several hours of extraction time. The results indicate that there is a significant improvement in the extraction efficiency of the blue dye from Butterfly pea flower due to use of magnetic stirring process and microwave irradiation method.**

***Index Terms*—Keywords: Butterfly Pea flower, Aquoues Extraction, Microwave Irradiation method, Magnetic Stirring process for extraction, UV-visible spectrophotometer.**

I. Introduction

Natural colors have been part and parcels of our life since ancient times. Until the unexpected invention of widely available and cheaper synthetic dye "Perkin Mauve" in 1856 [1],[2],[3]. People are using few natural sources like stem, bark, leaves, roots and flowers to get many colors for dyeing clothes. But today the growing demand for the material of natural origin is because some of the synthetic dyes are harmful due to their negative ecotoxicological effects and associated with hazards effecting human life, creating skin diseases, lungs problems and environmental problems also. Due to these drawbacks, natural dyes are becoming widelyrecognized throughout the world. Natural colorants are dyes and pigmentary molecules that are obtained from plant, animal or mineral sources with or without chemical processing. The advantages of natural dyes are cost effective, renewable, ecofriendly i.e., they do not create any environmental problems at the stage of production or use, maintains ecological balance and has no allergic reaction on skin. Use of natural dyes replaces and reduces significantly on the amount of toxic effluent resulting from the dye process. It is the need of the day to identify the various resources for the extraction of these dyes. In India huge amount of flowers and herbal materials are wasted daily. For the purpose of our work, indigo blue Butterfly Pea (Clitoria ternatea) is chosen as natural source for dye extraction. It is an annual creeper that flowers almost throughout the season.

II. Experimental

A. Aqueous Extraction method (control experiment):

The freshly collected flowers petals with average size of 1 cm are used for the experiments. Typically different amount of sample (0.1gm, 0.2gm, 0.5gm, 1gm and 2gm) is taken and 50 ml distilled water is added in each conical flask and kept into the Hot air woven at different temperatures (60 ^{o}c to 90 ^{o}c) and room temperature also. Extract samples are taken at different time intervals (30min, 45min, 60min, 90min, 120min, 180min). All extracts are filtered and dried using Hot air woven .The optical density is determined with the help of UV-VIS spectrometer after suitably diluting the extracted dye and then calculated the total weight of the colorant extract per gram of the Butterfly Pea.

B. Microwave extraction method:

Different amount of freshly collected sample (0.1gm, 0.2gm, 0.5gm, 1gm and 2 gm) are weighed and transferred into 50 ml distilled water in each conical flask. The flasks are covered using aluminum foil to prevent loss of solvent by evaporation. The effect of Microwave time on the yield of colorant is examined at time intervals (10sec, 30 sec, 50 sec, 60 sec, 75 sec, 90 sec and 120 sec) with the extraction power (330w, 600w, 800w). Like aqueous extraction procedure, all extracts are filtered and dried using Hot air woven .The optical density is determined with the help of UV-VIS spectrometer and then calculated the total weight of the colorant extract.

C. Extraction using Magnetic Stirring:

Different amount of freshly collected sample (0.1gm, 0.2gm, 0.5gm, 1gm and 2 gm) are weighed and transferred into 50 ml distilled water in each beaker. This beaker are stirred magnetically for different time intervals (5, 10, 15 20, 25

TABLE I
A COMPARATIVE STUDY OF EXTRACTIONS OF DYE FROM 1 GM BUTTERFLY PEA FLOWER.

	Aqueous	Magnetic stirrer	Microwave
Reaction Time	3hrs	30 mins	2 mins
Total Dye in Solution in mg/l	2022	2860	3985
Absorbance	1.373	2.112	4.605

and 30 min). Like above two procedures, all extracts are filtered and dried using Hot air woven .The optical density is determined with the help of UV-VIS spectrometer and then calculated the total weight of the colorant extract.

III. RESULTS AND DISCUSSIONS

Colourful dyes from Butterfly Pea are extracted by above mentioned procedures and the extraction processes are carried out at different temperature, different extraction time and different amount of flowers to get the optimization point of the process.

A. Effect of extraction time:

The effect of time on extraction rate of dye is important. The time effect is investigated at the different extraction time range for these three techniques. Over the examined range, the extraction rate of dye from butterfly pea increased as the time rise.

B. Effect of amount of flower:

The effect of amount of flower on extraction of dye is analyzed over an amount range 0.1 gm to 2 gm. It is observed that the amount of dye extraction from butterfly pea flower varied with flower's amount. In these three techniques, the dye extraction significantly increased along with an increase in the amount of butterfly pea.

It is found that the extraction of dye from Butterfly Pea employing microwave irradiation throughout is finished in just 2 minutes with 4.605mg/l dye extract in solution and using magnetic Stirrer Process, it is completed in 30 minutes with 2860mg/l dye extract. On the other side the conventional method (aqueous extraction method) reported to take 3 hours for yielding of 1.373mg/l blue dye extract. This comparative study reveals that not only the reaction time is reduced from 3 hours to 2 minutes but also the yield of extract material is better in our case.

The visible spectrum of colorant extracted by Microwave irradiation method at 2 min is compared to that obtained by Aqueous extraction method at 180 min. Fig. 1 shows that the maximum absorbance obtained at λ max 575 nm for Microwave extract is higher than the latter extract.

IV. CONCLUSION

The most important features of our work are to help the considerable improvisation in both the reaction times and yields. We are interested in looking environmentally safer and cost effective technology for producing the natural blue dye from Butterfly Pea.

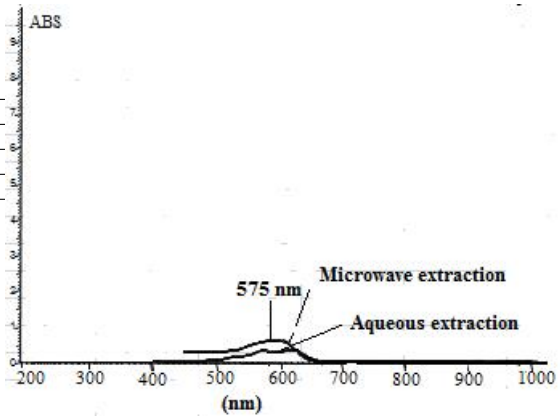

Fig. 1. Spectrum of natural colorant extracted by Microwave Irradiation method and aqueous extraction method

REFERENCES

[1] Parkes C. H, Creating colour in Yarn: An introduction to natural Dyes, Knitter's Review, 2002-200.
[2] Natural dyes, Avaliable at : http://www.housebarra.com/EP/ep03/03dyes.html, December 22, 2003.
[3] Making Natural Dyes from Plants, Available at: www.pioneerthinkinking .com, June 25 2003.

Elastic Recovery Lithography: A Simple Technique for Fabrication of Patterns with Different Feature Height Using a Single Stamp

Sudeshna Roy, Nandini Bhandaru, Suruchi and Rabibrata Mukherjee
Department of Chemical Engineering, Indian Institute of Technology Kharagpur,
West Bengal, 721 302, India
Email: nandini.bhandaru@gmail.com, sudeshna714@gmail.com, rabibrata@che.iitkgp.ernet.in

***Abstract*— A simple technique for creation of patterns with different feature heights, using a single stamp on thin elastomeric films is reported here. The proposed technique can be used to generate imprinted patterns with lateral dimension identical to that of the stamp but having controlled feature height (h) between 0 and h_0, where h_0 is the height of the feature on the stamp. Generating patterns with different h would require multiple numbers of stamps in any existing soft lithography method. However, the same can be accomplished with a single stamp which is the key novel feature of this work. The technique is based on elastic recovery of a visco-elastic liquid Sylgard 184 (a commercial elastomer). Thermal annealing results in films with progressively higher levels of cross linking until the material gets fully crosslinked. In this work, thermal pre-curing of as–coated Sylgard 184 films is done for different duration of time which results in partially cross linked films having different levels of visco elasticity. Subsequently, the same stamp under the same external force is used for imprinting the films. Owing to the elasticity of the film, the deformations due to imprinting tend to flatten out as the external force is withdrawn. The extent of deformation amplitude vis–a–vis the level of elastic recovery depends on the extent of elasticity of the film, which in turn is a function of pre curing time. Thus, pre cured films with different extents of reduction in the amplitude of the imprinted patterns results in features with different h. The films along with the stamps are subsequently cured for complete cross-linking, making the patterns permanent. Even after withdrawal of the external force, the presence of the stamp on the film surface ensures no lateral distortion to the imprinted patterns and hence the lateral feature periodicity of the imprinted patterns remains identical to that on the stamp.**

Electrochemical Reduction of Nitrate on Iron Phthalocyanines

Rajmohan K.S, Raghuram Chetty
Department of Chemical Engineering
Indian Institute of Technology Madras
Chennai, India
thanjaiksr@gmail.com

I. Introduction

Nitrated organic compounds are widely used as fertilizers, herbicides, insecticides, wood preservatives, pharmaceuticals, etc and are also produced either as intermediates or by-products during the manufacture of paints, plastic, polymers, solvents, etc. Concerns over the toxicity of these organic contaminants have been confirmed by the recent studies, which showed dramatic increase in toxicity to marine life and sea birds, when the waste enters uncontaminated streams at concentrations of 400 ppb. In humans, a variety of health effects including disruption of the endocrine system, as well as impact on the reproductive and immune systems were reported. Most nitrated contaminants are highly resistant to chemical attack; hence, until recently, it has only been possible using highly energetic methods, such as incineration. However new technologies which are emerging may provide more selective and also more economic methods for the destruction of nitrated contaminants.

II. Technologies Available

Current treatment methods often require initial pre-concentration of the contaminants such as solvent extraction when they are present in trace quantities. Biological and physicochemical techniques are being predominantly used. Owing to the disadvantages with the different techniques available, for example, biological treatment produces contaminants, slow reaction rate, difficult to control, produces residues and requires intensive maintenance, a constant supply of the organic substrate is needed and cannot be used above the concentration of 1000 mg/liter, whereas chemical reduction is limited by its cost, effectiveness and system stability/safety (as they produce toxic by-products). There are several advantages in the electrochemical method over the other methods mentioned above, which include [1]: (a) electrochemical degradation of waste is very efficient and selective degradation of waste may be achieved by controlling either the current or the potential of the electrode, (b) large volumes of waste may be treated by electrochemical cells incorporating continuous flow loops and high electrode area/volume ratio, (c) electrochemical reactions occur at room temperature and atmospheric pressures in contrast to the high temperature and pressure required by the other methods discussed above. Electrochemical reduction of nitrate generally requires a high negative potential, where non-noble metals undergo cathodic corrosion. Hence, expensive noble metal-based catalysts are commonly used as cathode. In the present investigation, we report on the reduction of nitrate on low cost metal phthalocyanines, which was found to be an efficient cathode for the reduction of nitrate.

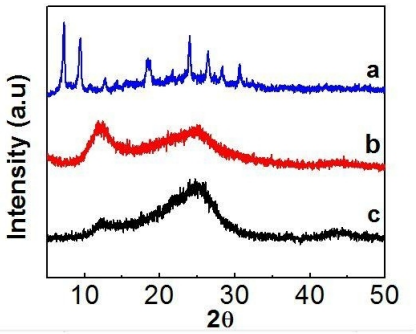

Fig. 1. X-ray diffractogram of (a) commercial FePc, (b) 10 wt. % FePc/C with heat treatment, and (c) untreated 10 wt.% FePc/C.

III. Experimental

Metal phthalocyanines (M-Pc, where M = Fe, Co, Ni) with metal loadings of 10 wt. % on carbon were prepared by impregnation method as reported in the literature [2].

A known quantity of FePc was added to dichloro methane and sonicated for 15 minutes, to which carbon black (Vulcan XC72R) was added and sonicated further for 30 minutes. The suspension was magnetically stirred overnight, and rest of the solvent was vaporized, and the obtained black powder was dried in oven at 85C for three hours. A part of the catalyst was also subjected to heat treatment, at a temperature of 650C in a tubular furnace under high pure nitrogen for 1 hour, with a heating rate of 10C min^{-1}. The prepared catalysts were characterized by high resolution scanning electron microscopy (HR-SEM) and X-Ray diffraction (XRD) to examine the morphology and structure. The electrochemical characterization was carried out to test the suitability of the catalyst for nitrate reduction. 2.5 mg of catalyst was added to 1.5 ml Millipore water and 0.96 ml ethanol and the mixture was sonicated for 60 minutes, and 10

1 of ink was deposited on the glassy carbon electrode and allowed to dry for 4 hours, served as the working electrode. Platinum wire and Ag/AgCl were used as counter and reference electrode, respectively. 20 mM perchloric acid solution was used as the supporting electrolyte (blank), and with 100 mM sodium nitrate for the nitrate reduction. All of the solutions studied were deaerated by bubbling nitrogen prior to the electrochemical measurements. The working electrode was cycled between 0.1 and -1.5 V at a scan rate of 100 mV/s five times before collecting the voltammograms.

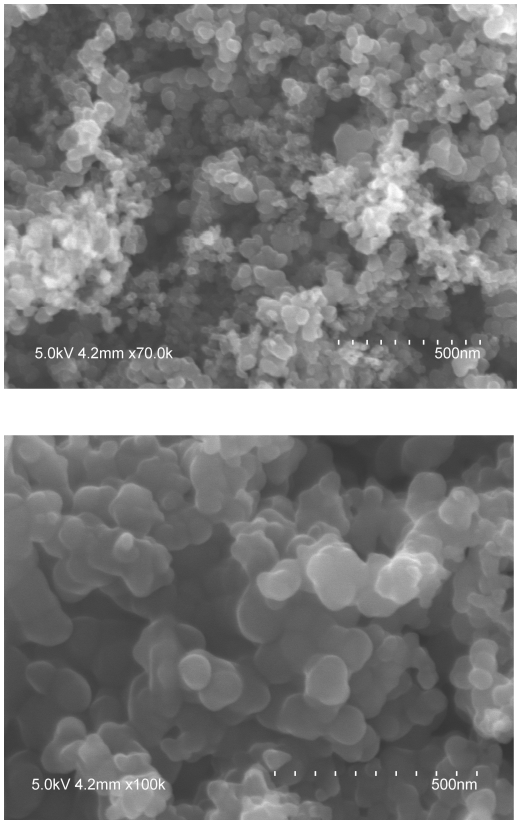

Fig. 2. Scanning electron micrographs of (a) untreated FePc/C and (b) heat treated FePc/C.

IV. Results and Discussions

Through trial runs, it was inferred that iron phthalocyanine (FePc) supported on carbon was found to be the best among the three metal phthalocyanines (CoPc, NiPc and FePc) evaluated for the reduction of nitrate in acidic media. It is reported in the literature that carbon black supported transition metal macrocycle show increase in catalytic activity when pyrolysed at higher temperature (¿ 650C) and the heat treatment changes the characteristics of macrocyclic compounds and alters the active sites, morphology, and particle size, which significantly influence the electrocatalytic activity. Hence in the present investigation, FePc supported on carbon was evaluated with and without heat treatment for the reduction of nitrate. The XRD patterns of FePc/C with and without heat treatment are shown in Figure 1, along with the diffraction patterns of as-received FePc presented for a comparison. Due to the amorphous nature of the FePc/C, no characteristic peaks were observed after the addition of carbon. Scanning electron micrographs of the synthesized catalyst

depicted in Figure 2 show aggregates of FePc particles dispersed on the carbon support. Comparison of cyclic voltammograms of untreated and heat treated FePc/C is shown in Figure 3. The voltammograms show an increase in cathodic current density for 100 mM sodium nitrate in perchloric acid solution compared to the blank solution which confirms the reduction of nitrate. The current density increased for the FePc/C catalyst heat treated at 650 C in comparison to the untreated catalyst. The onset potential and current density at

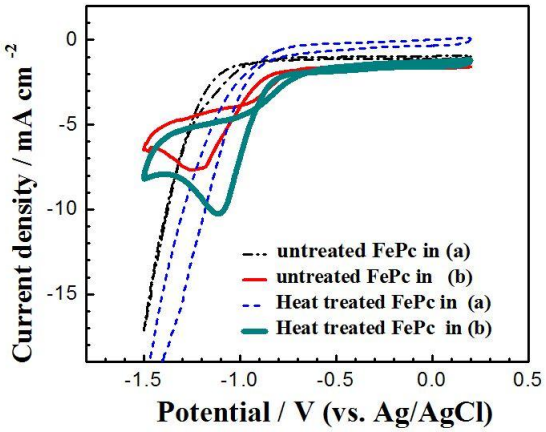

Fig. 3. Scanning electron micrographs of (a) untreated FePc/C and (b) heat treated FePc/C.

-1.0 V are -0.67 V and -7.06 mA cm^{-2} for the heat treated and -0.72 V and -4.01 mA cm^{-2} for the untreated FePc/C catalyst.

V. Conclusion

M-phthalocyanines (M = Fe, Co, Ni) supported on carbon were synthesized by impregnation method and their catalytic activity was compared towards nitrate reduction in acidic media. An increase in onset potential towards positive direction and higher current density signifies FePc/C as a promising catalyst for the reduction of nitrate. Moreover, heat treatment of the FePc/C at 650C showed improved catalytic activity than the untreated catalyst.

Acknowledgement

We thank the Department of Chemical Engineering, IIT Madras for the financial assistance.

References

[1] M Iizuka, Y Sakamura and T Inoue. "Electrochemical reduction of (U-40Pu-5Np) O2 in molten LiCl electrolyte." Journal of Nuclear Materials, vol. 359, pp. 102-113, 2006.

[2] K.D. Beard, M.T. Schaal, J.W. Van Zee and J.R. Monnier. "Preparation of highly dispersed PEM fuel cell catalysts using electro less deposition methods." Applied Catalysis B: Environmental, vol. 72, pp. 262-271, 2007.

Studies On a Single-Bed PSA With Different Cyclic Pressure Patterns

R.K.Gupta†, R.S. Thakur†, Nitin Kaistha† and D.P. Rao‡
†Department of Chemical Engineering, Indian Institute of Technology, Kanpur
‡Process Intensification consultants, Hyderabad
Email: rkgupta@iitk.ac.in, rsthakur@iitk.ac.in

I. Introduction

Pressure swing adsorption (PSA) is used as an alternative to cryogenic distillation and absorption process for gas separation and purification. Fractionations of air, CO_2 capture from flue gas, hydrocarbon recovery from landfill gas and hydrogen production from syngas are examples where PSA is used. The industrial PSA units usually have 3-10 beds that undergoes series of steps namely adsorption, blowdown, purge, pressure equalization and pressurization in a cycle to affect separation. As a bed of PSA unit goes through these steps of a cycle the pressure variation with time in a cycle forms a pattern characteristic of the PSA cycle. Several PSA cycles have been proposed to get one product of high purity and a waste product or both products of high purity. Low productivity and large footprints of PSA units are major concerns of these PSA processes.

Keller and Kuo (1982) in their patent (US Patent: 4,354,859) proposed a molecular-gate PSA (MGPSA) process that has a single bed connected with pistons at both the ends to vary the pressure. The resulting pressure pattern with time is sinusoidal. The MGPSA process is claimed to yield 95mol% pure oxygen at productivity of 39.4 LSTP of O_2 /h.kg adsorbent from air. Also 99.9 mol% pure CH_4 and H_2 products were produced at CH_4 productivity of 142.3 LSTP of CH_4/h.kg adsorbent from an equimolar mixture of CH_4 and H_2. The cycle frequencies were in the range of 30-50 RPM. The performance of MGPSA is far superior to the conventional PSA multibed units. However, the scale up of piston PSA for industrial purpose is difficult and hence it has limited use.

Hirose (1991) and independently Leavitt (1992) proposed a two-bed PSA called duplex PSA which is different from conventional PSA and MGPSA. Leavitt claimed that O_2 and N_2 purity in excess of 99mol% could be achieved from fractionation of air even with the low adsorption/desorption pressure ratio of 1.05 bar/0.7 bar. Sivakumar and Rao (2011) proposed a modification to enhance the productivity and purity of the duplex PSA.The modified duplex was shown to yield 99 mol% O_2 with 99% recovery from an equimolar mixture of N_2-O_2 at productivity of 120 LSTP of O_2 /h.kg adsorbent.

In this work we have proposed a single bed PSA with two surge tanks as alternative to MGPSA and duplex PSA. With the aid of programmable mass flow controller a desired pressure pattern in a cycle can be obtained. Proposed PSA is modular and thus several beds can be used in parallel to increase the capacity of the unit.

II. Simulation Studies

We have carried out simulation studies with different pressure patterns with time such as sinusoidal, rectangular and trapezoidal type to understand the performance of proposed PSA. Fractionation of air over zeolite 5A was chosen for the study.

III. Results and Discussions

ation for isothermal condition are reported in the table below. Table shows the purities and energy requirements for identical P_H/P_L at nearly same feed throughput for different pressure patterns. The modified duplex pressure pattern is far superior to the other two. The advantages and disadvantages of the proposed single bed PSA were presented. Typical results of the simul

Pressure pattern		Sinusoidal	Duplex PSA	Modified Duplex
Feed (LSTP $h^{-1}kg^{-1}$		439.5	439.5	457.8
$P_H/P_I/P_L$(bar)		4.0/-/1.9	4.0/-/1.9	4/2.5/1.9
Blowdown1 time(s)		25	5	3
Blowdown1 time(s)		-	-	2
Purge time(s)		-	20	25
Pressurization time(s)		25	5	3
Feed time(s)		-	20	15
Purity(mol%)	N_2	81.1	91.3	99.9
	O_2	29.2	73.8	100
Productivity (LSTP $h^{-1}kg^{-1}$)	N_2	307.3	336.5	364.0
	O_2	17.6	59.6	92.8
Energy (kJ/mol feed)		7.1	2.1	3.5

References

[1] Hirose T, A simple design method of a new PSA process consisting of both rectifying and stripping sections. Proceedings of the 2nd China-Japan-USA Symposium on Adsorption, 123. 1991.
[2] Keller II G.E. and Kuo C.H.A. Enhanced Gas Separation by Selective Adsorption, US Patent 4,354,859, 1982.
[3] Leavitt FW. Duplex adsorption process. US Patent 5,085674. 1992.
[4] Sivakumar SV, Rao DP. Modified duplex PSA.2. Sharp separation and process intensification for N2-O2-5A zeolite system. Ind. Eng. Chem. Res. 2011; 50: 3437–3445.
[5] Sivakumar SV. Sharp separation and process intensification on adsorptive separation processes. Ph.D. Thesis, Indian Institute of Technology Kanpur, India. 2007.

Colloidal Synthesis of Co-Mo Bimetallic and Core-Shell Nanoparticles

Rupesh Singh, Alok P. Singh, Dr. D. Kunzru, Dr. SriSivakumar
Department of Chemical Engineering,
IIT Kanpur,
Kanpur, India
rupeshs@iitk.ac.in

***Abstract*— Magnetic nano particles have lot of potential applications in various fields which include data storage, waste water treatment, MRI, and genetic engineering etc. In nano phase, particles shows property that can be entirely different from that of their bulk phase. The magnetic property of nanoparticles can be tuned by varying the applied magnetic field. For this application we had synthesized CoMo bimetallic and CoMo core shell nano particle.**

***Index Terms*—Magnetic nano particles, Bimetallic, core shell**

I. Introduction

Colloidal synthesis is Common technique used for the synthesis of nano particles because of low equipment cost, low temperature synthesis and control over the size of the nanoparticles. The precursor salts and reducing agents are dissolved in a common (usually organic) solvent and heated to the reaction temperature. The solvent is chosen such that it has little solubility with the product so that the product starts to nucleate and form particles. At some stage, a surfactant or capping agent is added to the solution which binds to the surface of these particles and stops further growth in size.

II. Experimental

Cobalt-Molybdenum bimetallic and core-shell particles were prepared using colloidal synthesis method. For Co-Mo bimetallic and core shell nano particle synthesis molybdenum hexacarbonyl, Mo(CO)6 and cobaltous acetate tetrahydrate ($(CH_3COO)2Co.4H_2O$) were used as the precursor salt. Oleic acid was used as a ligand to stop further growth of nanoparticles. The hydrophilic -COO- end of oleic acid binds to the surface of the nanoparticles and the remaining hydrophobic end prevents the particles from coming close to each other (reverse micelle like structures are formed). Diphenyl ether(DPE) is used as the solvent due to its high boiling point and good solubility with the precursor salts.

III. Results and Discussions

The prepared nano particles were characterized by using TEM, SEM-EDX, FTIR and XRD. TEM analysis shows that the average particle size of the prepared CoMo bimetallic nano particles and CoMo core-shell nano particles was found to be 12 nm and 30 nm respectively. For Biomedical applications particles need to show super paramagnetic property. Hysteresis loop of CoMO bimetallic and CoMo core-shell nano particle shows that the synthesized nano particles are showing super paramagnetic property. XRD analysis of CoMo particles shows the MoO3 phase of the prepared CoMo bimetallic nanoparticles. Whereas the XRD analyses of CoMo core- shell nanoparticles shows CoO and MoO3 phase. EDAX analysis shows the presence of Co and Mo in Co, Mo bimetallic and CoMo core shell nanoparticles. FTIR characterization proves the presence of carboxylate ions on the surface of nanoparticles, the peaks at 1549 and 1422 cm^-1 represent the symmetric and asymmetric vibrations of -COO species which clearly suggest that the oleic acid is attached to the surface of the nanoparticles and the absence of peak 1710 cm^-1 Shows that there is no free oleic acid is present after the washing steps is done. The peaks at 2928 and 2850 cm^-1 represent the asymmetric and symmetric vibrations of $-CH_2$ bonds, respectively Similarly in case of Core-Shell nano particles the peaks at 1567 and 1407 cm^-1 represent the symmetric and asymmetric vibrations of -COO species. Whereas the peaks at 2835 and 2924 cm^-1 represent the asymmetric and symmetric vibrations of $-CH_2$ bonds.

Bimetallic nano particles

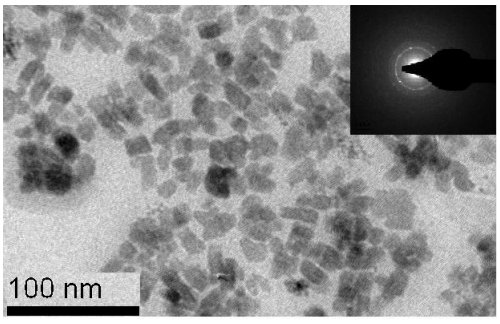

Fig. 1. TEM Image of Bimetallic nano particles

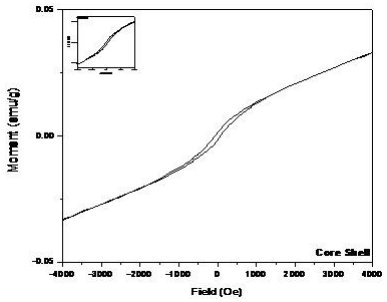

Fig. 2. Hysteresis Curve of bimetallic nano particles

Core-Shell nano particles

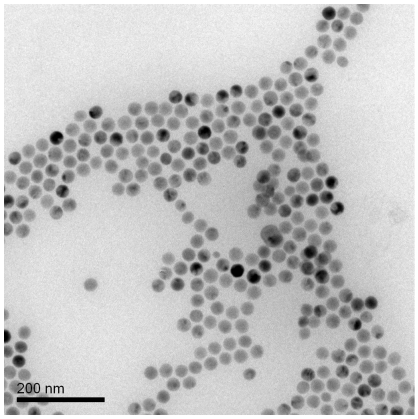

Fig. 3. TEM image of Core- Shell Nano particle

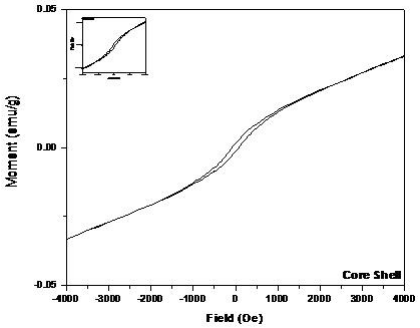

Fig. 4. Hysteresis curve of Core- Shell Nano particle

REFERENCES

[1] Park, J.C., and Song, H., ”Synthesis of Polycrystalline Mo/MoOx Nanoflakes and Their Transformation to MoO3 and MoS2 Nanoparticles”, Chem. Mater., 2007, 19 (11), pp 2706-2708

[2] Kim, C.W., Cha, H.G. , Kim, Y.H.,. Jadhav, A.P., Ji, E.S. , Kang, D.I., and Kang, Y.S., ”Surface Investigation and Magnetic Behavior of Co Nanoparticles Prepared viaSurfactant-Mediated Polyol Process”, J. Phys. Chem. C 2009, 113, 5081-5086.

[3] Su1, Y.K., Shen C.M., Yang, T.Z., Yang, H.T. , Gao, H.J., Li, H.L., ”The dependence of Co nanoparticle sizes on the ratio of surfactants and the influence of different crystal sizes on magnetic properties ”Applied physics A, Volume 81, Issue 3, pp.569-572.

Influence of Substrate Surface Energy on the Morphology of Thin Polymer Films Spin Coated on Topographically Patterned Substrates

Sudeshna Roy, Surendra Sasi Kumar Jampa, Khalid Jamal Ansari and Rabibrata Mukherjee
Department of Chemical Engineering, Indian Institute of Technology Kharagpur,
West Bengal, 721 302, India
Email: Sudeshna714@gmail.com, rabibrata@che.iitkgp.ernet.in

***Abstract*— The influence of substrate wettability on the morphology of a thin polymer film directly spin coated onto a topographically patterned substrate has been investigated. In addition to other parameters like concentration of the polymer solution (c_n), spinning speed, and duration, it has been shown that substrate surface energy (γ_s) has a strong effect on the final morphology. At a specific spin speed and dispensed drop volume, spin coating on a topographically patterned substrate will also lead to a continuous film as in case of a flat surface but only above a critical polymer solution concentration (c_t^*). It is generally believed that above c_t^* the resulting continuous film on a topographically patterned substrate has an undulating top surface where the undulations are in phase with the underlying substrate pattern. In this work we show that the undulations on the film surface are in phase with the substrate pattern only when the substrate surface energy is high but for a low surface energy substrate the undulations are 180 ^{o} out of phase to the substrate patterns. We show this effect with the specific example of spin coating of Polystyrene (PS) thin films on meso patterned substrates comprising stripes. Moreover, below c_t^*, depending on c_n, a variety of ordered and disordered structures like array of aligned and/or extended droplets, isolated strips of polymers etc., result on both high and low surface energy patterned substrates. Further, on a flat as well as on topographically patterned substrates, c_t reduces with increase in substrate surface energy (γ_s), which allows much thinner and continuous films to be cast on a preferentially wettable substrate.**

Ionic Liquids: Advantage Beyond Green Technology

S.A. Dharaskar, K.L. Wasewar, M.N. Varma, D.Z. Shende
Chemical Engineering Department
Visvesvaraya National Institute of Technology
Nagpur, India

***Abstract*— In recent years researchers have started to explore a particular class of organic solvents called room temperature ionic liquids or simply ionic liquids to identify their unique advantages for green technology. Because they lack vapour pressure, ionic liquids hold potential as green solvents. Ionic liquids can be considered as green solvents due to their very low vapor pressure and wide range of applications with unique physical and chemical properties. The potential of ionic liquids have been recognized worldwide. Scientists and engineers have been working in the advancement of preparation and applications of ionic liquid so that it can provide a range of options to industrialists looking to minimize the environmental impact of their chemical processes and processing cost. In petroleum and hydrocarbon industries, various solvents have been used such as ethers, amines, alcohols and other volatile organic compounds for the options like extraction, absorption, azeotropic distillation etc. These solvents have their own limitations as environmental issue, recycle ability etc. These limitations can be overcome by the use of ionic liquids.**

To minimize the negative health and environmental effects from automobile exhaust, many countries recently have mandated a drastic reduction in the sulfur content in transportation fuel. In petroleum industry, low-sulfur fuels are often obtained from hydrocracking processes or hydrotreating processes. Although hydrotreating processes have been highly effective for the reduction of sulfur levels, further improvement of the hydrodesulfurization efficiency is limited to increasing severe operational conditions at escalated cost with high energy and hydrogen consumption and other undesired side reactions.

In present paper, the attempts are made to write a critical review on various aspects of ionic liquids with the aim of their applications in petroleum and hydrocarbon industries and the various factors affecting their activity in removal of sulfur from transportation fuels.

***Index Terms*—Ionic liquids, desulfurization, review, refinery streams, various parameter.**

I. Introduction

Ionic Liquids (ILs) are usually composed of heterocyclic organic cations and various anions and have unique properties such as non-volatility, non-flammability, and a wide temperature range for liquid phase. The reality is that ionic liquids can be liquid at temperatures as low as -96^{o}C and some are liquid at over 4000^{o}C. Furthermore, room-temperature ionic liquids (RTILs) are frequently colourless, fluid, and easy to handle. In the patent and academic literature, the term "ionic liquids" now refers to liquids composed entirely of ions that are fluid around or below 100^{o}C.

Research into RTILs is booming. In the past few years significant literature has become available in the area of preparation, characterization and application of ILs for synthesis, catalysis and separation. Different ILs can be synthesized having a wide range of physical and chemical properties that can be fine-tuned by using different cations and anions to meet the requirement of specific applications. ILs are good solvents for a wide range of both inorganic and organic materials, and unusual combinations of reagents can be brought into the same phase. They are often composed of poorly coordinating ions, so they have the potential to be highly polar yet no coordinating solvents. They are immiscible with a number of organic solvents and provide a no aqueous, polar alternative for two-phase systems. Hydrophobic ionic liquids can also be used as immiscible polar phases with water. Ionic liquids are non-volatile, hence they may be used in high-vacuum systems and eliminate many contaminant problems.

II. Applications of Ionic Liquids

The potential of ionic liquids for new chemical technologies is beginning to be recognized as they have different application in many areas like as solvent for synthesis, catalysis or extraction, as an enzyme-friendly co-solvent, in batteries, as lubricant additives, in polymerization, in synthesis of nanoparticles, in analytical chemistry, etc. A few applications to mention are like in purification of essential oils by extraction, separation of azeotropic mixtures, in hydrogen purification, in extraction of rare earth metals, in extraction of carboxylic

acids, for removal of sulphur from refinery streams, in separation of isomers, for microfuidic separation using enzymatic reaction, in microextraction, for separation of fission products, in extraction and recovery of dyes, for extraction of ethanol etc. In addition to these applications of ionic liquids, it can be found that these noble solvents are very useful in many other fields with its recycle ability and without any impact on environment which is the most impressive factor in the present era of environmental concern.

REFERENCES

[1] Wasserschied, P., Roy van H. and Bosmann A. Green Chemistry, 2002, 4, 400-404.

[2] Nakashima, K., Kubota, F., Maruyama, T. and Goto M., Ind. Eng. Chem. Res., 2005, 44, 4368-4372.

[3] Rogers R. D. and K. R. Seddon, Science, 2003, 302(5646), 792-793.

[4] Seddon, K. R., in The International George Papatheodorou Symposium: Proceedings, S. Boghosian et al., Eds. (Institute of Chemical Engineering and High Temperature Chemical Processes, Patras, Greece, 1999), pp. 131-135.

[5] Marszall, M. P., M. J. Mrkuszewski and R. Kaliszan, J. Pharmaceutical and Biomedical Analysis, 2006, 41, 329-332.

[6] Welton T., Chem. Rev., 1999, 99, 2071-2083.

Aakar Group

(ISO 9001-2008, ISO 14001:2004 Certified Company)

Head Office - Aakar House Mathura Palace Begum bridge Meerut (U.P)
Phone & Fax - 0121-4033987, E-mail:-info@aakarinfra.com

- ✓ Aakar Infra Engineers Pvt. Ltd. (Building & Road)
- ✓ Aakar Engineers and contractors. (Civil Works)
- ✓ Aakar Construction Company. (Pipe Line & civil work)

ESSAR
OIL & GAS

Essar Oil is a fully integrated oil & gas company of international scale with strong presence across the hydrocarbon value chain from exploration & production to oil retail. It has a global portfolio of onshore and offshore oil and gas blocks, with about 45,000 sq km available for exploration. Essar Oil has over 300,000 bpsd (barrels per stream-day) of crude refining capacity that is being expanded to 750,000 bpsd. There are over 1300 Essar branded oil retail outlets in various parts of India.

www.essar.com

WITH BEST COMPLIMENTS

FROM

Binary Computer Systems.
WA-83, Mother Dairy Road,
Shakarpur, Delhi – 92 (INDIA)

Phone: 22468018, 22410367,

22430933, 43053872

Fax-22410367

WITH BEST COMPLIMENTS

FROM

QUALITY INDUSTRIES

W-50, MIDC, PHASE II,

DOMBIVLI – 421 204,

DIST.THANE MAHARASHTRA

PHONE : 0251-2443333

FAX : 0251-2449191

MANUFACTURE OF ANTI-OXIDANTS

WITH BEST COMPLIMENTS

FROM :- M/S SWASTIK OIL PRODUCTS MFG. CO. NAVSARI

MANUFACTURER OF FOLLWING PRODUCTS

- ETHYLENE GLYCOL MONO ETHYLE ETHER
- DI ETHYLENE GLYCOL MONO ETHYL ETHER
- ETHYLENE GLYCOL MONO METHYL ETHER
- DI ETHYLENE GLYCOL MONO METHYL ETHER
- EHYLENE GLYCOL MONO BUTYL ETHER
- DI ETHYLENE GLYCOL MONO BUTYL ETHER
- EHTYLENE GLYCOL MONO PHENYL ETHER
- FUEL SYSTEM ICING INHIBITOR AL-31
- FUEL SYSTEM ICING INHIBITOR AL-41
- URF (UNIVERSAL RECOIL FLUID) 80:20, 75:25, URF PLAIN
- BRAKE FLUID- DOT-3, DOT-4 & DOT-5
- ENGINE COOLANT
- PEG-200
- TETRA ETHYLENE GLYCOL
- TRI ETHYLENE GLYCOL
- ETHYLENE GLYCOL MONO ETHYL ETHER ACETATE
- ETHYLENE GLYCOL MONO METHYL ETHER ACETATE
- ETHYLENE GLYCOL MONO BUTYL ETHER ACETATE

Office Address
M/s. Swastik Oil Products Mfg. Co. Navsari
118/P, Hirji Govindji Compd.,
T.J. Road, Sewree,
Mumbai-400 015
Tel : 022-24131351/24130398
Fax: 022-24138512
Email : sanatswastikoil@gmail.com
Website: www.swastikoil.com

Factory address
M/s.Swastik Oil Products Mfg. Co. Navsari
Plot No.251, Village : Unn,
P.O. Khadsupa Boarding,
Tal & Dist : Navsari-396 433
Tel : 02637-225613
Fax: 02637-225013
Email : anup@swastikoil.com
Website: www.swastikoil.com

Promise what we deliver.

Deliver what we promise.

That's certainty

Critical situations. Ruthless competition. Unforgiving customers. Thankfully you can be absolutely sure of your IT solutions with Tata Consultancy Services (TCS). As one of the world's fastest growing technology and business solutions providers, TCS has built a reputation of delivery excellence based on world-class IT solutions that are on time, within budget and consistently deliver superior quality. So, it comes as no surprise that we pioneered the concept of the Global Network Delivery Model™. Developed Innovation Labs and Solution Accelerators. Achieving a level of delivery excellence that provides greater value to our customers and is the industry benchmark. Enabling our clients to experience certainty.

TATA CONSULTANCY SERVICES

Experience certainty.

IT Services ■ Business Solutions ■ Outsourcing

To learn how your business can experience certainty, visit www.tcs.com

NOTES

NOTES

NOTES

SABIC Innovative Plastics™

Performance, Innovation, Value

SABIC Innovative Plastics is a world leader in providing engineering thermoplastic resins, film and sheet products that are widely used in automotive, healthcare, consumer electronics, transportation, performance packaging, building & construction, telecommunications, and optical media applications. With over 75 years of success and a legacy that has defined the industry since its inception, we have an unmatched ability to provide solutions to customers, both globally and locally.

Through SABIC Innovative Plastics' legacy of innovation, we bring leading edge technology to our customers for improved performance and ground breaking style. Each innovation we develop to meet the changing needs of our customers combines the rich tradition of our materials expertise with market insight. Around the globe, we are helping to redefine the way our customers design, from concept to reality.

Through our Global Application Technology Centers, we collaborate with our customers to provide tailor-made and added-value solutions for their application challenges. From customer needs analysis to concept development; from engineering analysis to the development of actual parts, our emphasis on innovation, advanced engineering, and flexibility is demonstrated in each stage of the application development process. With our people, cutting-edge process, materials technology capabilities, and global expertise, we help our customers meet marketplace challenges and grow their businesses.

Sharing our futures

The passion to create the extraordinary everyday.

We are the pioneer in engineering thermoplastics. Everyday our people redefine the industry with passion, creativity and innovation to create breakthrough solutions that enable safer, more durable and higher performing products. We work side-by-side with our customers to transform new ideas into extraordinary solutions that enable their success.

Product Portfolio

Lexan* Resins Clarity & Superior Impact		Lexan (PC), Cycoloy* (PC/ABS), Lexan* SLX, Lexan* EXL, Lexan* XHT, Lexan* DMX
Noryl* Resins Dimensional Stability & Electrical Performance		Noryl* (PPE/HIPS), Flexible Noryl*, Noryl GTX* (PPE/nylon), PPO* (PPE)
Crystaline Performance Polymers Chemical Resistance & Excellent Impact		Valox* (PBT), Xenoy* (PC/PBT) Xylex* (PC/polyester), Valox* iQ, Xenoy* iQ
High Performance Polymers Superior Heat & Mechanical Strength		Ultem* (PEI), Extem* (TPI) Siltem* (PEI/Siloxane)
Cycolac* & Geloy* Resins Medium Impact & Weatherable Performance		Cycolac* (ABS) Geloy* (ASA)
LNP* Compounds Specialty Performance through Compounding		Thermocomp*, Lubricomp* Lubriloy*, Stat-Kon*, Faradex* Verton*, Starflam*
Specialty Sheet & Film High Temp. Film & High Impact Sheet		Lexan* PC film/sheet, Ultem* film/sheet, Thermoclear*sheet

Contact Details

West
781, Solitaire Corporate Park
Andheri Ghatkopar Link Road
Chakala, Andheri East
Mumbai-400093
Phone : (022) 6697 2382
Fax : (022) 6697 2383

North
Gateway Tower, 8th Floor
DLF Phase III, NH-8
Gurgaon-122002
Phone : (0124) 401 8001
Fax : (0124) 401 8022

South
5th Floor, "The Residency"
No 133/1, Residency Road
Bangalore, 560 025, INDIA
Phone : (080) 4053 9600
Fax : (080) 4053 9605

www.sabic-ip.com